

See discussions, stats, and author profiles for this publication at: <https://www.researchgate.net/publication/265058788>

Practical CIE5315 Computational Hydraulics

Technical Report · June 2014

DOI: 10.13140/2.1.3131.5842

CITATIONS

0

READS

134

1 author:



Adrià Moya

Delft University of Technology

3 PUBLICATIONS 0 CITATIONS

SEE PROFILE

Practical

CIE5315 Computational Hydraulics

Adrià Moya Ortiz
4314581



Faculty of Civil Engineering and Geosciences
Delft University of Technology
The Netherlands
June 2014

Contents

1	1D Modelling of Forced and Free Behaviour	1
1.1	Swash Code	1
1.2	Estimation of Required Simulation Time	1
1.3	Calculation of Eigen Frequencies and Spin-up Times	3
1.4	Propagating and Standing Waves	7
1.5	Bottom Friction Influence Assessment	8
1.6	Conditions for Linear Wave Behaviour	10
1.7	Spin-up Time Overview	10
1.8	Optimal Time Step Determination	12
1.9	Influence of Latitude	14
2	Modelling River Flow and Backwater Curves	16
2.1	Swash Code	16
2.2	Nikuradse Roughness Length	17
2.3	Minimization and Maximization of Backwater Curves	18
2.3.1	Fixed water level at the mouth of the river	18
2.3.2	Roughness	19
2.3.3	Discharge upstream	20
2.4	Horizontal Adaptation Length Scale	21
2.5	Assessment of Different Combinations of Boundary Conditions	22
2.5.1	Two discharge boundaries	23
2.5.2	Two velocity boundaries with different initial water levels	24
2.5.3	Upstream a discharge and downstream a water level condition	26
2.5.4	Explanation of findings	27
3	The Use of Advection Scheme	29
3.1	Introduction	29
3.2	Advection Scheme Assessment	30
3.3	Friction and Local Geometry Losses	38
3.4	Different Advection Schemes for Momentum	41
3.5	Interpolation of the Water Depth to the Velocity Points	45
4	Rectilinear Grids with Staircases vs. Curvilinear Grids	49
4.1	Water Level Head Differences	49
4.2	Time Step Assessment	52
5	The Vertical Structure of Barotropic Currents: Wind Driven Circulation in a Lake	53
5.1	Assessment of the Vertical Gradient of the Flow Velocity	54

5.2	Influence of the Background Viscosity on the Spin-Up Time	55
5.3	The Turbulent Kinetic Energy Profile	59
5.4	Gradually Increasing (Ramping) Wind	60
5.5	Two-Dimensional System	60
5.6	Differences With Depth-Averaged Simulations	67
6	Standing Short Wave in a Closed Basin	69
6.1	Creating a Standing Wave in a Closed Basin	69
6.2	Creation of a Short Wave	71
6.3	Number of Grid Points per Wave Length	74
6.4	Linear Wave Modelling	75
6.5	Assessment of the Phase Speed (fixed bottom level)	77
6.6	Hydrostatic and non-Hydrostatic Modes	79
6.7	Assessment of the Phase Speed (variable bottom level)	81
6.8	Different Number of Layers	82
6.9	θ -scheme	84

List of Figures

1.1	Water level for original conditions (18 days of simulation time.)	4
1.2	Different (imposed) frequencies of the forcing wave.	6
1.3	(Top) S2 tidal component water level (sinusoidal tide + oscillations due to conditions difference) and at the (bottom) detailed shape of a single oscillation.	7
1.4	(Top) Water level at the harbour basin with constant friction along the bottom (constant coefficient equal to (by default) and (bottom) water level at the harbour basin for a frictionless situation. Both situations belong to a harbour basin of 10 m depth.	9
1.5	Water level at $x = 0$ m for the set of conditions: $\zeta_{ic}(10,000, 0) = \zeta_{bc}(10,000, 0) = 1$ m and $u_{ic}(10,000, 0) = u_{bc}(10,000, 0) = 0$ m/s.	10
1.6	(a) Water level for $\phi = 0^\circ$ and $\zeta = 0$ m initially at the harbour, (b) water level for $\phi = 90^\circ$ and $\zeta = 0$ m initially at the harbour and (c) water level for $\phi = 0^\circ$ and $\zeta = 1$ m initially at the harbour.	12
2.1	Backwater curve for different roughness coefficients at $t = t_f$	18
2.2	Backwater curve for different water levels at the mouth at $t = t_f$	19
2.3	Increasing water levels (maximized backwater curves) for larger roughness values (lower Chezy coefficient).	20
2.4	Increasing water levels (maximized backwater curves) for larger discharges q upstream.	21
2.5	Adaptation length for the original backwater curve ($C = 50$ m ^{0.5} /s, $q = 4$ m/s, $b = 500$ m, $i_b = 10^{-4}$ and $h_0 = 7$ m).	22
2.6	<i>Test 1</i> water level variations at the different control points.	23
2.7	<i>Test 2</i> water level variations at the different control points.	24
2.8	<i>Test 1</i> water level variations at the different control points.	25
2.9	<i>Test 2</i> water level variations at the different control points.	26
2.10	Water level variations at the different control points.	27
2.11	Backwater curves for each of the combinations explained above.	28
3.1	Arrangement of the unknowns in a staggered grid.	30
3.2	Water level along a saw-tooth profile for different stepwise designs and sudden expansion disposition.	31
3.3	Water level along a saw-tooth profile for different stepwise designs and sudden contraction disposition.	31
3.4	Mass balance (sudden expansion case).	32
3.5	Momentum balance (sudden expansion case).	33
3.6	Energy head balance (sudden expansion case).	33
3.7	Mass balance (sudden contraction case).	34
3.8	Momentum balance (sudden contraction case).	34

3.9	Energy head balance (sudden contraction case).	35
3.10	Water level along a smoothly varying bottom profile for different amplitudes.	36
3.11	Mass balance (smoothly varying bottom profile).	37
3.12	Momentum balance (smoothly varying bottom profile).	37
3.13	Energy head balance (smoothly varying bottom profile).	38
3.14	Water levels (at last time step) and energy head levels (out of scale) for various bed roughnesses (sudden expansion case with a stepwise of 10 m).	39
3.15	Water levels (at last time step) and energy head levels (out of scale) for various bed roughnesses (sudden contraction case with a stepwise of 10 m).	40
3.16	(Left) water level using no space discretization and (right) water level for advective terms discretization using a upwind scheme with momentum conservation everywhere.	41
3.17	(Left) water level using no space discretization and (right) water level for advective terms discretization using a upwind scheme with momentum conservation everywhere.	42
3.18	(Left) velocities using no space discretization and (right) velocities for advective terms discretization using a upwind scheme with momentum conservation everywhere.	42
3.19	(Left) water level using no space discretization and (right) water level for advective terms discretization using a upwind scheme with energy head conservation everywhere.	43
3.20	(Left) water level using no space discretization and (right) water level for advective terms discretization using a upwind scheme with energy head conservation everywhere.	43
3.21	(Left) velocities using no space discretization and (right) velocities for advective terms discretization using a upwind scheme with energy conservation everywhere.	44
3.22	(Left) water level using no space discretization and (right) water level for advective terms discretization using a upwind scheme with energy head conservation everywhere.	45
3.23	(Left) velocities using no space discretization and (right) velocities for advective terms discretization using a upwind scheme with energy conservation everywhere.	45
3.24	Arrangement of the unknowns in a staggered grid where water depth is interpolated to velocity points.	46
3.25	Water levels for a the sudden expansion case (10 m stepwise). (Discontinuous line) original case and (continuous line) interpolation of water depth to velocity points.	46
3.26	Mass balance for a the sudden expansion case (10 m stepwise). (Discontinuous line) original case and (continuous line) interpolation of water depth to velocity points.	47
3.27	Momentum balance for a the sudden expansion case (10 m stepwise). (Discontinuous line) original case and (continuous line) interpolation of water depth to velocity points.	47
3.28	Energy head balance for a the sudden expansion case (10 m stepwise). (Discontinuous line) original case and (continuous line) interpolation of water depth to velocity points.	48
4.1	Curvilinear grid (left) and rectilinear/Cartesian grid (right).	50
4.2	Water level and velocity magnitude in a river bend with a rectilinear (Cartesian) grid.	51
4.3	Water level and velocity magnitude in a river bend with a curvilinear grid.	51
4.4	Curvilinear grid superposed over the rectilinear grid.	52

5.1	(a) Vertical distribution of the flow velocity, (b) vertical distribution of the vertical eddy viscosity per layer interface (in m^2/s) and (c) vertical distribution of the turbulent kinetic energy per layer interface (in cm^2/s^2).	54
5.2	Water level at the lake.	55
5.3	Time-evolution of the velocity profile (over depth) for the absence of background viscosity situation.	56
5.4	Time-evolution of the velocity profile (over depth) for a background viscosity of $10^{-3} \text{ m}^2/\text{s}$	57
5.5	Time-evolution of vertical distribution of the flow velocity with and without background viscosity.	58
5.6	Time-evolution of vertical distribution of the vertical eddy viscosity per layer interface with and without background viscosity.	58
5.7	Time-evolution of vertical distribution of the turbulent kinetic energy per layer interface with and without background viscosity.	59
5.8	Evolution of the turbulent kinetic energy profile.	60
5.9	Bathymetry of the lake (vertical borders).	62
5.10	Water levels and wind directions (vectors) at the lake (vertical borders).	62
5.11	Bathymetry of the lake (gradually sloping borders).	63
5.12	Water levels and wind directions (vectors) at the lake (gradually sloping borders).	64
5.13	Flow circulation at a latitude of 160 m ($y=5$) (vertical borders).	65
5.14	Flow circulation at a latitude of 160 m ($y=5$) (sloping borders).	65
5.15	Flow circulation at a latitude of 320 m ($y=9$) (vertical borders).	66
5.16	Flow circulation at a latitude of 320 m ($y=9$) (sloping borders).	66
5.17	Flow circulation near the easternmost border (vertical borders).	67
5.18	Flow circulation near the easternmost border (sloping borders).	67
6.1	Computed time series of surface elevation at gauge point for the standing wave in closed basin of 10 m depth.	71
6.2	Computed time series of surface elevation at gauge point for the standing wave in closed basin (deeper).	72
6.3	Computed time series of surface elevation at gauge point for the standing wave in closed basin (shallower).	73
6.4	Computed time series of surface elevation at gauge point for the standing wave in closed basin (different longitudes).	74
6.5	Validity of wave theories.	76
6.6	Computed time series of surface elevation at gauge point for the standing wave in closed basin (different amplitudes).	77
6.7	The dispersion relationship, the phase velocity c and the group velocity c_g (depth 100 m).	78
6.8	Application of hydrostatic and non-hydrostatic modes for different scales.	79
6.9	Computed time series of surface elevation at gauge point for the standing wave in closed basin (hydrostatic and non-hydrostatic simulations).	80
6.10	Computed time series of surface elevation at gauge point for the standing wave in closed basin (different layers).	83
6.11	Computed time series of surface elevation at gauge point for the standing wave in closed basin (different layers).	84
6.12	Computed time series of surface elevation at gauge point for the standing wave in closed basin (different θ_s).	85
6.13	Computed time series of surface elevation at gauge point for the standing wave in closed basin (different θ_s in detail).	86

List of Tables

1.1	Eigen frequencies, period and recommended simulation times for the original port situation and different resonance modes.	3
1.2	Forcing frequency, period and recommended simulation time.	3
1.3	Different harbour lengths and boundary conditions with corresponding eigen frequencies and spin-up times.	5
1.4	Courant number calculation for a series of time steps.	14
2.1	Different combinations regarding the two velocity boundaries case.	23
2.2	Different combinations regarding the two velocity boundaries case.	24
6.1	Dispersion relationship and phase speed results for a depth of 10 m.	78
6.2	Dispersion relationship and phase speed results for depths of 10 m to 50 m.	82
6.3	Dispersion relationship and phase speed results for a depth of 10 m (different horizontal layers).	82

Chapter 1

1D Modelling of Forced and Free Behaviour

1.1 Swash Code

```
PROJECT 'Exercise1' '1'
'1D Modelling of forced and free behaviour'
MODE DYN ONED
CGRID 0. 0. 0. 10000. 0. 100 0
INPGRID BOTTOM 0. 0. 0. 1 0 10000. 0.
READINP BOTTOM 1. 'flat.bot' 1 0 FREE
INIT ZERO
BOUND SIDE EAST BTYPE WLEV CON FOURIER 0. 1. 1.454E-4 90.
TIMEI METH IMPLICIT
POINT 'Buoy' 10000. 0.
TABLE 'Buoy' HEAD 'har01.tbl' TSEC WATL OUT 20140424.000000 1 MIN
COMPUTE 20140424.000000 2.5 MIN 20140429.000000
STOP
```

1.2 Estimation of Required Simulation Time

Estimate the required simulation time based on the imposed and eigen frequencies.

The Swash manual addresses this topic in the *numerical parameters* section. The following information is specified:

It is recommended to take into account both the spin-up time and the duration of the time series at the wavemaker boundary. In this way a steady-state condition will be obtained. We assume that the spin-up time takes at most 10 to 15% of the total time of the simulation. For a suitable simulation time at least 500 to 1000 waves are needed.

In the above example the cycle period equals 30 minutes, which is supposed to be at least 85% of the total simulation time. So, the duration of the intended simulation would be 35 minutes, or more safely, 40 minutes.

We can base the estimation on the imposed and eigen frequencies. The eigen frequencies for a given harbour length can be found by assuming that resonance occurs when the length of the basin (harbour) is approximately a quarter (or any other odd multiple) of the length of the incoming wave.

Therefore, for a frictionless situation (standing wave), the resonance condition:

$$\cos kL_b = 0 \rightarrow kL_b = (2n - 1)\frac{\pi}{2} \quad (1.1)$$

$$kL_b = \frac{2\pi}{L}L_b = (2n - 1)\frac{\pi}{2} \rightarrow L_b = \frac{(2n - 1)}{4}L \quad (1.2)$$

Frequency will occur not only for $L_b = 1/4L$, but for different resonance modes $L_b = 3/4L, L_b = 5/4L, L_b = 7/4L$, etc.

Considering the initial harbour size L_b (10,000 m), the length of the incoming wave L should be equal to 40,000 m so that resonance occurs. The frequency can be found by using the following expression, valid for shallow water:

$$T = \frac{4L_b}{(2n - 1)\sqrt{gh}} \rightarrow f = \frac{(2n - 1)\sqrt{gh}}{4L_b} \quad (1.3)$$

with $n = 1, 2, 3, \dots$

The above formula can be easily computed using the following **Matlab** script. Also, the recommended simulation time can be estimated by multiplying each period by a reasonable number of waves (see above). Here it has been considered that 750 waves would do the work (between 500 – 1000, as suggested by the manual).

```
% Calculation of the eigen frequencies of a harbour, tidal basin
n = input('Total number of resonance modes:');
L = 10000;
h = 10;
g = 9.81;

file = fopen('eigenfreqorig.txt','wt');
fprintf(file,'Length\tMode\tFreq [Hz]\tPeriod [s]\tSimultime [d]\n\n');

for i = 1:n
    f = (2*i-1)*sqrt(g*h)/(4*L);
    T = 1/f;
    t = T*750/86400;
    fprintf(file,'%d\t%d\t%.6f\t%.2f\t%.2f\n',L,i,f,T,t);
end
```

yielding the following values:

Table 1.1: Eigen frequencies, period and recommended simulation times for the original port situation and different resonance modes.

Length [m]	Mode	Freq [Hz]	Period [s]	Simultime [d]
10,000	1	0.000248	4038.55	35.06
10,000	2	0.000743	1346.18	11.69
10,000	3	0.001238	807.71	7.01
10,000	4	0.001733	576.94	5.01
10,000	5	0.002229	448.73	3.90
10,000	6	0.002724	367.14	3.19
10,000	7	0.003219	310.66	2.70
10,000	8	0.003714	269.24	2.34
10,000	9	0.004209	237.56	2.06
10,000	10	0.004705	212.56	1.85

For the imposed frequency, the required simulation time can be estimated in the same way as it has been done for the natural frequencies. We have been proposed to force the system by a S2 tidal component, the frequency of which is equal to inverse of the period, which is half a solar day (12 hours). Therefore, the simulation time would yield a much more large simulation time. For this solution it has been assumed that a tidal cycle would be understood as a single wave (however, one may differ with respect to such assumption).

Table 1.2: Forcing frequency, period and recommended simulation time.

Length [m]	Freq [Hz]	Period [h]	Simultime [d]
10,000	0.000023	12.00	375.00

The simulation time could be also computed on the basis of the spin-up time. It is also suggested in the manual that the spin-up time covers around a 10 to 15 % of the total simulation time. Therefore, as the spin-up time is estimated in the following section (approximately 15 days), it can be concluded that the simulation time should take up to 150 days, which is less than half the simulation time computed above.

1.3 Calculation of Eigen Frequencies and Spin-up Times

Estimation of the eigen frequencies using hand-calculations.

The eigen frequencies for a given harbour length can be found reference to formula. The spin-up time, however, will be estimated from the model outputs. The so-called spin-up is the time that the system takes to reach a steady behaviour. When the incident wave propagates inside the harbour, wiggles will first appear and gradually smooth out until the system reaches the equilibrium. The existence of such wiggles is due to the initial condition imposed inside the harbour and the boundary condition (wave forcing), in this case, at the east side of the domain. It is primordial to match the initial and boundary conditions so that the spin-up time is minimized.

Anyhow, wiggles will occur regardless the matching between the initial and boundary conditions (unless the basin is very small or the wave state inside the basin is exactly a continuation of the boundary condition). The tidal component will propagate towards the end of the harbour and water level oscillations will be significant (due to superposition of incident and reflected waves) at the beginning and will decrease in time (see standing waves section). The amount and strength of this wiggles will vary in function of the matching previously explained. This will be however further discussed in the corresponding section.

The spin-up time for the original situation can be visualized from the wave record at the end of the harbour (see Fig. 1.1). One can see that after approximately 15 days the function becomes practically smoothed.

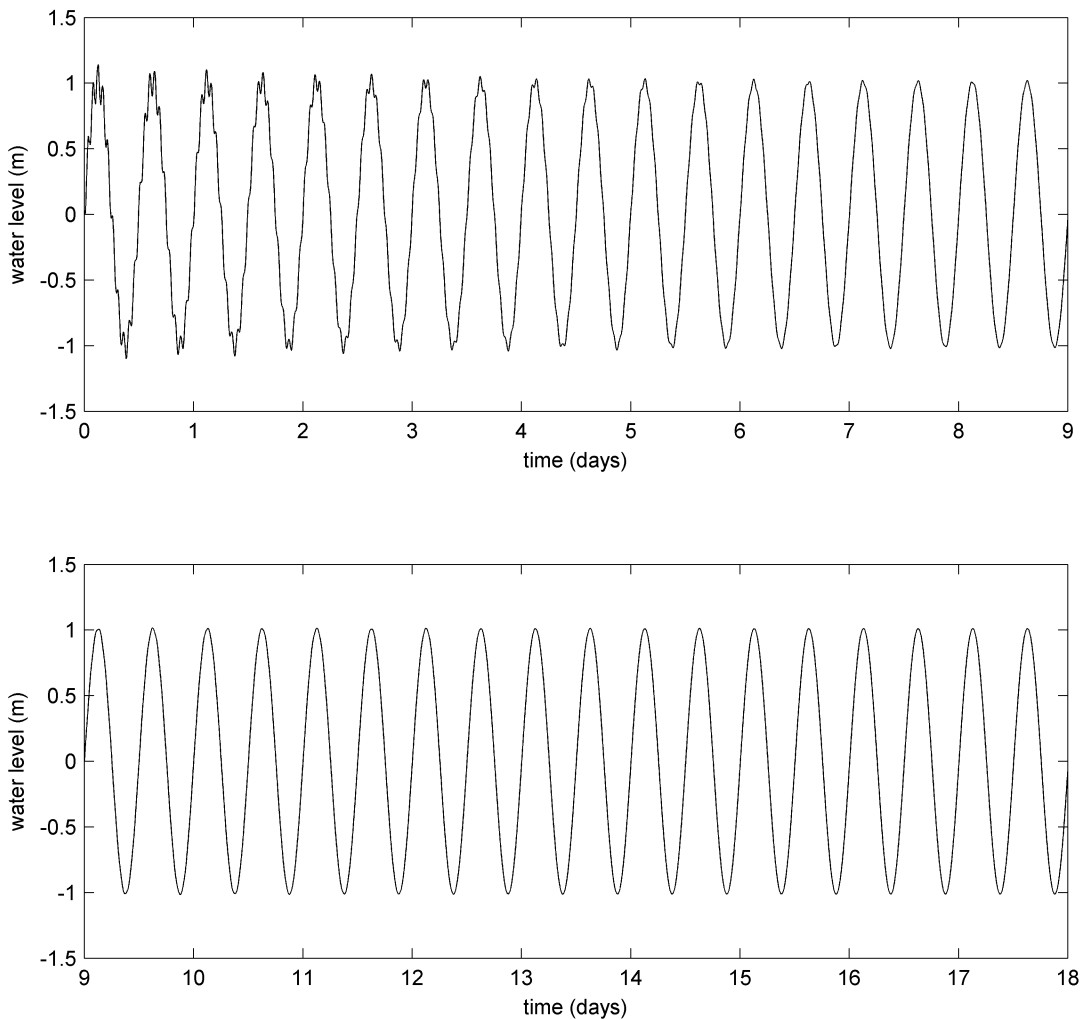


Figure 1.1: Water level for original conditions (18 days of simulation time.)

A simple Matlab script has been developed in order to compute the eigen frequencies for the various boundary conditions:

Listed below (see Table 1.3) one may find the different eigen frequencies (also angular frequencies) for various modes (different forcing) and harbor sizes.

```
% Calculation of the eigen frequencies of a harbour, tidal basin
L = input('Length of the basin [m]:');
h = input('Depth of the basin [m]:');
n = input('Total number of resonance modes:');
g = 9.81;

file = fopen('eigenfreq.txt','wt');
fprintf(file,'Length\tMode\tFreq [Hz]\tAng freq [rad/s]\n\n');
for j = 0.25:0.25:2
    Lb = j*L;
    for i = 1:1:n
        f = (2*i-1)*sqrt(g*h)/(4*Lb);
        w = f*2*pi;
        fprintf(file,'%d\t%d\t%.6f\t%.6f\n',Lb,i,f,w);
    end
end
```

Table 1.3: Different harbour lengths and boundary conditions with corresponding eigen frequencies and spin-up times.

Length [m]	<i>n</i>	Freq [Hz]	Freq [rad/s]	Length [m]	<i>n</i>	Freq [Hz]	Freq [rad/s]
2,500	1	0.000990	0.006223	12,500	1	0.000198	0.001245
2,500	2	0.002971	0.018670	12,500	2	0.000594	0.003734
2,500	3	0.004952	0.031116	12,500	3	0.000990	0.006223
2,500	4	0.006933	0.043562	12,500	4	0.001387	0.008712
5,000	1	0.000495	0.003112	15,000	1	0.000165	0.001037
5,000	2	0.001486	0.009335	15,000	2	0.000495	0.003112
5,000	3	0.002476	0.015558	15,000	3	0.000825	0.005186
5,000	4	0.003467	0.021781	15,000	4	0.001156	0.007260
7,500	1	0.000330	0.002074	17,500	1	0.000141	0.000889
7,500	2	0.000990	0.006223	17,500	2	0.000424	0.002667
7,500	3	0.001651	0.010372	17,500	3	0.000707	0.004445
7,500	4	0.002311	0.014521	17,500	4	0.000990	0.006223
10,000	1	0.000248	0.001556	20,000	1	0.000124	0.000778
10,000	2	0.000743	0.004667	20,000	2	0.000371	0.002334
10,000	3	0.001238	0.007779	20,000	3	0.000619	0.003890
10,000	4	0.001733	0.010891	20,000	4	0.000867	0.005445

Estimation of the eigen frequencies using the model.

For this purpose, and for a given harbour dimension, the model will be run several times for different forcing waves (different frequencies). The larger the amplitude recorded at the study point ($x = 0$ m), the closer to the eigen frequency (resonance).

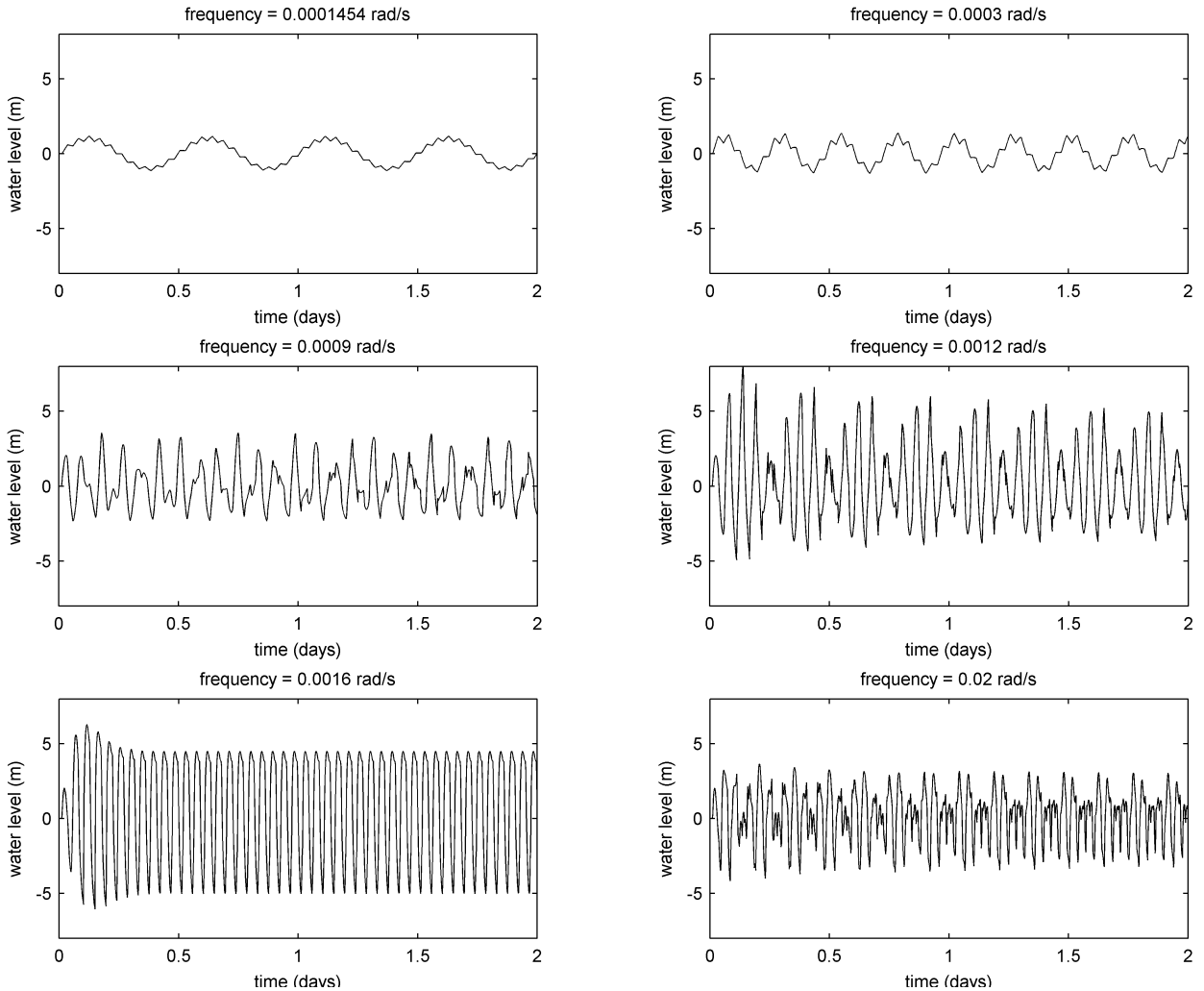


Figure 1.2: Different (imposed) frequencies of the forcing wave.

As it can be seen in the Fig. 1.2, the amplitude is maximum for a frequency approximately equal to 0.0016 rad/s , thus proving the previous estimation using the formula. This issue could be also solved by analysing, i.e. the water level record for the $1.454 \cdot 10^{-4} \text{ rad/s}$ frequency of the forcing. By zooming in onto one of the crests it would be possible to determine the eigen frequencies by checking the size of the irregular pattern although the resolution of the computation should be much larger (in order to properly define the wiggles).

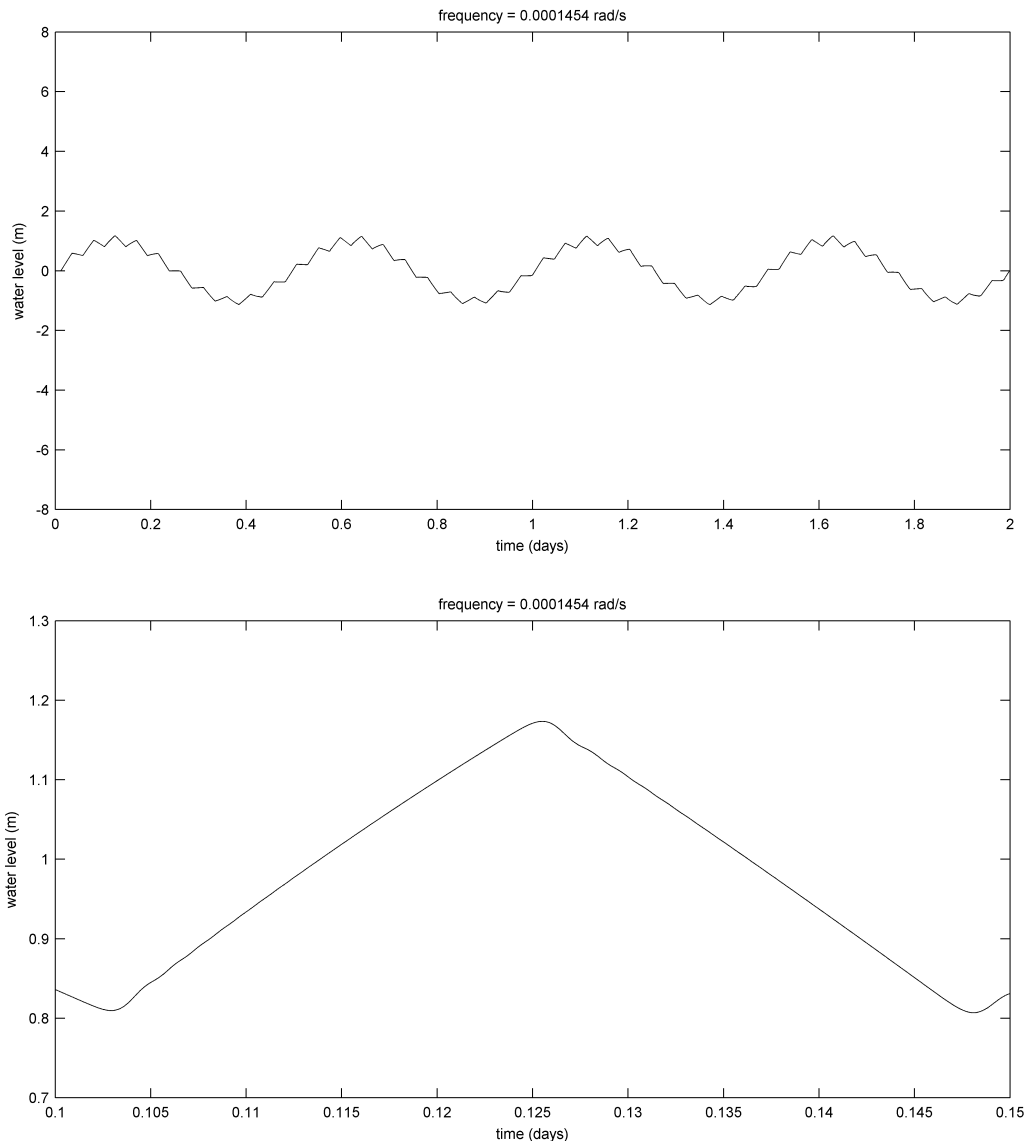


Figure 1.3: (Top) S2 tidal component water level (sinusoidal tide + oscillations due to conditions difference) and at the (bottom) detailed shape of a single oscillation.

It is then possible to estimate the period of the wiggle (which is associated with the natural frequencies of the harbour) from the Fig. 1.3. The (first mode eigen)period would approximately equal to 0.045 days ($0.1475 - 0.1025$, see Fig. 1.3). This results in a frequency of $2.572 \cdot 10^{-4}$ Hz or, alternatively, 0.0016 rad/s. It is then proved that the eigen frequencies of the harbour can be computed in several ways and are listed on the Table 1.1.

1.4 Propagating and Standing Waves

Investigate the difference between standing and propagating waves.

A **propagating wave** is a disturbance that travels through the ocean from one location

to another, transporting energy as it moves. The mechanism by which a wave propagates itself through a medium involves particle interaction; one particle applies a push or pull on its adjacent neighbour, causing a displacement of that neighbour from the equilibrium or rest position. As a wave is observed traveling through a medium, a crest is seen moving along from particle to particle. This crest is followed by a trough that is in turn followed by the next crest. In fact, one would observe a distinct wave pattern (in the form of a sine wave) traveling through the ocean.

Propagating waves are observed when a wave is not confined to a given space along the medium. If a wave is confined in a small region such as a basin or a lake. The wave will quickly reach the end of basin, reflect and travel back in the opposite direction. Any reflected portion of the wave will then interfere with the portion of the wave incident towards the fixed end. This interference produces a new shape in the medium that seldom resembles the shape of a sine wave. Subsequently, a propagating wave (a repeating pattern that is observed to move through a medium in uninterrupted fashion) is not observed in a (semi)enclosed basin. Indeed there are propagating waves although they are not easily detectable because of their interference with each other. In such instances, rather than observing the pure shape of a sine wave pattern, a rather irregular and non-repeating pattern is produced on the surface that tends to change appearance over time. This irregular looking shape (also referred as wiggles) is the result of the interference of an incident (sinusoidal) wave pattern with a reflected (sinusoidal) wave pattern in a rather non-sequenced and untimely manner. Both the incident and reflected wave patterns continue their motion through the medium, meeting up with one another at different locations in different ways. For example, the middle of the basin might experience a crest meeting a half crest; then moments later, a crest meeting a quarter trough; then moments later, a three-quarters crest meeting a one-fifth trough, etc. This interference leads to a very irregular and non-repeating motion of the medium. The appearance of an actual wave pattern is difficult to detect among the irregular motions of the individual particles.

It is however possible to have a wave confined to a given space in a medium and still produce a regular wave pattern that is readily discernible. The wave pattern is only produced when one end of the basin is vibrated (wave forcing) at just the right frequency. When the proper frequency is met, the interference of the incident wave and the reflected wave occur in such a manner that there are specific points along the medium that appear to be standing still. Because the observed wave pattern is characterized by points that appear to be standing still, the pattern is often called a **standing wave** pattern. There are other points along the medium whose displacement changes over time, but in a regular manner. These points vibrate back and forth from a positive displacement to a negative displacement at regular time intervals such that the motion of the medium is regular and repeating.

1.5 Bottom Friction Influence Assessment

Assess the influence of bottom friction (roughness and depth).

The influence of bottom friction will outcome result in a (constant) energy dissipation along the harbour basin. This phenomenon will therefore yield to a faster dispersion of the wiggly pattern show in the Fig. 1.4. The generation of these wiggles has been already covered before and, due to the aforementioned wave energy dissipation effects that bottom friction implies, the spin-up time will be significantly reduced (see Fig. 1.4). For the

forcing condition and harbour size originally taken into account:

1. S2 tidal components ($\omega = 1.4544 \cdot 10^{-4}$ m/s),
2. 10,000 m harbour basin length,
3. 10 m harbour basin depth;

the corresponding outcomes regarding the water level (friction and frictionless situation) are shown in the already referred Fig. 1.4.

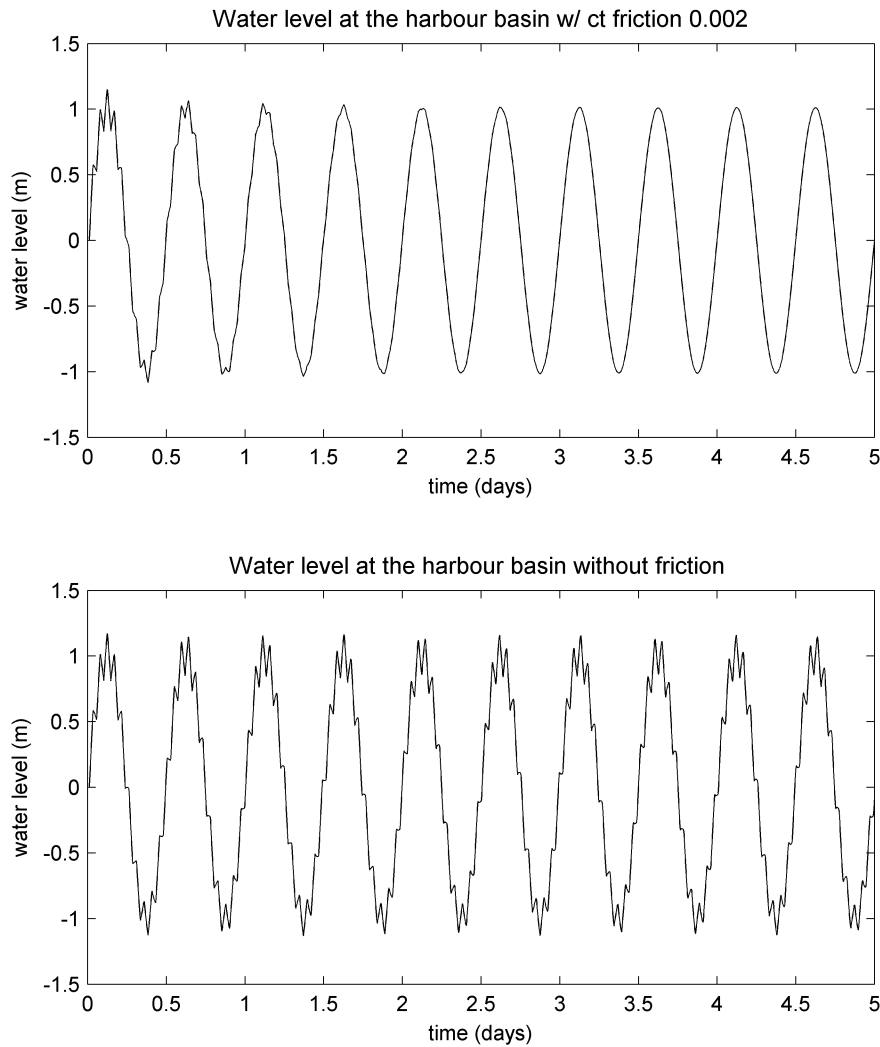


Figure 1.4: (Top) Water level at the harbour basin with constant friction along the bottom (constant coefficient equal to (by default) and (bottom) water level at the harbour basin for a frictionless situation. Both situations belong to a harbour basin of 10 m depth.

Following the depth, combined with the friction influence, will be analysed by maintaining the same forcing but modifying the basin depth. Therefore, in case we were supposedly dealing with larger depths, the model will output the following results:

1.6 Conditions for Linear Wave Behaviour

Under what conditions do the waves behave roughly linearly?

Linear waves will occur when a regular (sinusoidal) pattern is observed. For said effect, matching between initial and boundary conditions (both surface elevation and velocity) is required. A roughly linear behaviour can then be expected if the conditions discussed in the section 1.7 are implemented.

For instance, if velocities are forced to match at the entrance of the harbour, the external forcing should be set in such a way that the velocity is zero at $t = 0$ s. As it is considered to represent a sinusoidal wave, the amplitude at such location and time would be maximum (1 m) and therefore the harbour water level should be raised 1 m in order to catch up with the external forcing.

Linear behaviour should be expected after ensuring both initial and boundary conditions matching (see Fig. 1.5).

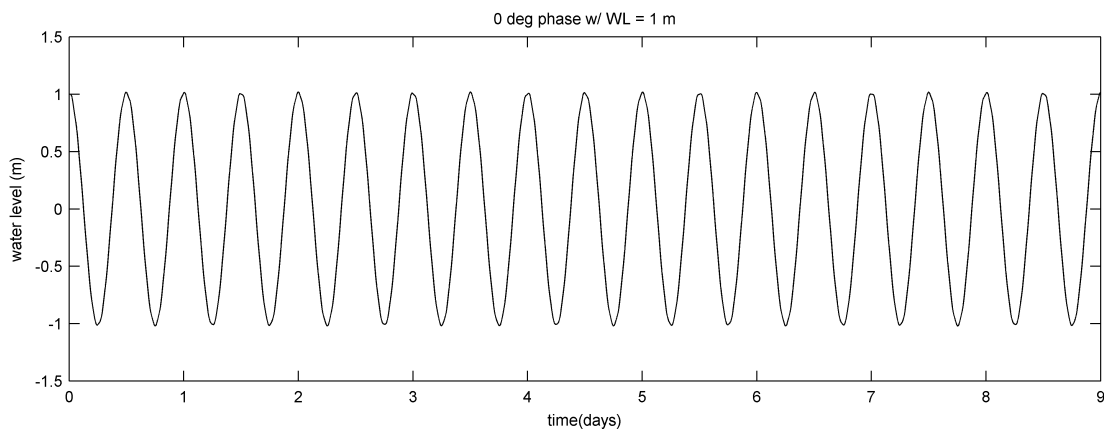


Figure 1.5: Water level at $x = 0$ m for the set of conditions: $\zeta_{ic}(10,000, 0) = \zeta_{bc}(10,000, 0) = 1$ m and $u_{ic}(10,000, 0) = u_{bc}(10,000, 0) = 0$ m/s.

1.7 Spin-up Time Overview

Try to minimize and maximize the spin-up time by varying the initial conditions (water levels and velocities) and boundary type (water levels and velocities).

Since the conditions inside and outside the harbour basin differ, an irregular, non-repeating pattern will characterize the water level record at the buoy location (see Section 1.4). The duration of such phenomena (until a regular pattern is observed) will be minimized if there exists a perfect match between the initial and boundary conditions. The matching needs to occur, in this case, with reference to the water level and velocity. The water level can be described using the following equation:

$$\zeta \sim \zeta_{max} \cos(\omega t + \phi) \quad (1.4)$$

so that, the velocity:

$$u = \frac{d\zeta}{dt} \sim u_{max} \sin(\omega t + \phi) \quad (1.5)$$

In case we consider a phase angle of $\phi = 0^\circ$, at the harbour basin mouth ($x = 10,000$ m) for $t = 0$ s (antinode) the equations (1.4) and (1.5):

$$\begin{aligned}\zeta &= \zeta_{max} \\ u &= 0\end{aligned}$$

However, this configuration would maximize the spin-up time since there is a mismatch between the velocity of the forcing (boundary condition) and inside the basin (initial condition).

This can be solved by shifting the phase to $\phi = 90^\circ$ in both equations (1.4) and (1.5), so that:

$$\begin{aligned}\zeta &\sim \zeta_{max} \cos\left(\omega t + \frac{\pi}{2}\right) = \zeta_{max} \sin(\omega t) \\ u &\sim u_{max} \sin\left(\omega t + \frac{\pi}{2}\right) = u_{max} \cos(\omega t)\end{aligned}$$

At $x = 10,000$ m and $t = 0$ s (node):

$$\begin{aligned}\zeta &= 0 \\ u &= u_{max}\end{aligned}$$

It should be noted that if linear wave theory was taken into account, it is known that wave amplitudes are small, so that the theory holds. This rather low amplitude would yield a not so much large velocity value when implementing the second initial-boundary set of conditions (node). This would be a way of adjusting the model run in terms of maximizing/minimizing the spin-up time. Therefore it is advisable to set a 90° phase so as to minimize the spin-up time.

However, there is still a second solution to prevent these conditions from mismatching. Velocity would indeed require to match the initial condition of the harbour basin; ergo be equal to zero. This would yield a maximum amplitude of the wave forcing (boundary condition) that would occur to be different from the water level (set to zero) of the harbour basin. Nevertheless, it could be fixed by rising the water level of the harbour by an amount equal to ζ_{max} (1 m). Therefore, this would have to be introduced into the initial conditions specifications.

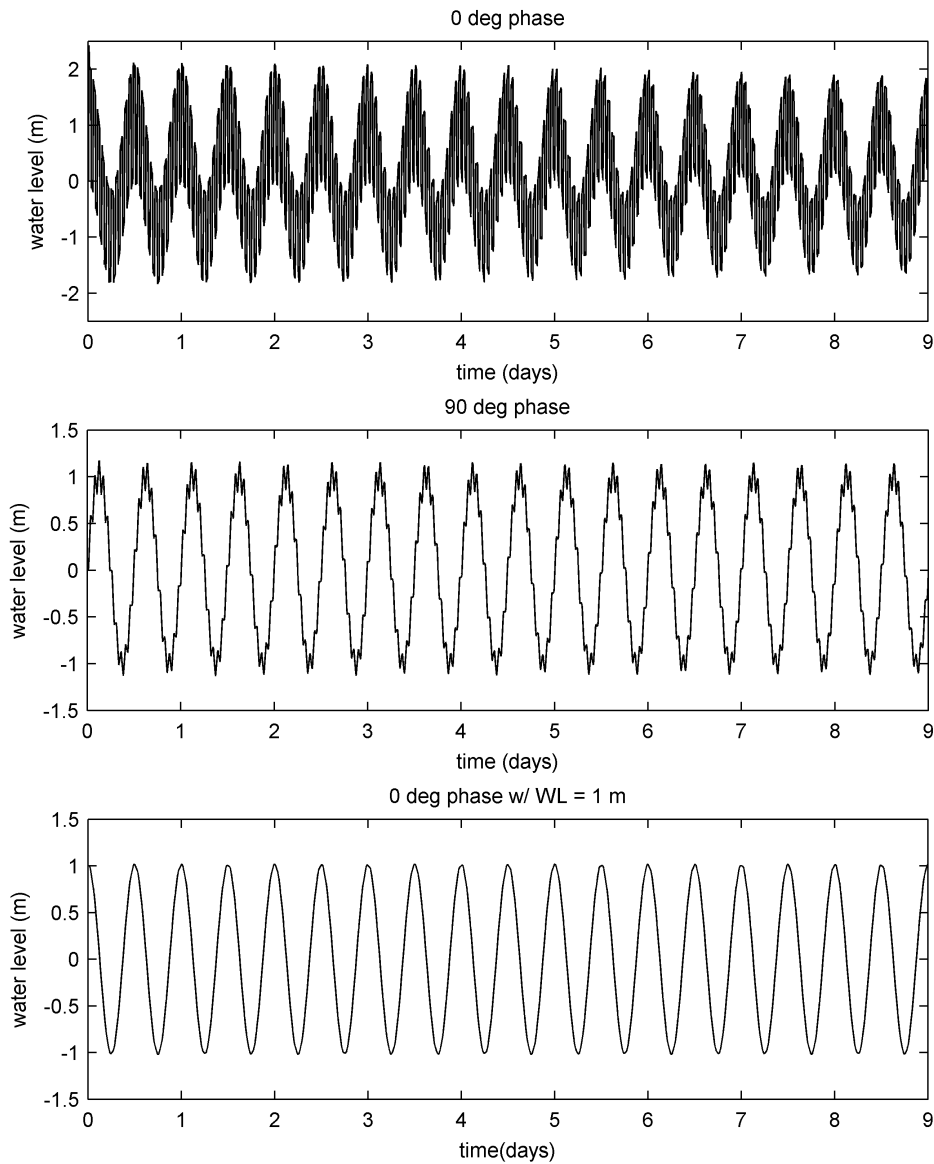


Figure 1.6: (a) Water level for $\phi = 0^\circ$ and $\zeta = 0$ m initially at the harbour, (b) water level for $\phi = 90^\circ$ and $\zeta = 0$ m initially at the harbour and (c) water level for $\phi = 0^\circ$ and $\zeta = 1$ m initially at the harbour.

1.8 Optimal Time Step Determination

Before using the proposed parameters, the adequate time step can be estimated from the model itself.

By checking the `harbour.prt` file, it has been possible to determine whether the model run has crashed or not. For the original conditions (see above), the following warning was found when the time step was larger than 2.5 minutes.

```
** Terminating error: INSTABLE: water level is too far below the bottom level!
** Message           : Please reduce the time step!
```

The S2 tide (imposed) frequency is equal to the inverse of the period, resulting in $2.315 \cdot 10^{-5} s^{-1}$ (or $1.454 \cdot 10^{-4} m/s$). In case we had considered the S4 tidal component (6 hour period), the frequency would be twice the S2 frequency, therefore equal to $4.630 \cdot 10^{-5} s^{-1}$ (or $2.909 \cdot 10^{-4} m/s$), the model would crash for the same time step of 2.5 minutes. For such reason, the time step has been reduced until 1.5 minutes (larger computational time), allowing the model to carry out the computations without crashing.

It will be further analyzed the case of a S6 tidal component with a 4 hour period ($6.944 \cdot 10^{-5} s^{-1}$ or $4.363 \cdot 10^{-4} m/s$). For such forcing condition, a time step of 0.8 minutes needs to be used.

From the previous analysis it can be concluded that the larger the (imposed) frequency, the shorter the time step and, therefore, larger computational cost.

The optimal time step is also assessed in the Swash manual by means of the Courant number. The time integration is of explicit type and thus requires strict conformity of stability criteria for a stable solution. The CFL condition for the (present) 1D case is shown in the equation (1.6):

$$C_r = \frac{\Delta t (\sqrt{gh} + |u|)}{\Delta x} \leq 1 \quad (1.6)$$

with Δx the mesh width, Δt the time step, u the flow velocity, and C_r the Courant number.

The time step is halved when this number becomes larger than a preset constant $C_{r,max} < 1$, and the time step is doubled when this number is smaller than another constant $C_{r,min}$, which is small enough to be sure the time step can be doubled. Usually, $C_{r,min}$ is set to 0.2, while the maximum Courant number $C_{r,max}$ is specified in the range of 0.5 to 0.8. It is advised not to choose a value higher than 0.8 since nonlinear processes, e.g. wave breaking and wave-wave interactions, can affect the stability condition. For high, nonlinear waves, or wave interaction with structures with steep slopes (e.g. jetties, quays), a Courant number of 0.5 is advised.

The following Matlab script has been built in order to estimate the Courant number given a time step. As it is suggested in the manual, a value of the Courant number equal to 0.5 will be considered to be optimal:

```
% Courant number estimation
x = 100;
g = 9.81;
h = 10;
t = 0;
Cr_u = 0;

file = fopen('Courant.txt', 'wt');
fprintf(file, 'Timestep [s]\tCourant\n');
while Cr_u >= 0.4 && Cr_u <= 0.8
    t = t+2.5;
    Cr_u = t*u/x;
    fprintf(file, '%.1f\t%.3f\n', t, Cr_u);
end
```

which outputs the following Table 1.4:

Table 1.4: Courant number calculation for a series of time steps.

Timestep [s]	Courant (u)
40.0	0.400
42.5	0.425
45.0	0.450
47.5	0.475
50.0	0.500
52.5	0.525
55.0	0.550
57.5	0.575
60.0	0.600
62.5	0.625
65.0	0.650
67.5	0.675
70.0	0.700
72.5	0.725
75.0	0.750
77.5	0.775
80.0	0.800

1.9 Influence of Latitude

Try one simulation in which you set the latitude of, for instance, 52° N. What happens?

Consideration of latitude directly involves the Coriolis effect, which diverts a moving particle to the right (left) on the Northern (Southern) hemisphere. This holds for large scale motions such as the one taken into consideration in the present analysis (S2 tidal component). Coriolis forces are balanced by a water level gradient and therefore entail a tilting of the sea surface that can be estimated from the momentum equation taking into account the aforementioned Coriolis force.

The acceleration at which a particle is deflected due to this force is expressed below (1.7).

$$a_c = fV = 2\omega_e V \sin \varphi \quad (1.7)$$

where

ω_e = angular velocity of the earth ($72.9 \cdot 10^{-6}$ rad/s)

V = current velocity (1 m/s)

φ = latitude (52°)

Coriolis forces are balanced by a water level gradient and therefore entail a tilting of

the sea surface that can be estimated by using the equation (1.8).

$$g \frac{d\zeta}{dx} = fV \rightarrow \Delta\zeta = \frac{fV\Delta x}{g} \quad (1.8)$$

Assuming we had a 2D grid of 2,000 m width (deflection would occur along the transversal direction). By substituting these values into (1.8), Coriolis-induced set up equals to 0.0234 m. Which is rather small compared to the basin size (10,000 km).

Chapter 2

Modelling River Flow and Backwater Curves

2.1 Swash Code

```

PROJECT 'Exercise2' '1'
'Modelling river flow and backwater curves'
MODE DYN ONED
CGRID 0. 0. 0. 100000. 0. 100 0
INPGRID BOTTOM 0. 0. 0. 1 0 100000. 0.
READINP BOTTOM 1. 'flat.bot' 1 0 FREE
INPGRID WLEV 0. 0. 0. 1 0 100000. 0.
READINP WLEV 1. 'surface.wlv' 1 0 FREE
INIT STEADY
BOUND SIDE EAST BTYPE WLEV CON -3.
BOUND SIDE WEST BTYPE DISCH CON 4.
TIMEI METH IMPLICIT
GROUP 'Section' SUBG 1 101 1 1
TABLE 'Section' NOHEAD 'riversect.tbl' DIST WATL
POINT 'Buoy_00' 0. 0.
TABLE 'Buoy_00' NOHEAD 'riv_00.tbl' TSEC WATL OUT 20140424.000000 10 MIN
POINT 'Buoy_80' 80000. 0.
TABLE 'Buoy_80' NOHEAD 'riv_80.tbl' TSEC WATL OUT 20140424.000000 10 MIN
POINT 'Buoy_90' 90000. 0.
TABLE 'Buoy_90' NOHEAD 'riv_90.tbl' TSEC WATL OUT 20140424.000000 10 MIN
POINT 'Buoy_100' 80000. 0.
TABLE 'Buoy_100' NOHEAD 'riv_100.tbl' TSEC WATL OUT 20140424.000000 10 MIN
COMPUTE 20140424.000000 2.5 MIN 20140429.000000
STOP

```

In the following, it will be referred as original conditions to the following parameters defining the backwater curve visible in Fig. 2.1.

$$C = 50 \text{ m}^{0.5}/\text{s}$$

$$q = 4 \text{ m/s}$$

$$i_b = 10^{-4}$$

$$h_0 = 7 \text{ m} \text{ (depth at the mouth)}$$

and, by means of the equation (2.1), the equilibrium depth is found ($h_e = 4 \text{ m}$).

$$h_e = \left(\frac{q^2}{C^2 i_b} \right)^{1/3} \quad (2.1)$$

2.2 Nikuradse Roughness Length

The use of a Chezy roughness value is very common in civil engineering. Chezy values have weird units, so we strongly advocate not using them. Try to impose the roughness with the z_0 or Nikuradse roughness in meters instead. Despite that, for a lot of cases, Chezy values are very useful for circulation models, because they implicitly contain a depth-dependent roughness.

The roughness of the sea floor varies over several orders of magnitude, from the diameter of a sediment grain to the size of large sand waves. The sediment bed is usually mobile and responds to energetic flows, and its roughness in turn impacts the flow. Hydrodynamics over mobile beds therefore involves feedback between the river bed and overlying flows.

Bed roughness scale forms a hierarchy from smallest-to-largest. At the smallest stage it is found:

Nikuradse roughness: The smallest form of roughness is that of the sediment grains themselves, called grain roughness or Nikuradse roughness. This is usually not the dominant form of roughness in coastal waters- but is used as a lower limit for physical roughness estimates. It is also needed as a roughness length scale for an inner boundary layer when bed forms are present. Nikuradse (1933) found an expression for this roughness scale using laboratory measurements of flow through smooth and roughened pipes.

According to different authors, it is found in literature that the Nikuradse roughness length k_s can be estimated using the median grain diameter D_{50} :

$$k_s = 2.5D_{50} \quad (2.2)$$

Considering the sediment size to lie around the gravel domain (larger than 2 mm up to 256 mm), the roughness length taken into account will range from 0.1 m to 0.3 m.

For a proper visualization of the variation with reference to the Chezy coefficient implementation, Chezy and Nikuradse (roughness coefficients) friction effects have been contrasted. A value of the Chezy coefficient equal to $50 \text{ m}^{0.5}/\text{s}$ is widely used in engineering applications and it will be therefore used in the following comparison. Different roughness lengths (Nikuradse), representing various grain sizes, will be plotted in order to understand the behaviour of a river when different sediments and bed forms that may be encountered.

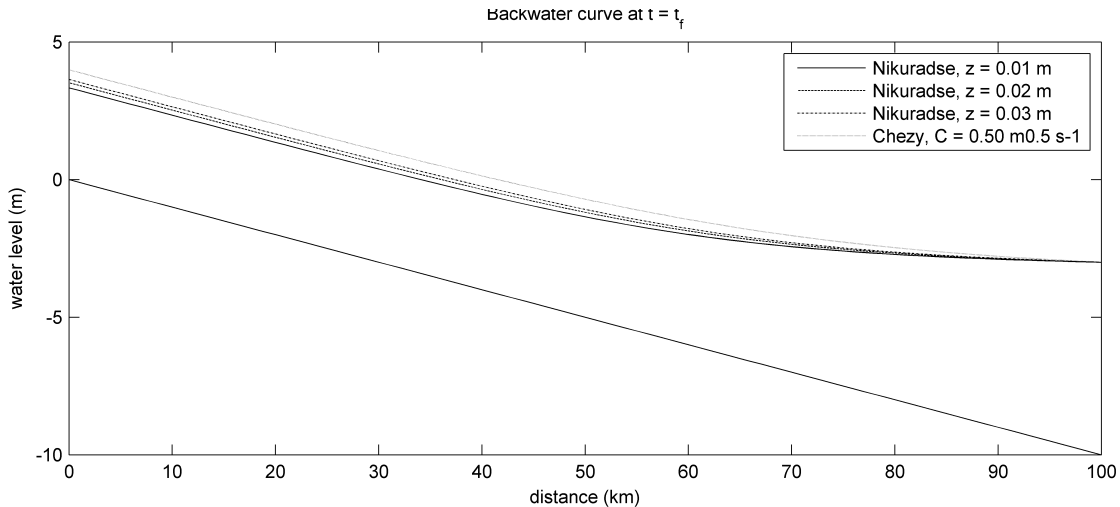


Figure 2.1: Backwater curve for different roughness coefficients at $t = t_f$.

As it can be observed in the Fig. 2.1, the water level in the Chezy-derivated friction case is larger than the water level using the roughness length. At a first glance, some conclusions can be extracted from the Fig. 2.1:

- The bed friction must be larger using the Chezy coefficient since velocities are lower and therefore water level rises.
- The adaptation length scale of the backwater curve seems to be larger for the Chezy's case given the smoother shape of the water surface. This is in contrast to the assumption previously exposed.

2.3 Minimization and Maximization of Backwater Curves

Try to minimize and maximize the backwater curves.

It is understood by minimizing and maximizing a backwater curve the fact of making it longer or shorter in terms of length. There are several factors that can influence the shape of the curves.

2.3.1 Fixed water level at the mouth of the river

Imagine that downstream the river reach presented in the previous figure there is i.e. a lake. The water level at the entrance of the basin would be then supposed to be constant. In case the water level rose at the lake, the backwater curve would require a much larger adaptation length, in other words, the influence of the lake (and its new water level) would be propagated further upstream.

On the contrary, if the water level were decreased, backwater curve would be shortened. This outcomes can be observed in the Fig. 2.2, where different boundary conditions regarding the water level downstream have been imposed.

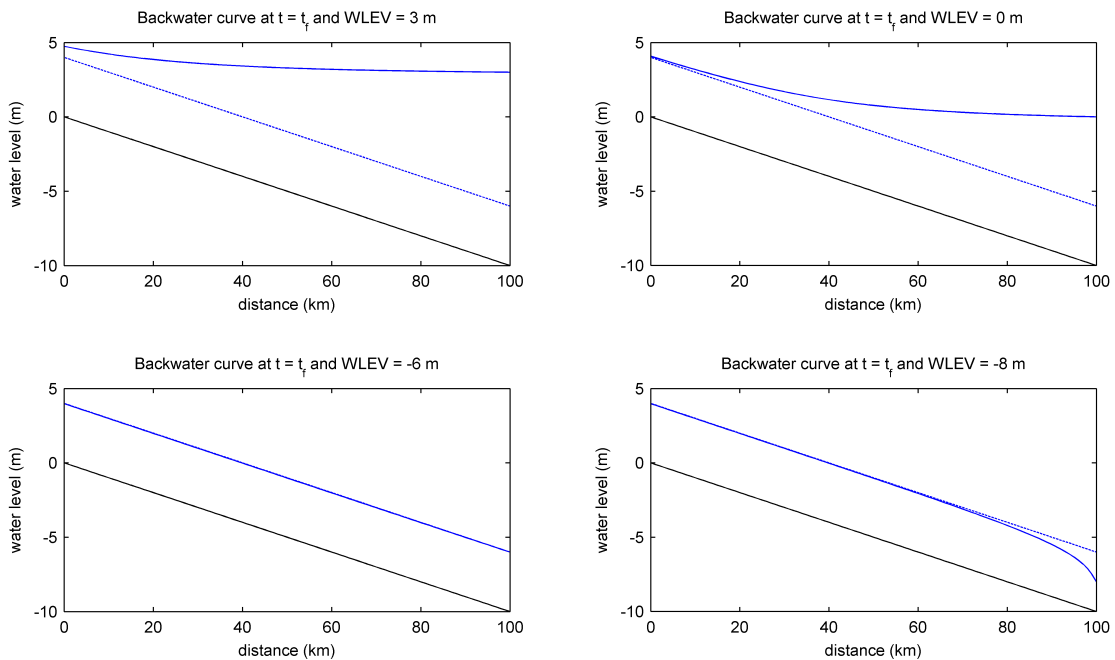


Figure 2.2: Backwater curve for different water levels at the mouth at $t = t_f$.

2.3.2 Roughness

As it has been demonstrated in the section 2.2, varying the friction magnitude of the river bed will result in different water levels and thus a maximization or minimization of the corresponding backwater curve. It is expected that a larger roughness (smaller Chezy coefficient) will lead to a larger adaptation length and therefore maximize the backwater curve Fig. 2.3 shows the different backwater curves formed as a result of different roughness coefficient values.

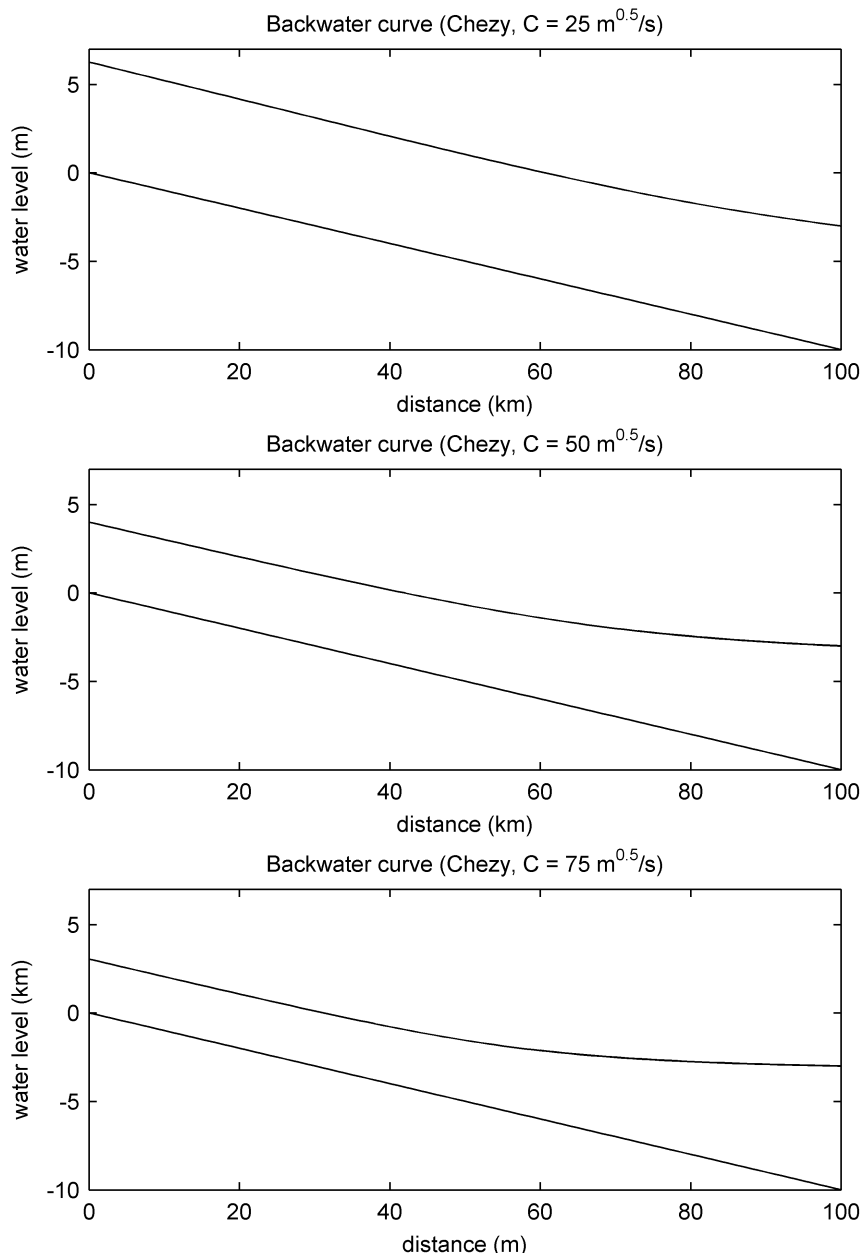


Figure 2.3: Increasing water levels (maximized backwater curves) for larger roughness values (lower Chezy coefficient).

2.3.3 Discharge upstream

In the same manner as seen above, a backwater curve will be maximized if the discharge upstream is larger (maintaining the water level constraint downstream). On the contrary, a lower discharge would therefore reduce the water level over the river reach and minimize the amplitude of the backwater curve. From Fig. 2.4, for a given roughness ($C = 50 \text{ m}^{0.5}/\text{s}$) the predicted effects are shown.

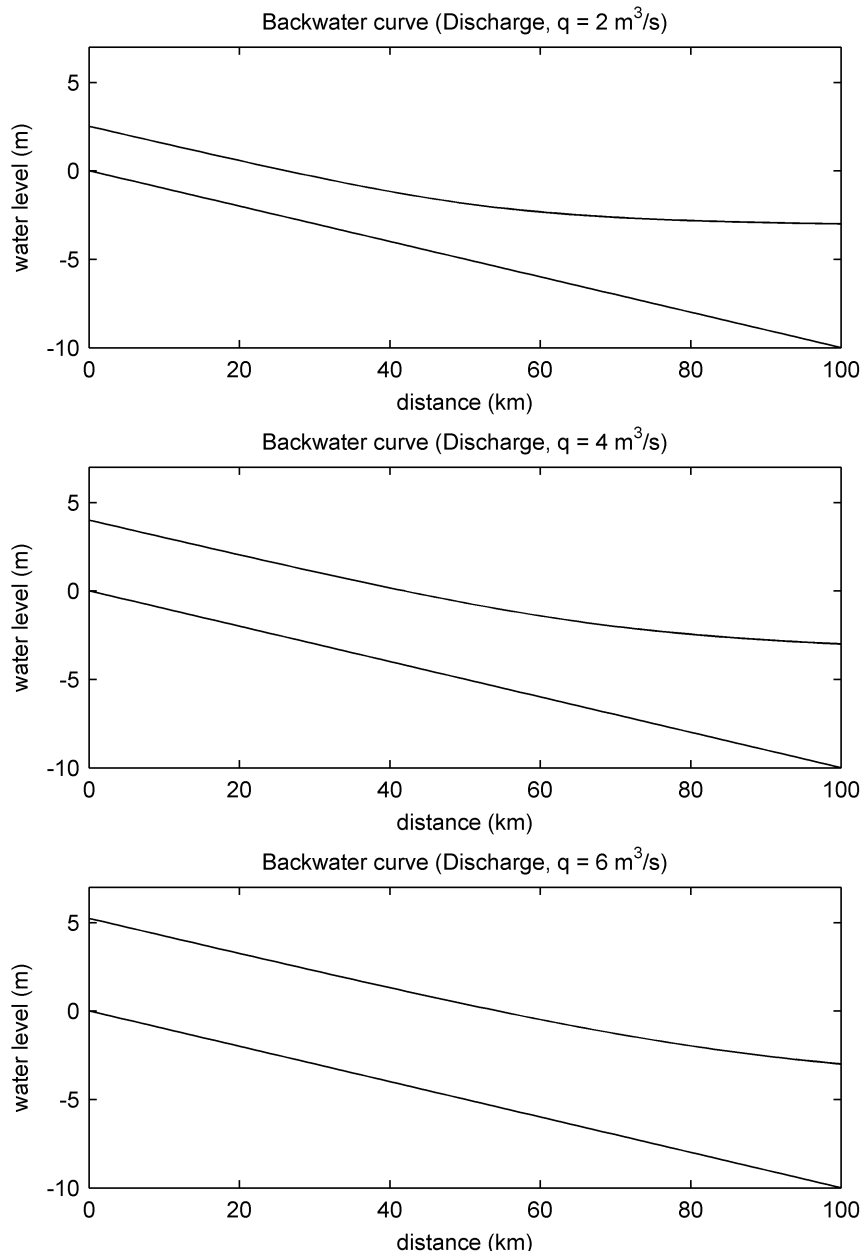


Figure 2.4: Increasing water levels (maximized backwater curves) for larger discharges q upstream.

2.4 Horizontal Adaptation Length Scale

Try to get a feeling for the horizontal adaptation length scale of the backwater curves in relation to the length of your model.

In terms of sediment transport, the adaptation length $L_{1/2}$, and also adaptation time $T_{1/2}$ are constant for uniform flow. They are defined as the interval (both in length and in time) required for the mean actual concentration to approach the mean equilibrium

concentration. The adaptation length represents the length scale and the adaptation time represents the time scale (Ribberink, 1986).

However, the concept of adaptation length (applied to hydraulics) was also introduced by Bresse (1860). The adaptation length can be found using the equation (2.3) and the subindex $1/2$ denotes that this length is equal to the distance between the origin of the backwater curve and the location at which the (vertical) amplitude of the curve has exactly decayed one half the total amplitude.

$$L_{1/2} = 0.24 \frac{h_e}{i_b} \left(\frac{h_0}{h_e} \right)^{4/3} \quad (2.3)$$

where

h_e = equilibrium depth (4 m)

h_0 = depth downstream (7 m)

i_b = bottom slope (10^{-4})

Therefore, the adaptation length for the given boundary conditions equals to 20,245 m, which can be largely represented within the length of our model (see Fig. 2.5). In case we took into consideration the modifications used in the section 2.3, the adaptation lengths would vary and, in some cases, the length of the model system would not be sufficiently large to cover the whole backwater curve (see Fig. 2.1).

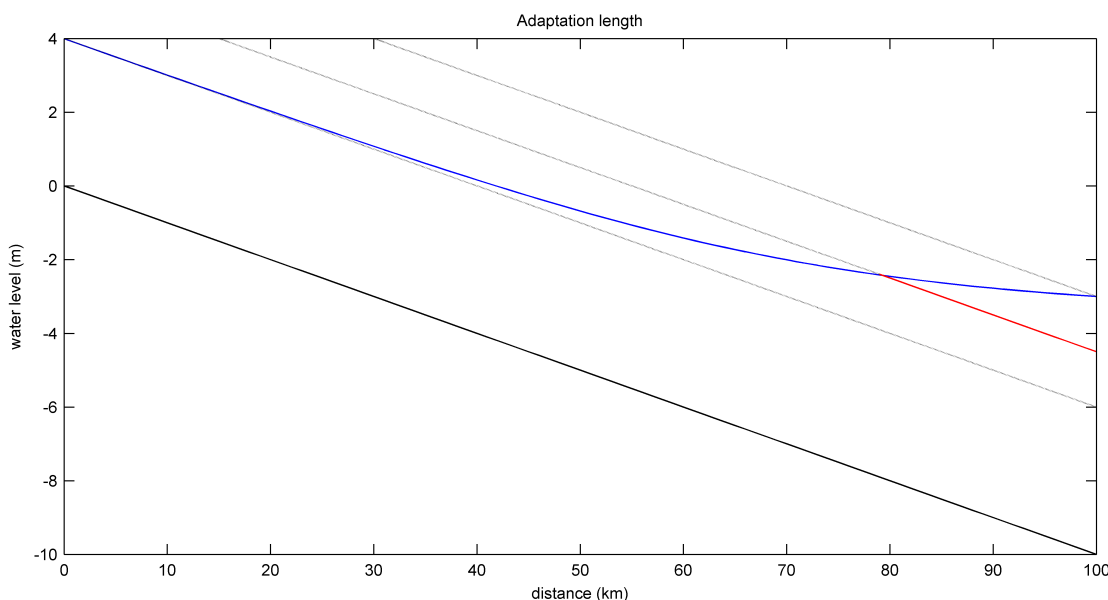


Figure 2.5: Adaptation length for the original backwater curve ($C = 50 \text{ m}^{0.5}/\text{s}$, $q = 4 \text{ m}/\text{s}$, $b = 500 \text{ m}$, $i_b = 10^{-4}$ and $h_0 = 7 \text{ m}$).

2.5 Assessment of Different Combinations of Boundary Conditions

Impose different combinations of boundaries and assess the effect on the final solution, and on the spin-up time required to get that solution. Assess at least the following combinations:

2.5.1 Two discharge boundaries

BOUND SIDE WEST BTYPE DISCH CON 4.
 BOUND SIDE EAST BTYPE DISCH CON 4.

For the present assessment, the boundary conditions presented in the Table 2.1 have been applied. In this particular case, it has been pursued to determine whether the spin-up time would be larger or shorter in case the water levels were different at both boundaries (assuming the same discharge at both sides, otherwise the computation would not be possible since water would be flushed away from the system). Furthermore, besides the construction of the backwater curves, several control points, equally spaced along the river, have been placed in order to measure the water level oscillation and thus calculate the spin-up time.

Table 2.1: Different combinations regarding the two velocity boundaries case.

	Test 1		Test 2	
	Discharge q [m ³ /s]	Water depth [m]	Discharge q [m ³ /s]	Water depth [m]
Upstream	4	4	4	4
Downstream	4	4	4	7

Below are shown the different water levels at the control points for both *test 1* and *test 2*.

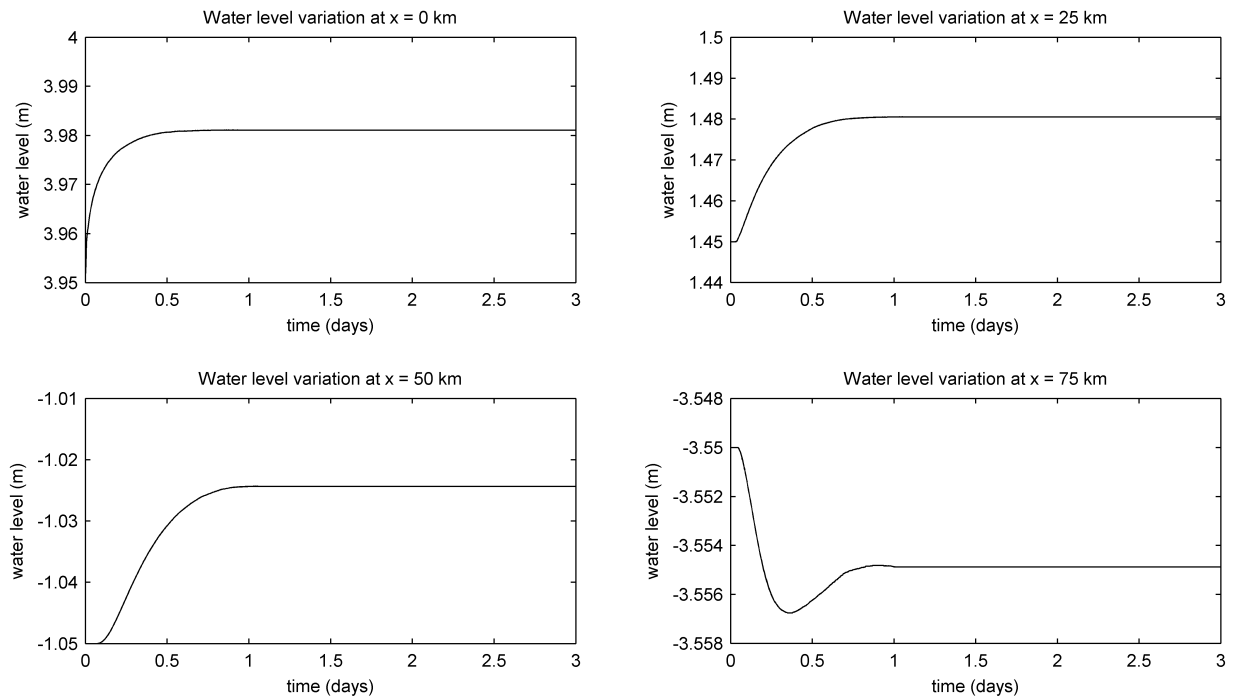


Figure 2.6: Test 1 water level variations at the different control points.

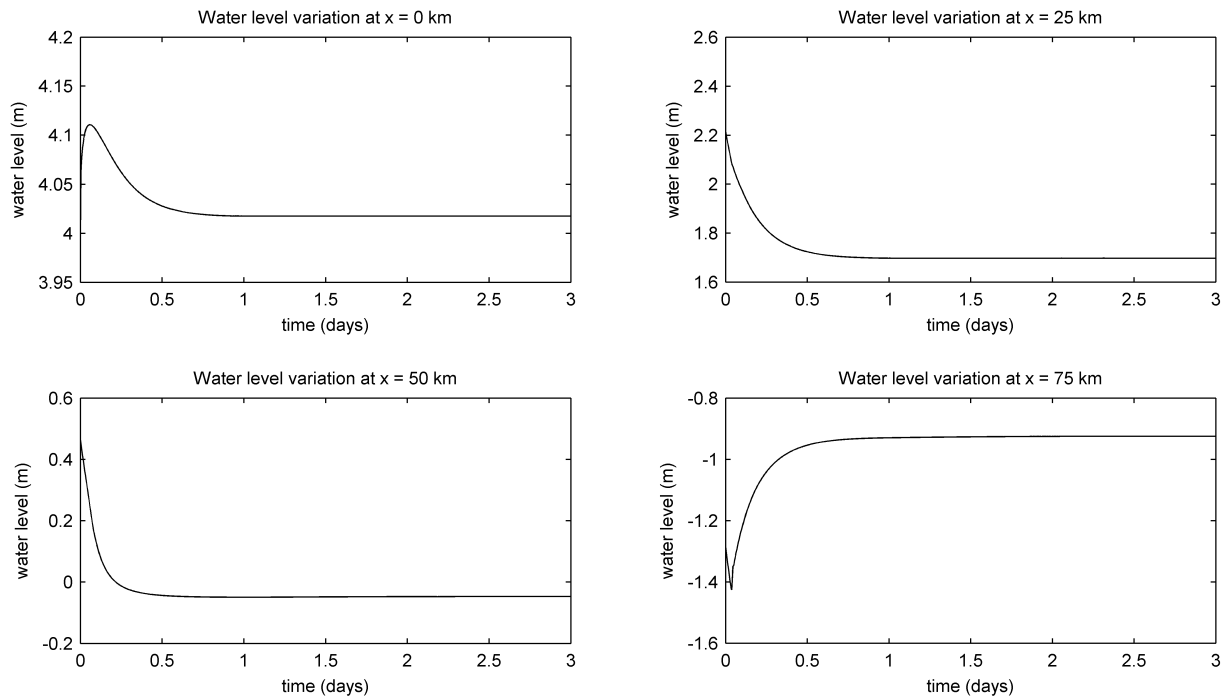


Figure 2.7: Test 2 water level variations at the different control points.

As it can be seen in the figures 2.6. and 2.7., the larger the difference in water level between both sides, the faster the water surface catches up with its equilibrium value (water has to readjust in more or less the same time regardless the difference and therefore the peak between both figures is displaced along the time line). It has been stated that this readjusting time is the same and can be proved by measuring the duration of the readjustment on both cases. It takes the system approximately one day to develop its equilibrium backwater curve. There may exist differences however, as it can be seen in the 50 km control point time series, where in the second test the water surface is stabilized faster than in the first one. This effect may be founded on the fact that the original and final water profile is much more different than the one in the first test.

2.5.2 Two velocity boundaries with different initial water levels

The velocity will be estimated using the depth averaged velocity formula (2.4):

$$U = C\sqrt{Ri_b} = \frac{1}{\sqrt{c_f}}\sqrt{gRi_w} \quad (2.4)$$

The value of the velocity for the original set of conditions is equal to 1 m/s.

Table 2.2: Different combinations regarding the two velocity boundaries case.

	Test 1		Test 2	
	Velocity U [m/s]	Water depth [m]	Velocity U [m/s]	Water depth [m]
Upstream	1	4	1	4
Downstream	1	4	0.5	7

Therefore, the boundary conditions implemented in Swash will vary depending on the simulation test.

For the *test 1*, the following will be introduced:

```
BOUND SIDE WEST BTYPE VEL CON 1.  
BOUND SIDE EAST BTYPE VEL CON 1.
```

whereas for the *test 2*:

```
BOUND SIDE WEST BTYPE VEL CON 1.  
BOUND SIDE EAST BTYPE VEL CON 1.
```

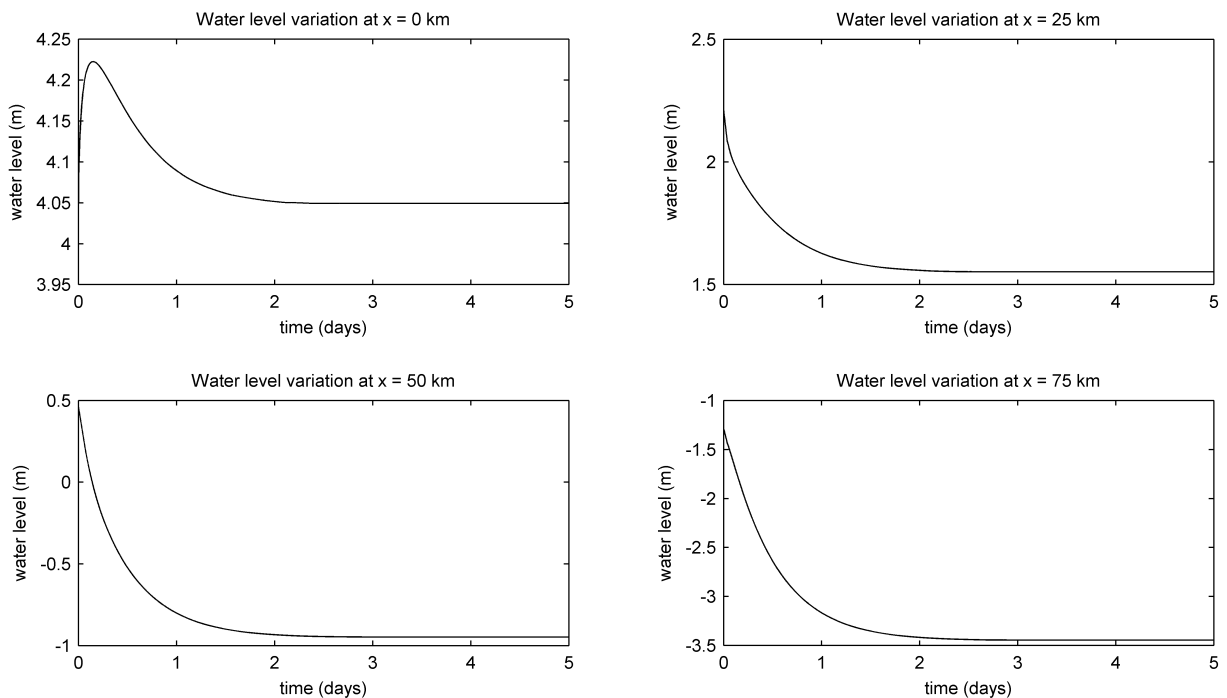


Figure 2.8: Test 1 water level variations at the different control points.

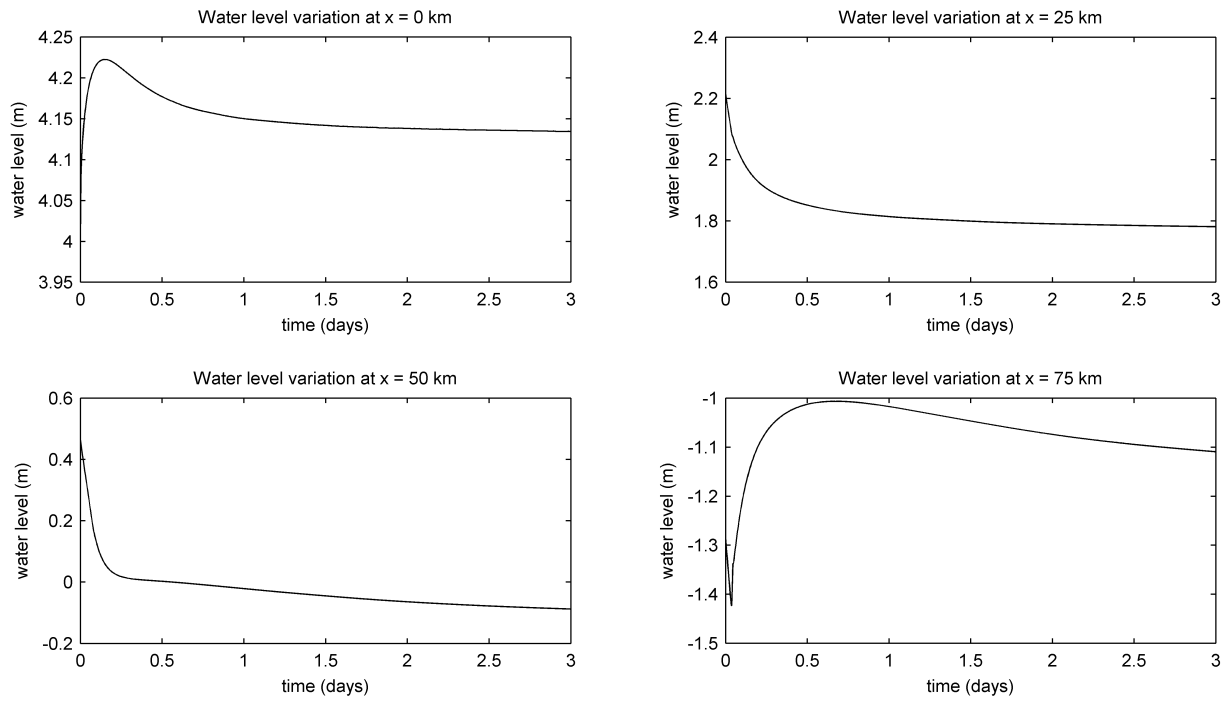


Figure 2.9: Test 2 water level variations at the different control points.

2.5.3 Upstream a discharge and downstream a water level condition

```
BOUND SIDE WEST BTYPE DISCH CON 4.
BOUND SIDE EAST BTYPE WLEV CON -3.
```

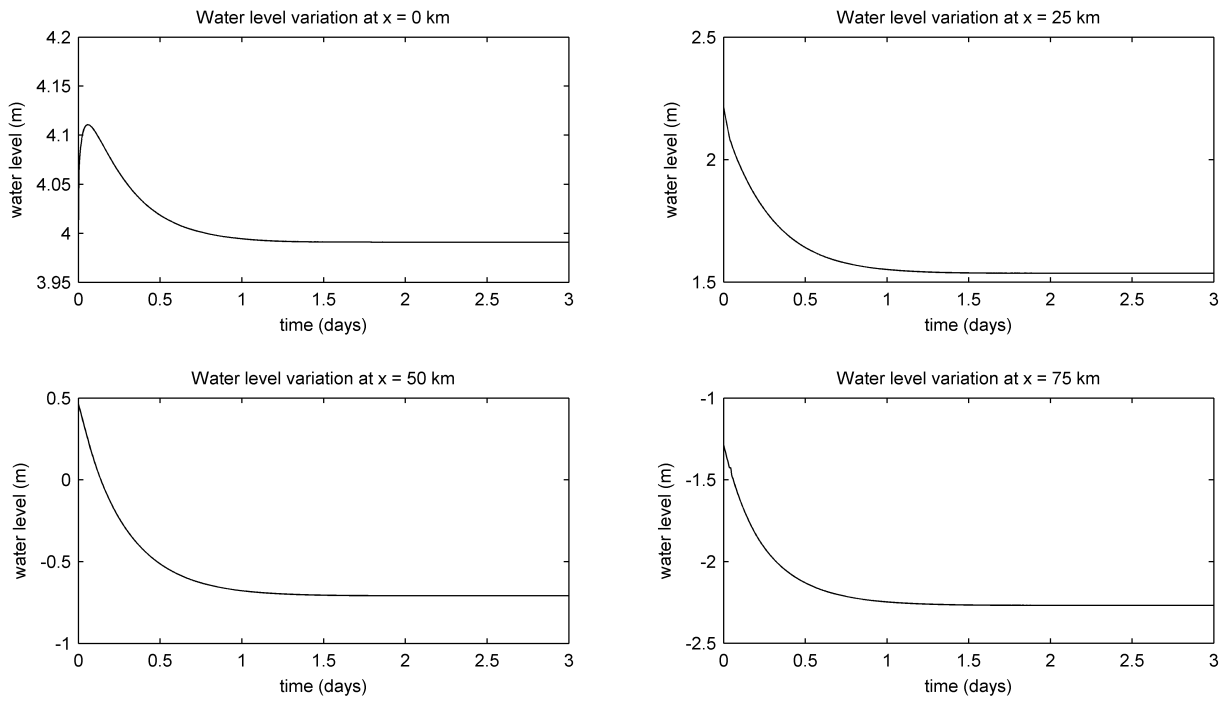


Figure 2.10: Water level variations at the different control points.

2.5.4 Explanation of findings

Bringing it all together, there are some aspects that can be discussed. The spin-up time varies from approximately one to one and a half days. It would not be precise to admit that the spin-up time does not depend on the (here analyzed) set of boundary conditions although the variance is not so large. Particles upstream will experience a rather small vertical rise/fall of the water level whereas downstream the amplitude of the vertical shifting will be significantly larger.

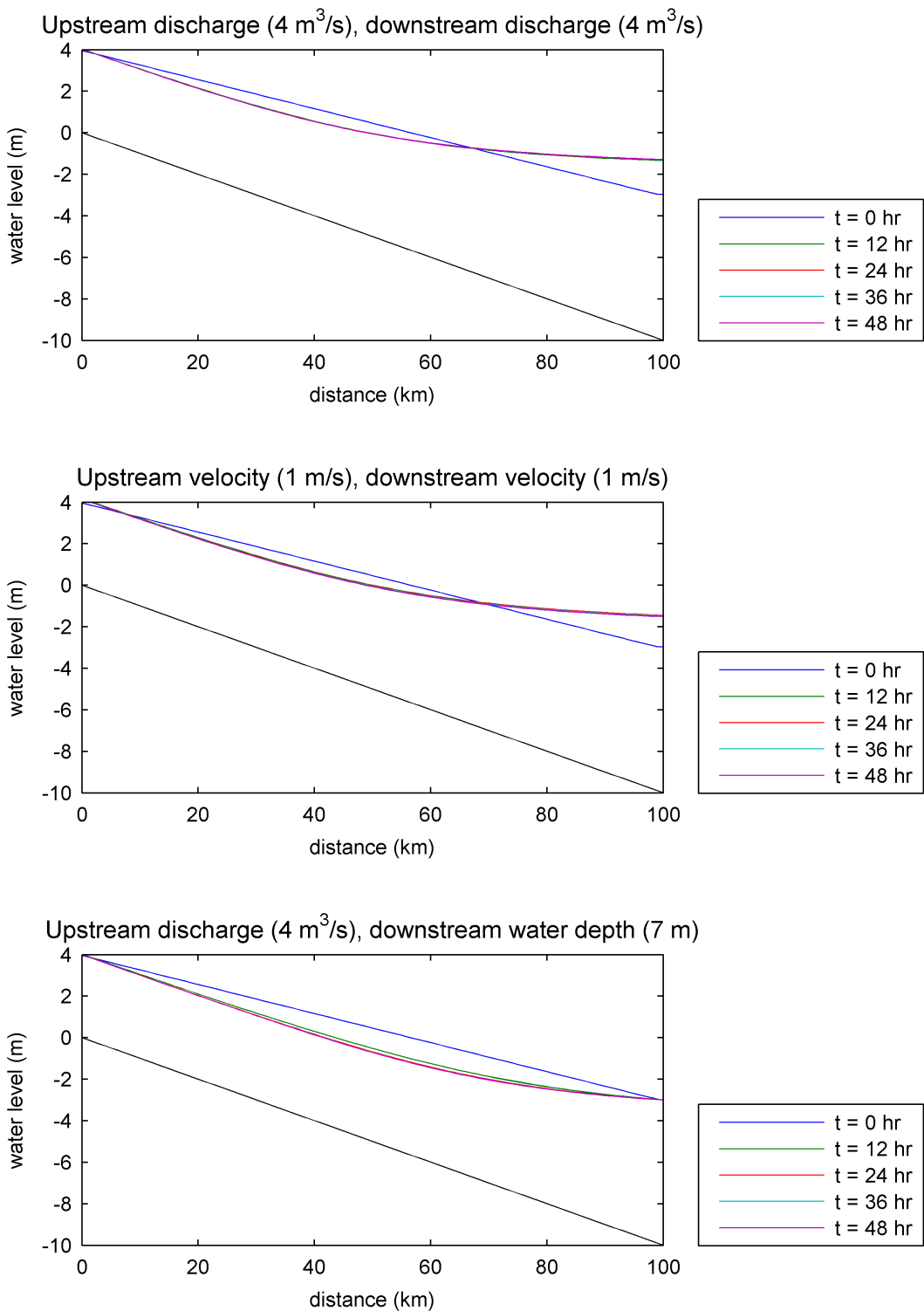


Figure 2.11: Backwater curves for each of the combinations explained above.

Chapter 3

The Use of Advection Scheme

3.1 Introduction

The three basic balances have to be reviewed prior to the assessment of the advection schemes that rule the model. These are conservation of mass, momentum and energy head.

Mass conservation:

$$u_i h_i = u_{i+1} h_{i+1} \quad \forall i = 1, \dots, n \quad (3.1)$$

Momentum conservation:

$$q_i u_i + \frac{1}{2} g h_i^2 = q_{i+1} u_{i+1} + \frac{1}{2} g h_{i+1}^2 \quad \forall i = 1, \dots, n \quad (3.2)$$

Energy head conservation:

$$\frac{1}{2} u_i^2 + g \zeta_i = \frac{1}{2} u_{i+1}^2 + g \zeta_{i+1} \quad \forall i = 1, \dots, n \quad (3.3)$$

where n is the number of grid points.

A staggered grid arrangement is employed (see Fig.3.1), in which the velocity component u is located at the center of the cell faces ($\dots, i-1, i, i+1, \dots$). The water depth h and water level ζ are however interpolated to the centers of the grid cell ($\dots, i-1/2, i+1/2, \dots$) although were initially given d at the grid points ($\dots, i-1, i, i+1, \dots$).

Therefore, care must be taken when the balances are calculated since velocities and water levels and depths are outputted at different points. A simple interpolation can be implemented in order to calculate the velocities at the centers of the grid cells.

This has been tested although no large differences have been found. Thereafter, even though not being strictly correct, in the following the different balances calculations will be carried out irrespective of the mentioned and little artifacts are expected to occur at the water level computations around the obstacles.

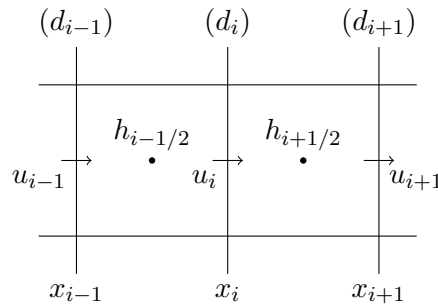


Figure 3.1: Arrangement of the unknowns in a staggered grid.

3.2 Advection Scheme Assessment

Test the advection scheme in Swash with the saw-tooth profile. Use a stepwise increase of the depth, and a stepwise decrease of the depth. Which basic balances hold at the steps? Check this by calculating the basic balances by hand. Optionally compare also runs with a smoothly varying bottom profile.

In order to visualize the effect of the steps in a clear way, the set-up will be kept constant throughout the course of this study. This can be achieved by making a short model (1 km length) and choosing a low friction coefficient. Nevertheless, assuring small flow velocities will contribute in guaranteeing a setup in which the overall flow does not change much.

The saw-tooth profile suggested in order to test the advection scheme has been laid out in such a way that sudden expansion and contraction can be assessed. Both sudden expansion and sudden contraction results from the computation can be found in the Figs. 3.2 and 3.3. Three different stepwise heights have been considered for the present study. Additionally, a situation with a flat bottom has been plotted so that the extreme case (no stepwise at all) is shown. The heights of such steps are 10 m, 6 m and 3 m (emerging from a bottom level of 10 m below the reference level). The water level has been set at 1 m above the reference level (initial water block). Moreover, a water level constrain at the east side forces the water level to be equal to 1 m and 4 m²/s are discharged at the west side. Regarding the dissipation by friction, a Chezy coefficient equal to 50 m^{0.5}/s has been chosen.

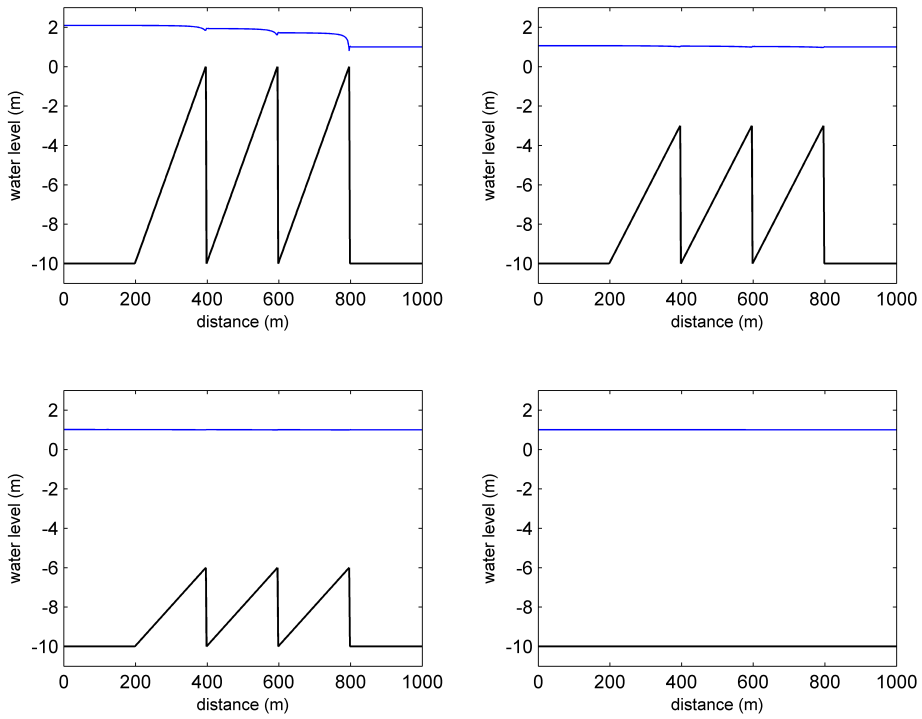


Figure 3.2: Water level along a saw-tooth profile for different stepwise designs and sudden expansion disposition.

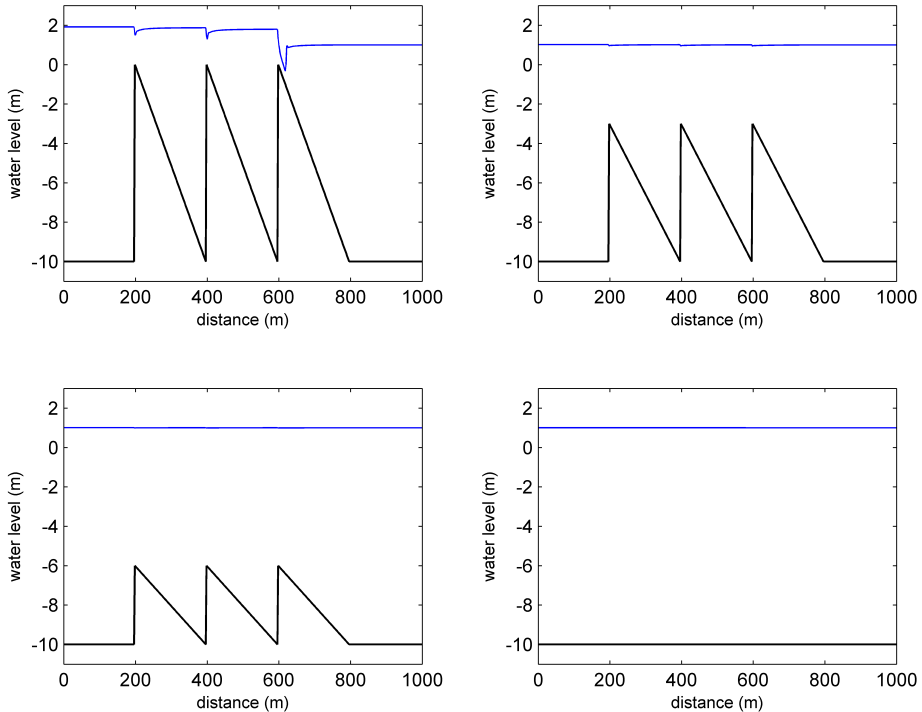


Figure 3.3: Water level along a saw-tooth profile for different stepwise designs and sudden contraction disposition.

It should be noted that the discharge at the west boundary is rather large and will yield to high velocity gradients ($u = 4\text{m/s}$). However, for this part of the analysis, local effects will be visually enhanced.

In order to assess whether a balance holds or not, involved variables of each balance are requested to the model (u , q , h and ζ). The equations (3.1), (3.2) and (3.3) are computed at each grid point yielding the following figures for the sudden expansion case (3.4, 3.5 and 3.6).

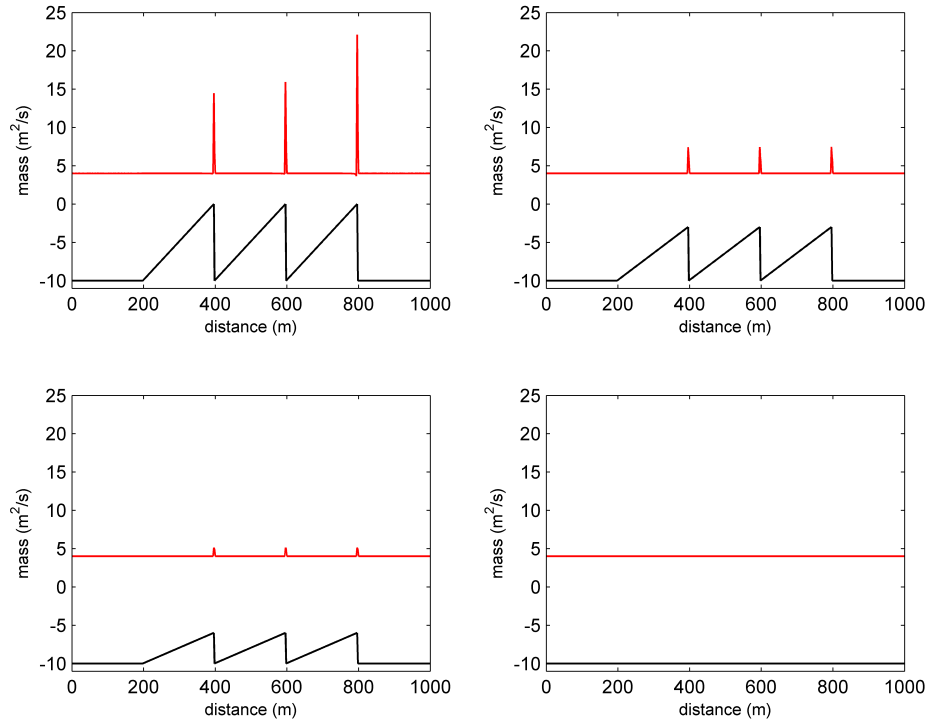
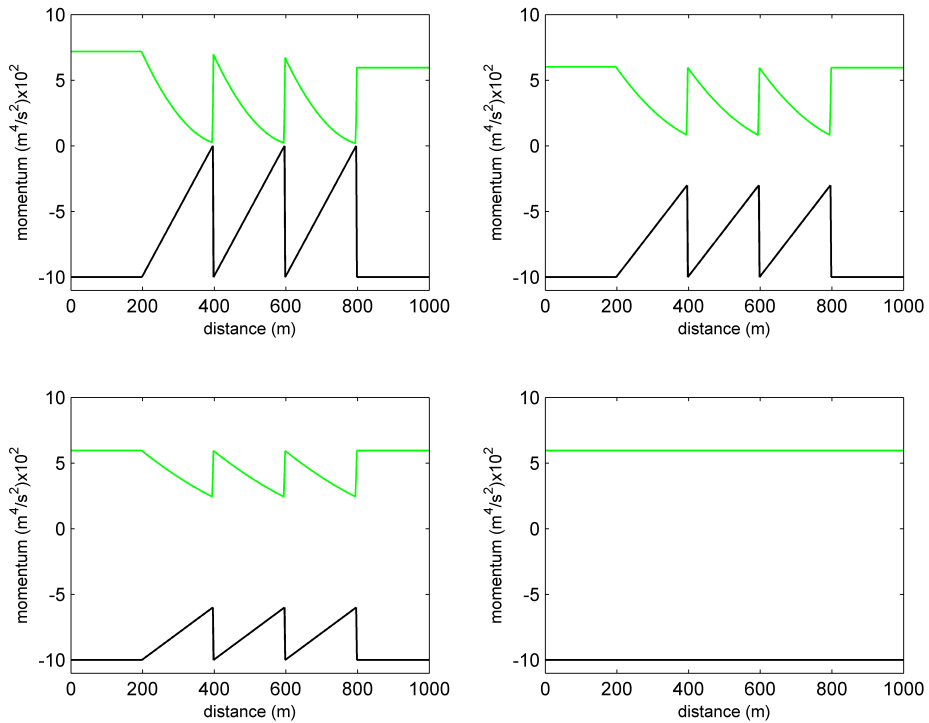
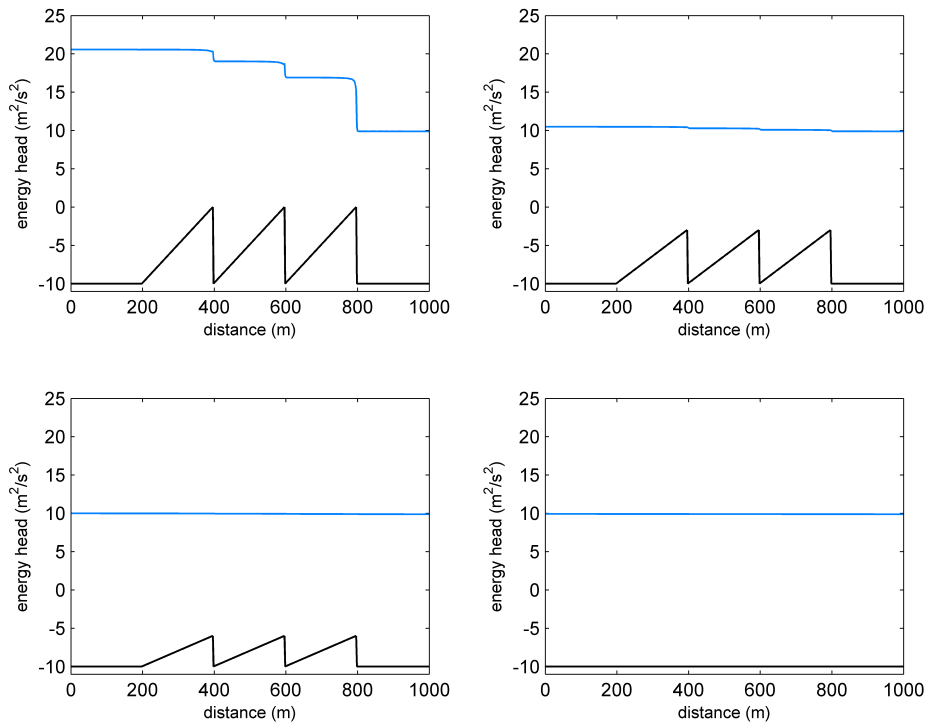
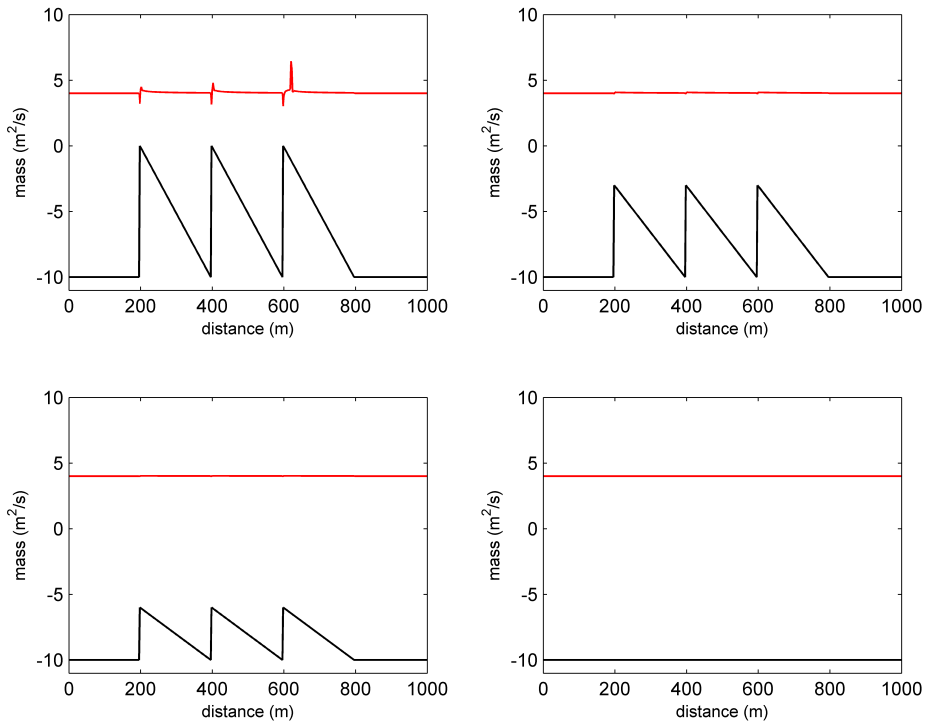
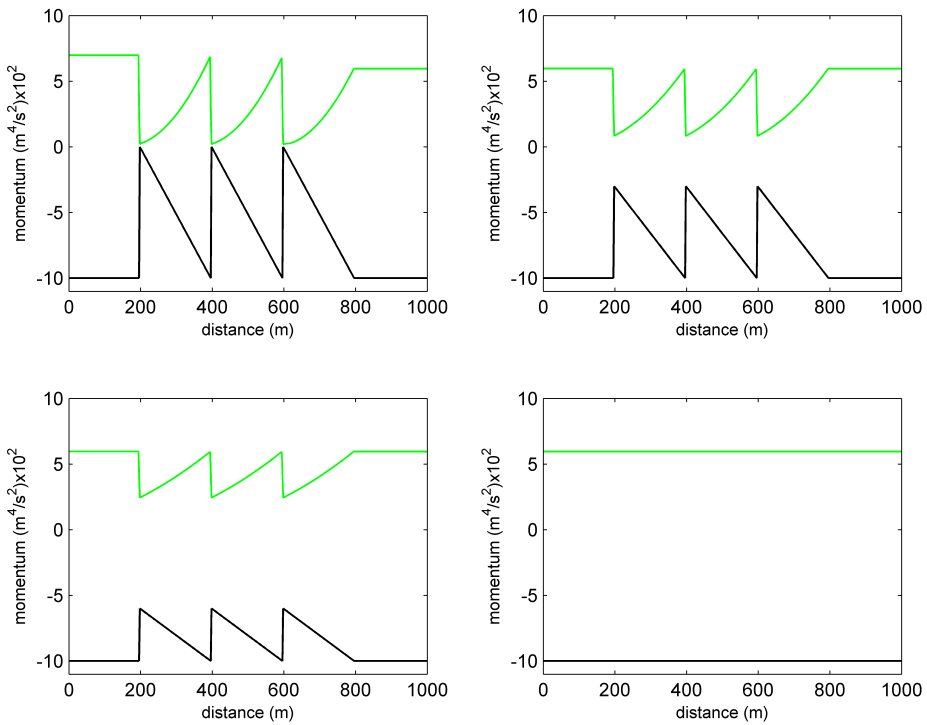


Figure 3.4: Mass balance (sudden expansion case).

**Figure 3.5:** Momentum balance (sudden expansion case).**Figure 3.6:** Energy head balance (sudden expansion case).

Similarly, the three balances have been computed for the sudden contraction case leading to the following results (Figs. 3.7, 3.8 and 3.9):

**Figure 3.7:** Mass balance (sudden contraction case).**Figure 3.8:** Momentum balance (sudden contraction case).

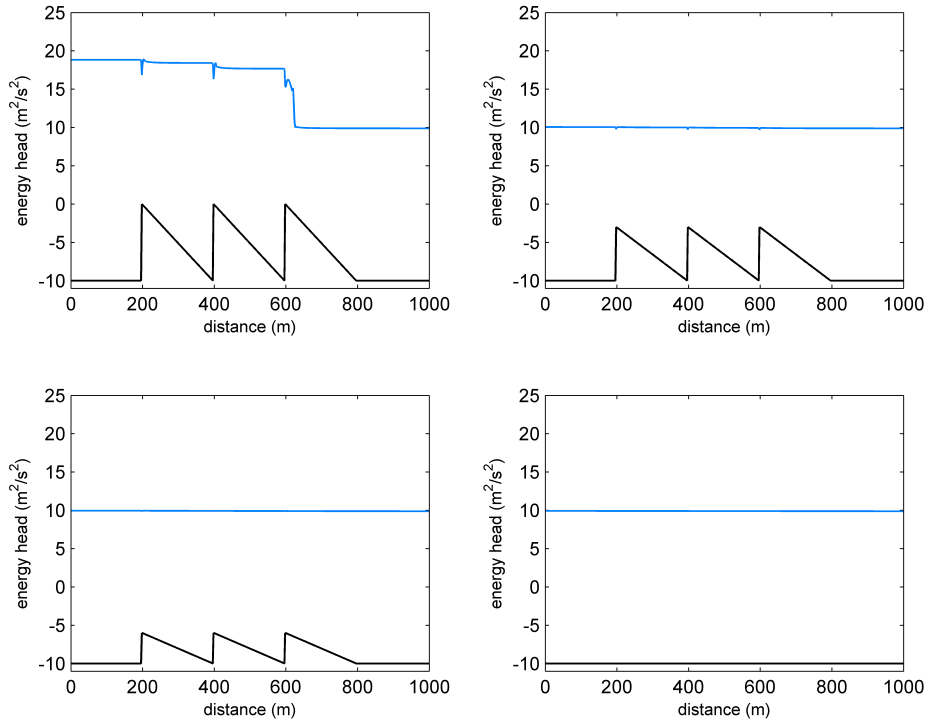


Figure 3.9: Energy head balance (sudden contraction case).

Differences between both step configurations can be seen from the figures (3.4, 3.5, 3.6 and 3.7, 3.8, 3.9). The mass balance does not hold in none of the two considered situations for a 10 m depth stepwise. However, conservation of the balance is achieved for the sudden contraction case (for stepwise depth equal or lower than 6 m). On the other hand, sudden expansion is more restrictive in terms of mass conservation. This is due to the rather large velocities that take place at each of the edges of the steps, which lead to large values of "mass" for slowly varying water depths.

The momentum balance does not hold as long as irregularities on the bottom profile are present. This statement remains truthful regardless the amplitude of the step. This variability is due to the square of the water depth in the second term of the balance (see equation 3.2) since the product of the discharge and velocity will be constant over the whole length of the system.

Lastly, the energy head balance is analyzed. It can be seen that the energy is significantly large when the depth of the stepwise is relatively high. Therefore, the energy head balance does not hold for such cases where the step is considerable, yielding to a local rise of the water level and, thus, the energy head. The rest of the situations (3 and 6 m stepwise depth) display a fairly conservation of the energy head.

The comparison has also been carried out taking into account a smoothly varying bottom profile. The bottom input file has been generated using the following Matlab script:

```

file = fopen('flat_smooth.txt','wt');
for i = 1:100
    fprintf(file,'10.000 \textbackslash n')
end
x = linspace(1,300,300);
y = 10+6*sin(x*5*pi()/300);
for i = 1:length(y)
    fprintf(file, '\%.3f \textbackslash n',y(i));
end
for i = 1:101
    fprintf(file,'10.000 \textbackslash n');
end

```

The model has been run for different amplitudes (stepwise heights) and basic balances are similarly represented in the figures 3.10, 3.11, 3.12 and 3.13.

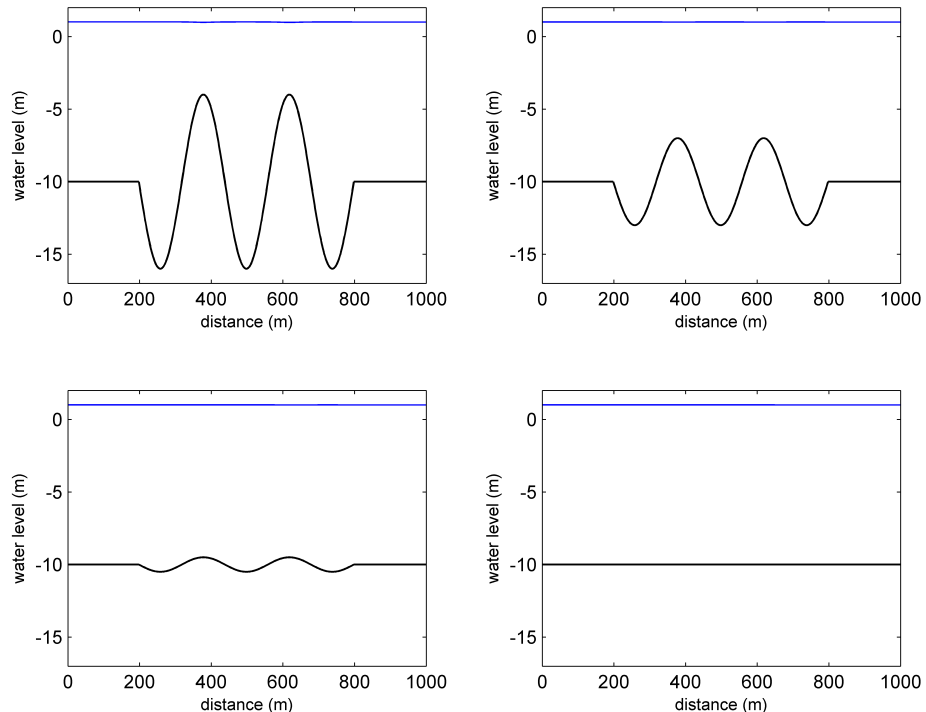


Figure 3.10: Water level along a smoothly varying bottom profile for different amplitudes.

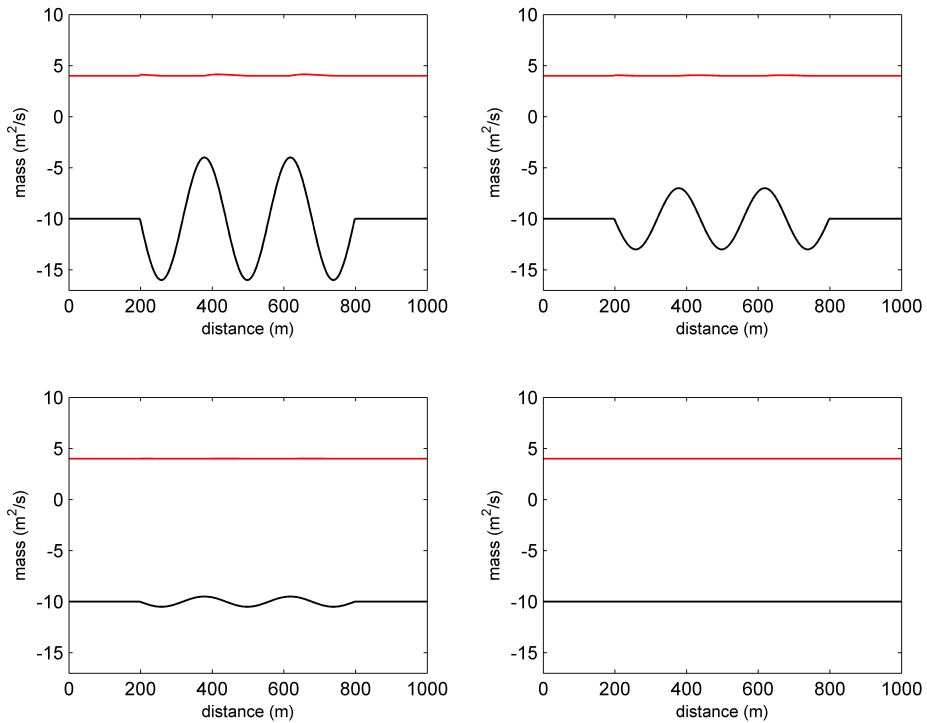


Figure 3.11: Mass balance (smoothly varying bottom profile).

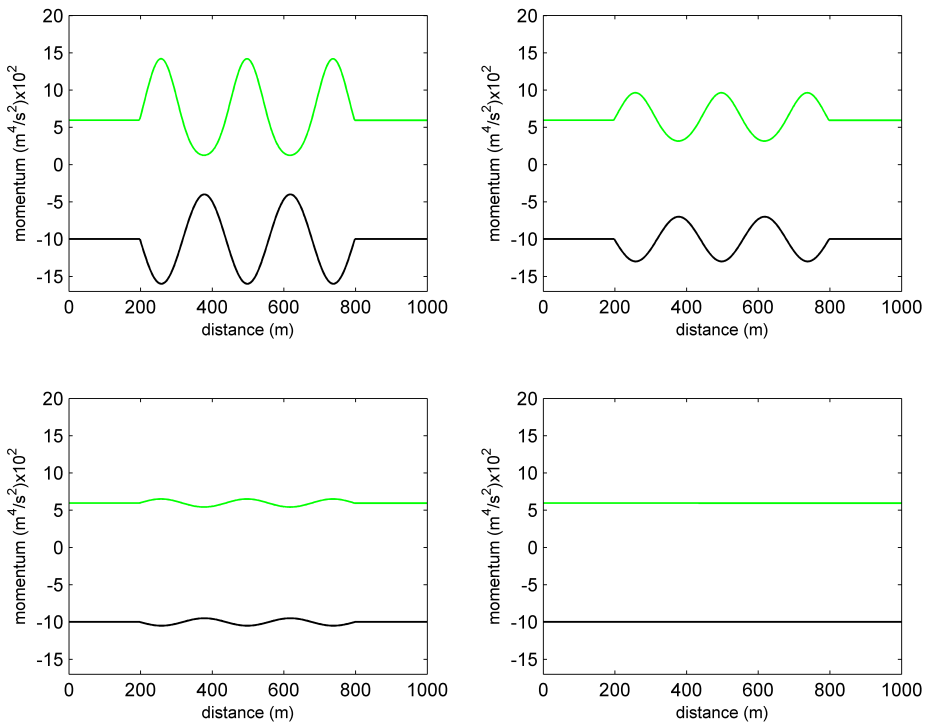


Figure 3.12: Momentum balance (smoothly varying bottom profile).

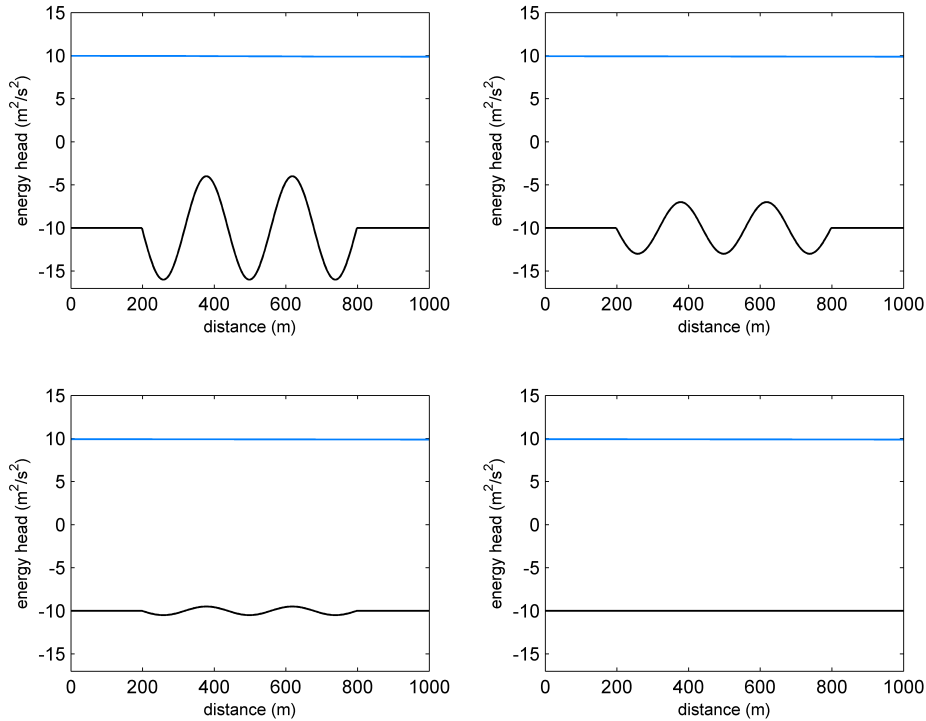


Figure 3.13: Energy head balance (smoothly varying bottom profile).

Fig. 3.10 shows the water level for different amplitudes of the varying profile. It can be noted that regardless the depth of the bottom level, the water level remains constant throughout the entire length. This will lead to a constant energy head for all considered situations since, as said before, the energy head depends largely on the water elevation. Therefore, it can be concluded that the energy head balance is conserved. On the contrary, the mass balance does not hold for such a case where the amplitude of the bottom level oscillations is fairly high. In a more markedly way, the momentum exhibits larger differences due to the direct dependence to the square of the wave height.

3.3 Friction and Local Geometry Losses

Compare bottom friction losses to local geometry losses.

This comparison has been realized enabling and disabling bottom friction dissipation. Therefore, by doing so, losses will be associated to either bottom friction or local geometry effects. Different Chezy values have been implemented and the evolution of the water level and other properties is assessed.

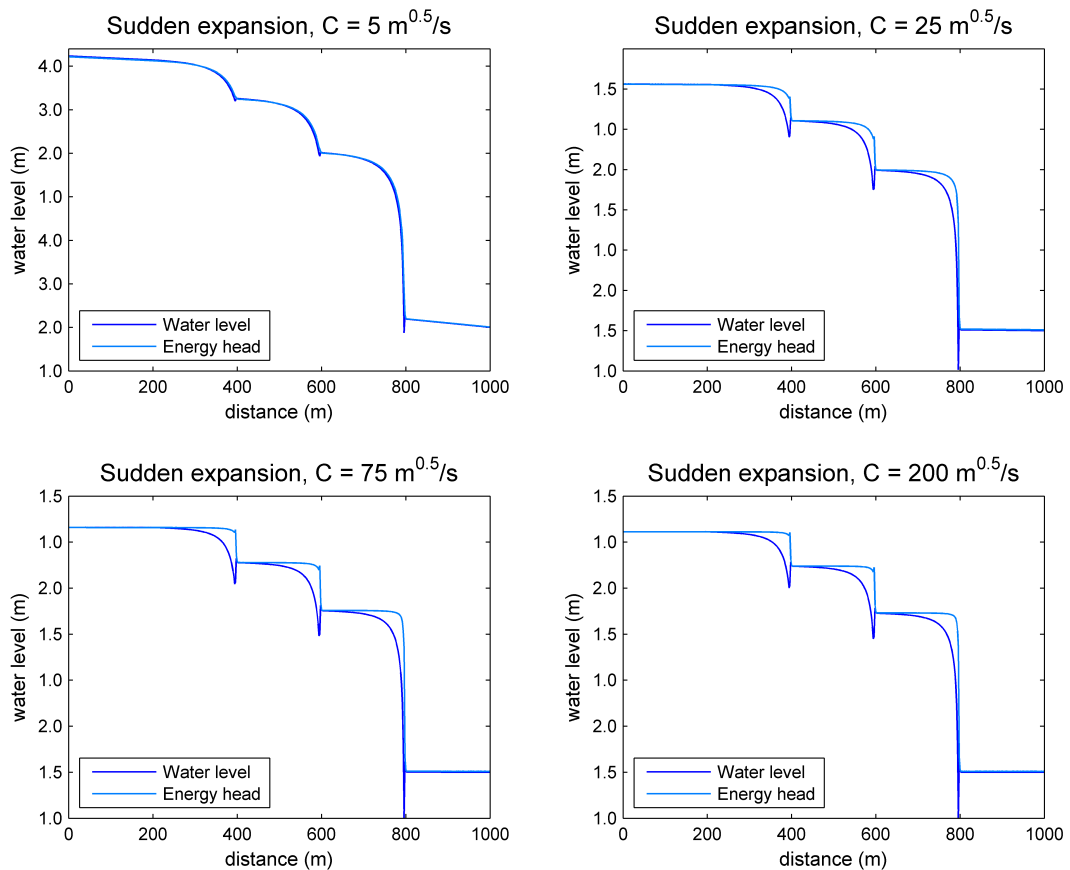


Figure 3.14: Water levels (at last time step) and energy head levels (out of scale) for various bed roughnesses (sudden expansion case with a stepwise of 10 m).

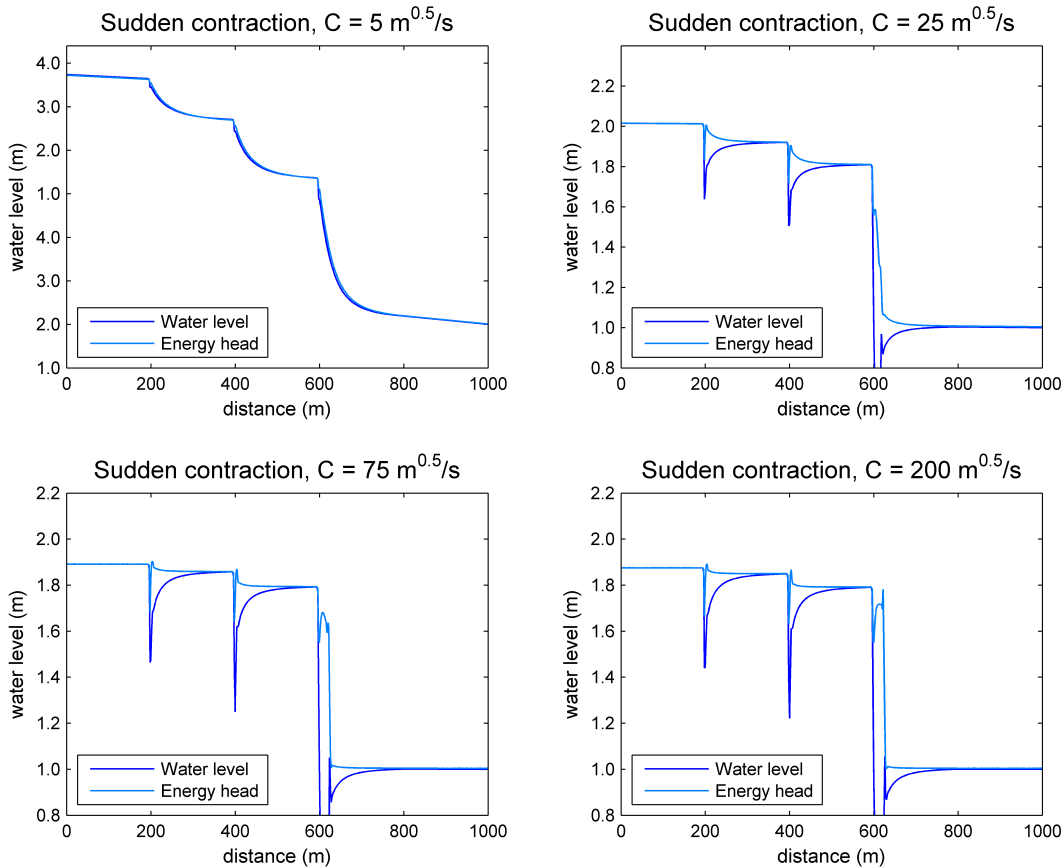


Figure 3.15: Water levels (at last time step) and energy head levels (out of scale) for various bed roughnesses (sudden contraction case with a stepwise of 10 m).

As it can be seen from the previous figures (3.14 and 3.15), the lower the friction dissipation (larger values of Chezy coefficient) the less energy loss. It can be pictured by measuring the vertical difference the energy level upstream (before the obstacles) and the energy level downstream the steps. Therefore, energy losses due to local geometry effects occur close to the edges of the obstacles, where the velocity gradients largely vary over a relatively short length.

The effect of bottom friction is based on the stresses that develop along the surface of the bed. Larger roughness imply larger energy losses due to bottom friction. The influence of the bottom friction can be seen as the area limited by the water level and the (non-scaled) energy head level and, therefore, the larger the friction coefficient the larger the area.

However, we already observed that smoothing the bed leads to larger spin-up times. The ideal case of a completely smooth bottom would result in an infinite spin-up time. Thereafter, there is another way to reduce the influence due to bottom friction. The aforementioned stresses produce energy dissipation (induced turbulence) and are proportional to the square of the velocity. In case flow velocities were smaller, it would be possible to reduce bottom friction regardless of the spin-up time.

3.4 Different Advection Schemes for Momentum

Assess the effect of choosing a different advection scheme for momentum (DISCRET UPW MOM and DISCRET UPW HEAD).

For convection-dominated flows it is possible that wiggles in the solution arise. In that case upwind discretization may be necessary. At this moment, three types of upwind schemes are implemented:

- the standard first order upwind scheme
- higher order upwind schemes obtained with the k-formulation
- TVD schemes with several classes of flux limiters.

Conservation properties become crucial for rapidly varied flows. These properties are often sufficient to get solutions that are acceptable in terms of local energy losses. In flow expansions, the horizontal advective terms in u - and v -momentum equations are approximated such that they are consistent with momentum conservation. In flow contractions, the approximation is such that constant energy head is preserved along a streamline, i.e. the Bernoulli equation.

The discretization employed for u/v (momentum equation) will be first implemented contraction forcing the system to conserve the momentum everywhere. This is achieved by introducing the following command:

DISCRET UPW UMOM MOM

Firsts implementation attempt yielded no results. The time step was re-calculated using Courant number and the discharge reduced to $1 \text{ m}^2/\text{s}$. Eventually, the model produced the outputs applying the upwind discretization for momentum conservation everywhere.

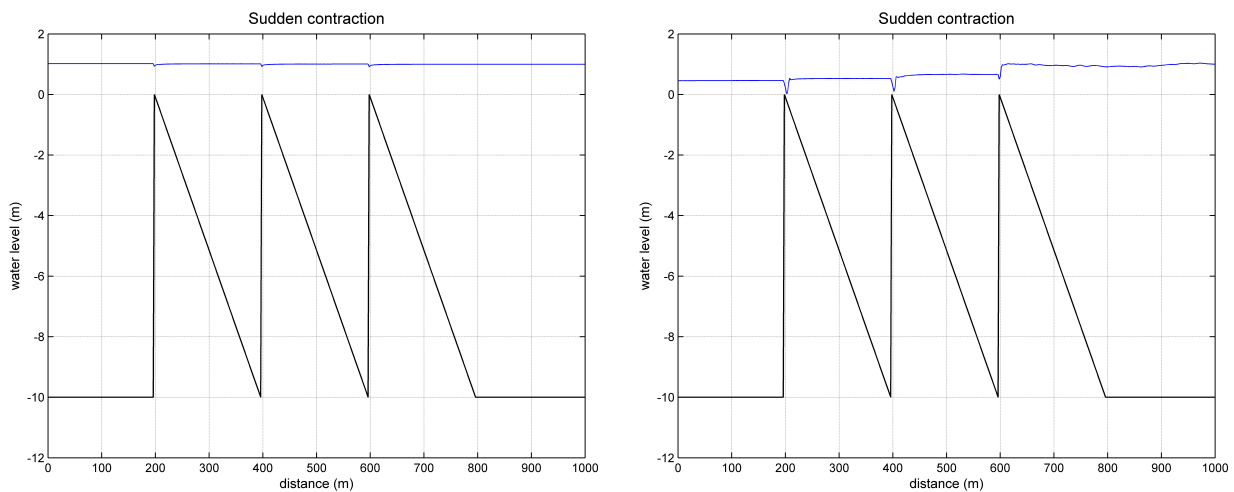


Figure 3.16: (Left) water level using no space discretization and (right) water level for advective terms discretization using a upwind scheme with momentum conservation everywhere.

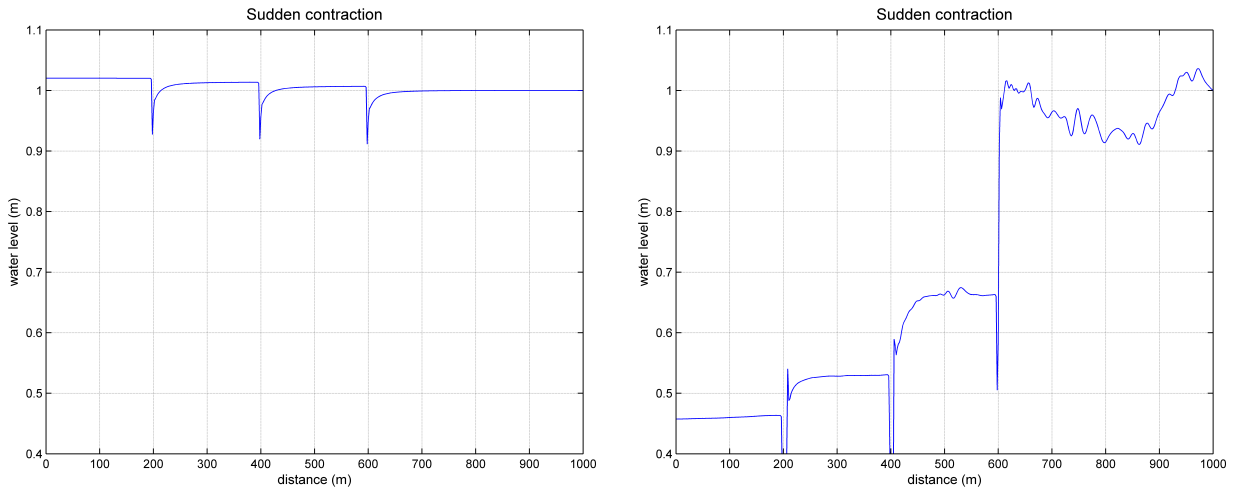


Figure 3.17: (Left) water level using no space discretization and (right) water level for advective terms discretization using a upwind scheme with momentum conservation everywhere.

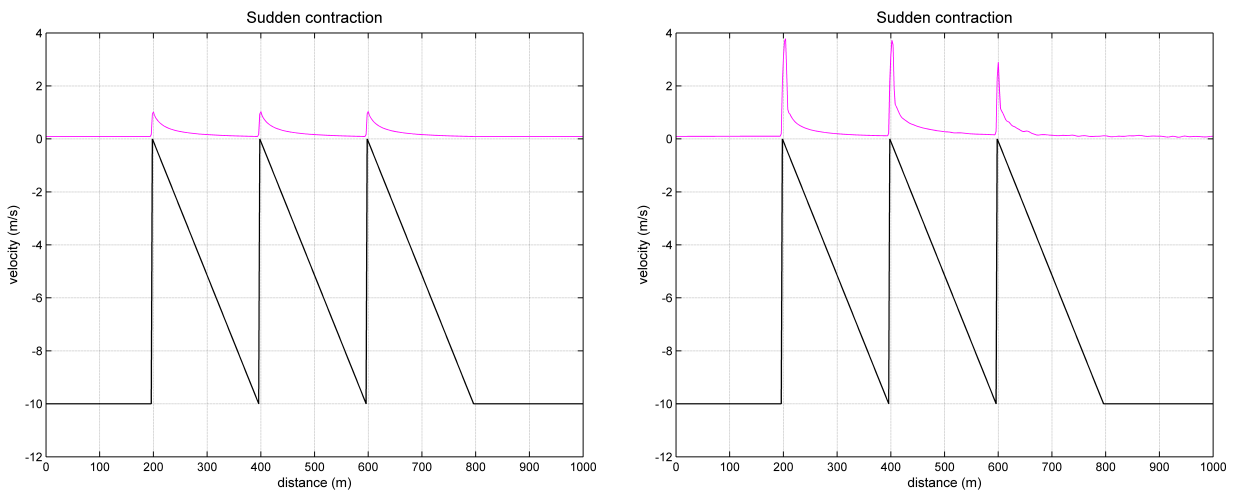


Figure 3.18: (Left) velocities using no space discretization and (right) velocities for advective terms discretization using a upwind scheme with momentum conservation everywhere.

Since the momentum balance is held over the entire length, the water level rises downstream due to the lower value of the flow velocity. Thus, the momentum balance (3.2) is conserved.

Once implemented such an option, the upwind scheme will be re-applied but this time conserving the energy head everywhere (the discretization is employed onto the horizontal advective terms).

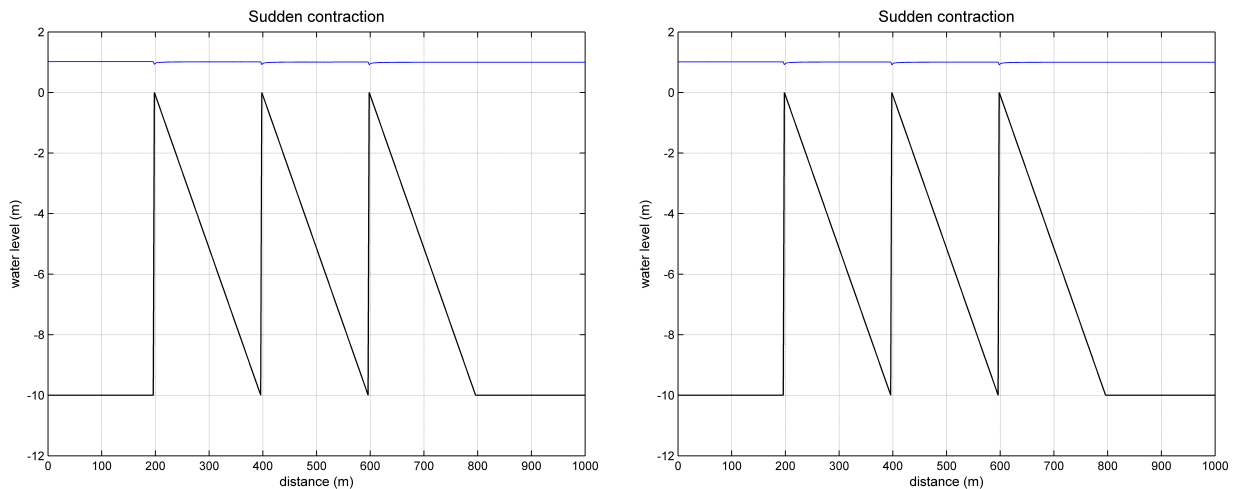


Figure 3.19: (Left) water level using no space discretization and (right) water level for advective terms discretization using a upwind scheme with energy head conservation everywhere.

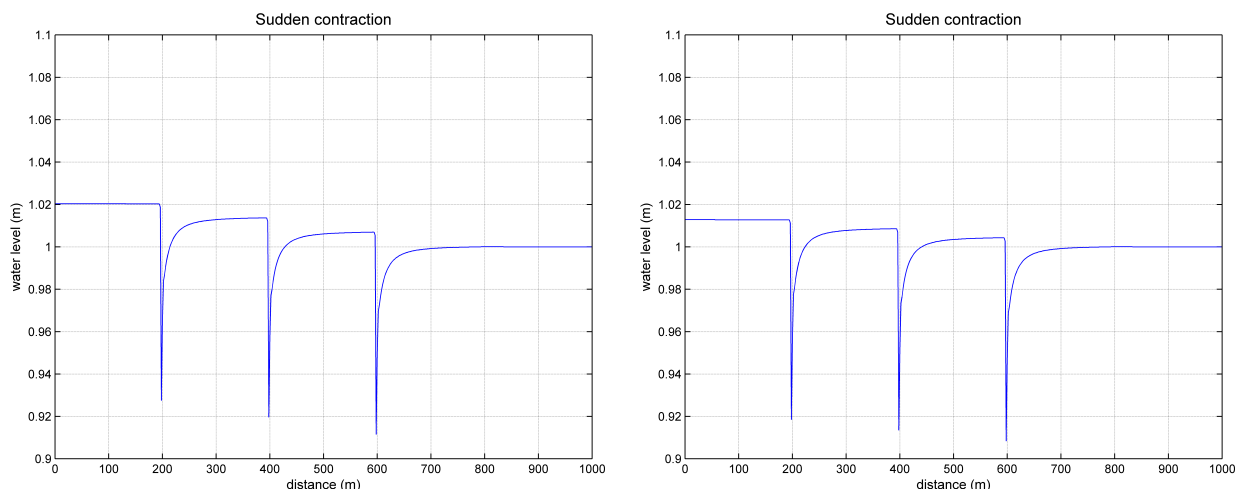


Figure 3.20: (Left) water level using no space discretization and (right) water level for advective terms discretization using a upwind scheme with energy head conservation everywhere.

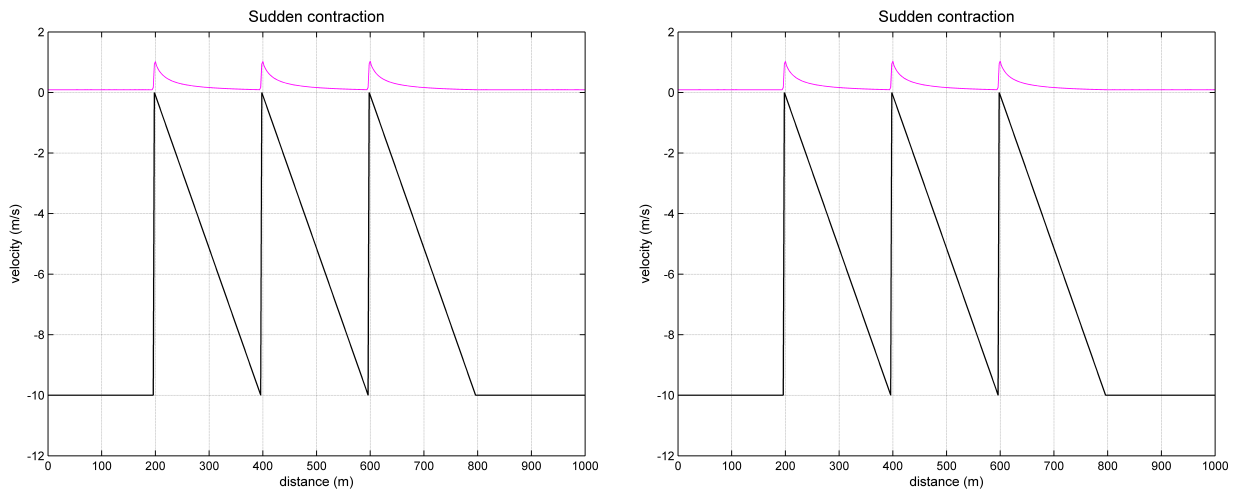


Figure 3.21: (Left) velocities using no space discretization and (right) velocities for advective terms discretization using a upwind scheme with energy conservation everywhere.

From the figures 3.19, 3.22 and 3.23 it can be seen that the model roughly behaves (applying a dynamic choice technique) employing the energy conservation everywhere when sudden contractions occur.

Dynamic choice agrees with the following algorithm:

```
If u(i+1) > u(i)
    Apply energy head balance
Else
    Apply momentum balance
End
```

Since flow contractions normally comply that $u_{i+1} \geq u_i$, conservation of energy is applied. However, the situation is rather different for the expansion case. It can be noted that significant differences do not take place between energy head and momentum conservation.

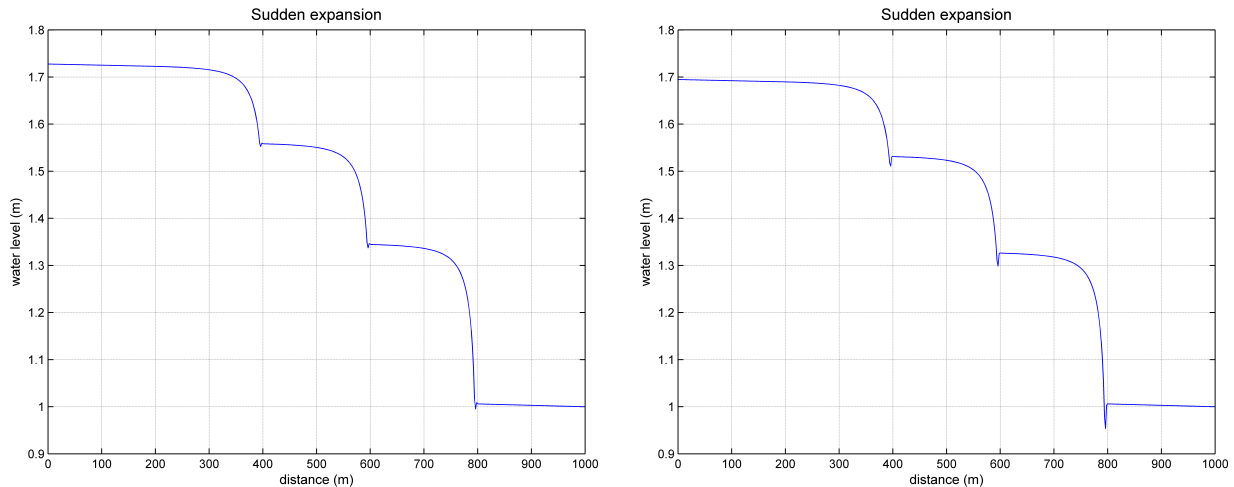


Figure 3.22: (Left) water level using no space discretization and (right) water level for advective terms discretization using a upwind scheme with energy head conservation everywhere.

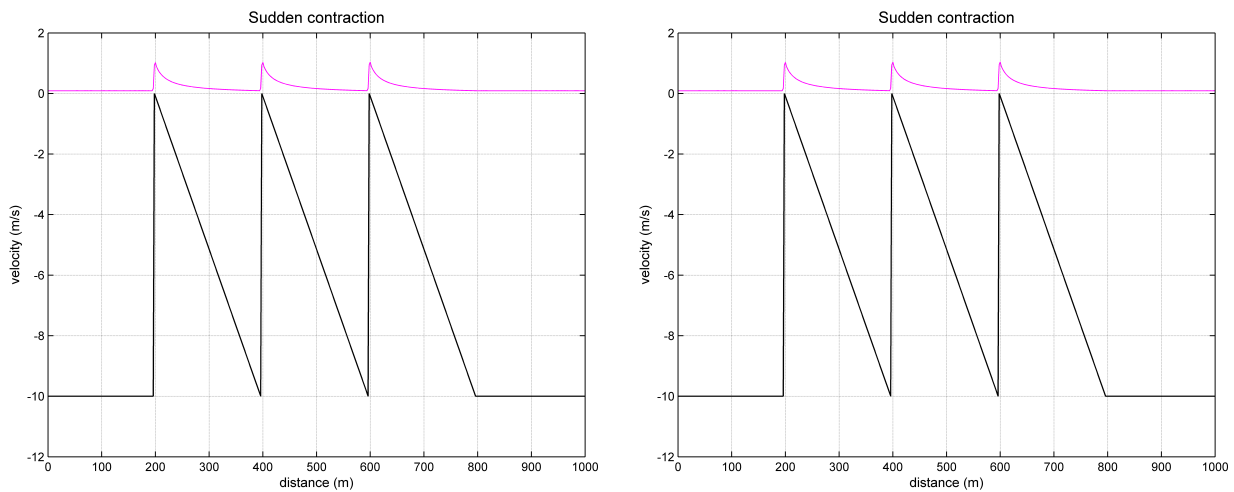


Figure 3.23: (Left) velocities using no space discretization and (right) velocities for advective terms discretization using a upwind scheme with energy conservation everywhere.

3.5 Interpolation of the Water Depth to the Velocity Points

The interpolation of the water depth to the velocity points may also has a profound impact on the numerical solution. Try the DISCRET CORRDEP interpolation method and assess the effect.

The interpolation of the water depth to the velocity points yields the following grid configuration (Fig. 3.24) where:

$$h_i = f(h_{i-1/2}, h_{i+1/2}) \quad \forall i = 1, \dots, n$$

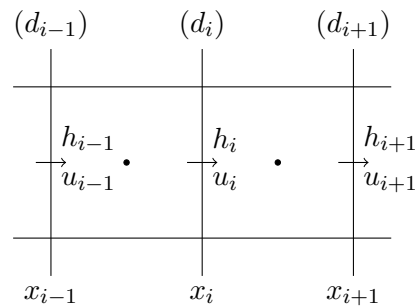


Figure 3.24: Arrangement of the unknowns in a staggered grid where water depth is interpolated to velocity points.

The following figures display the water levels and the three different balances (see equations 3.1, 3.2 and 3.3).

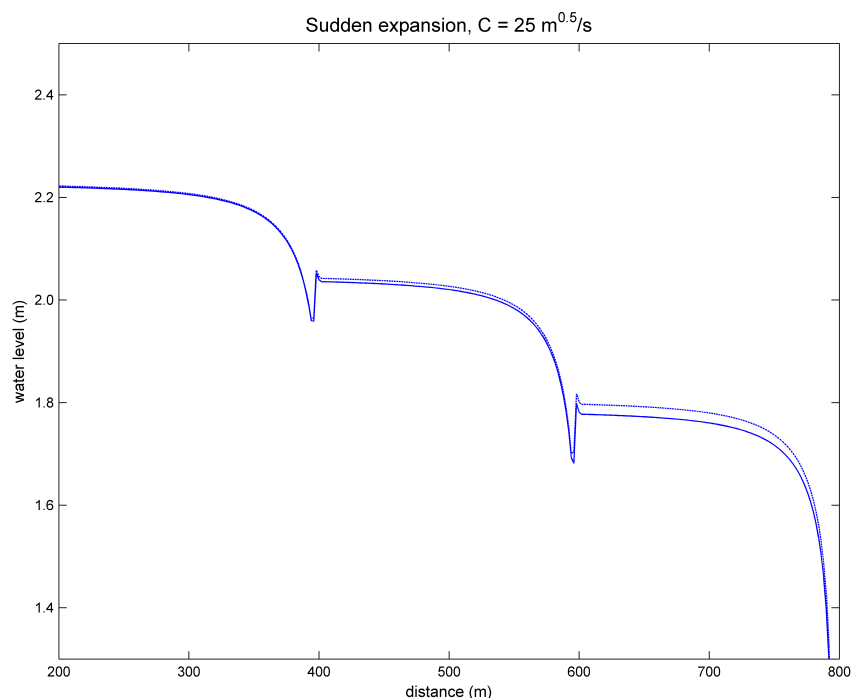


Figure 3.25: Water levels for a the sudden expansion case (10 m stepwise). (Discontinuous line) original case and (continuous line) interpolation of water depth to velocity points.

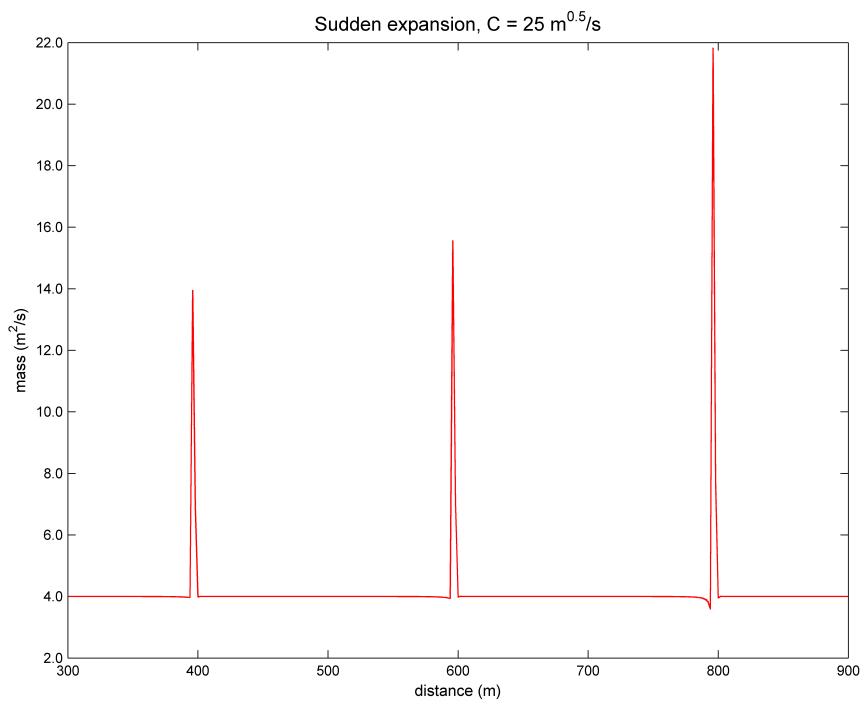


Figure 3.26: Mass balance for a the sudden expansion case (10 m stepwise). (Discontinuous line) original case and (continuous line) interpolation of water depth to velocity points.

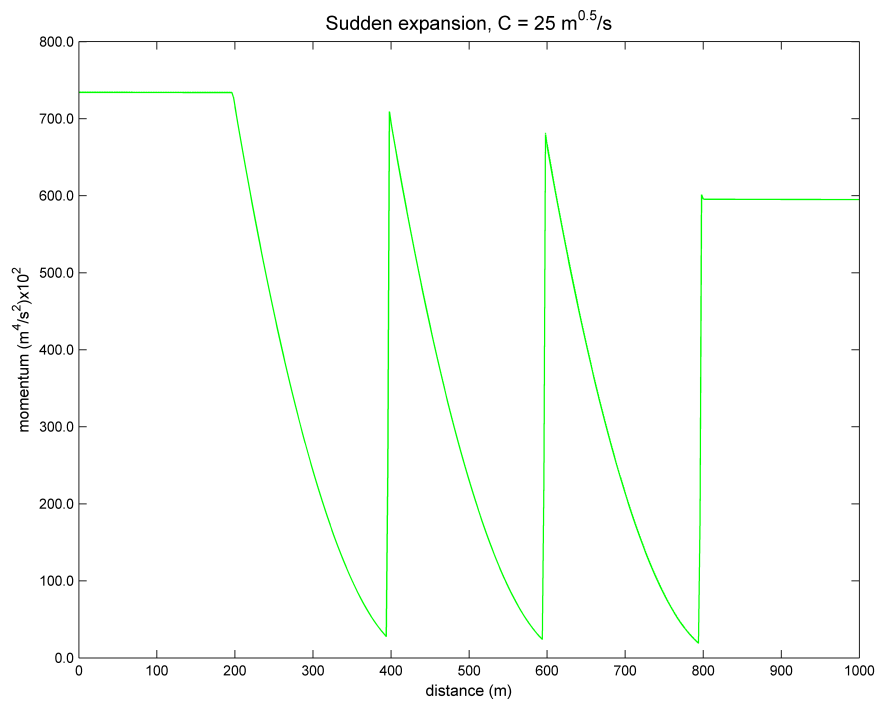


Figure 3.27: Momentum balance for a the sudden expansion case (10 m stepwise). (Discontinuous line) original case and (continuous line) interpolation of water depth to velocity points.

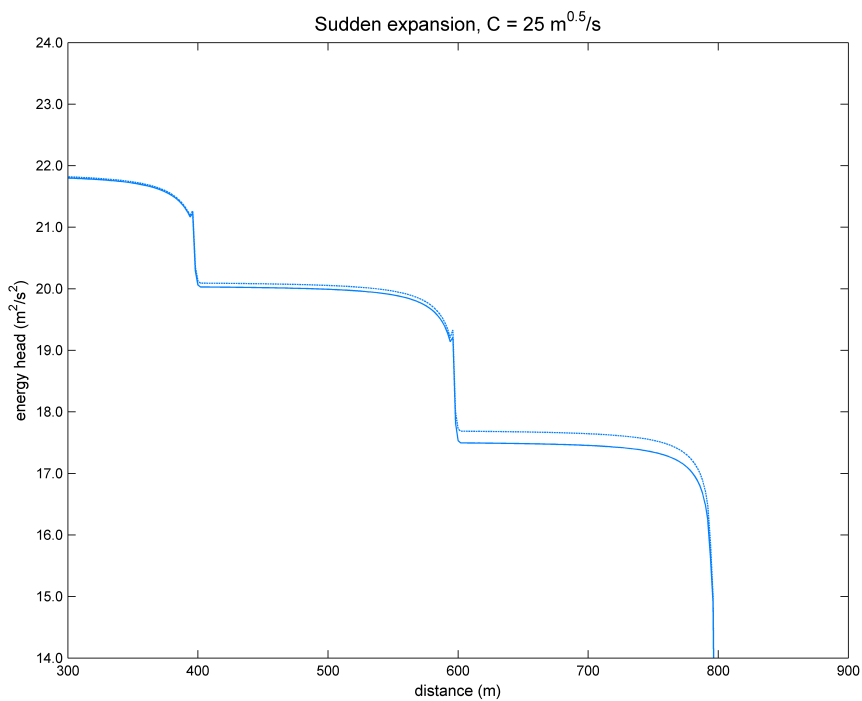


Figure 3.28: Energy head balance for a the sudden expansion case (10 m stepwise). (Discontinuous line) original case and (continuous line) interpolation of water depth to velocity points.

It can be seen from the Fig. 3.25 that the water level has been reduced due to the interpolation method. This will basically influence the energy head balance (see Fig. 3.28), thus reducing it slightly. However, the impact is negligible in the other two balances (Figs. 3.26 and 3.27) since the velocities do not vary and the the water depths are virtually the same (whereas the change influence in the water level is much higher and, hence, the energy balance varies).

Chapter 4

Rectilinear Grids with Staircases vs. Curvilinear Grids

Simulate one river bend with a rectilinear grid schematization and a smooth curvilinear grid schematization of the exact same river.

4.1 Water Level Head Differences

What is the difference in water level head when a prescribed discharge flows through the bend? Why? Clarify and analyze the results.

The first simulation corresponds to the river bend with a rectilinear grid and in the second a smooth curvilinear grid will be implemented. In the Fig. 4.1 one can observe the different grids implemented.

To accurately resolve flow and transport processes in topographically complex areas, a locally variable grid resolution is desirable. Curvilinear grids, either in Cartesian or spherical coordinates (Kernkamp et al. 2011), have greatly increased the possibilities of numerical flow modelling in shallow water applications.

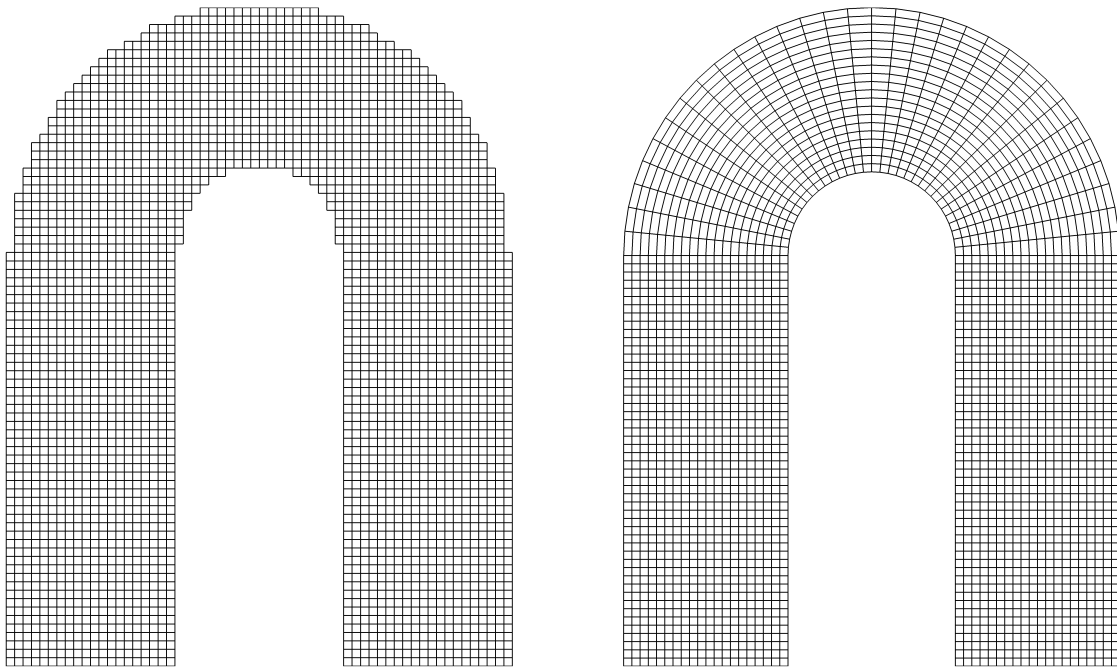


Figure 4.1: Curvilinear grid (left) and rectilinear/Cartesian grid (right).

The advection term integrated explicitly in time and is formulated in a momentum conservative way, basically following (Kramer and Stelling 2008). Since the other terms in the momentum are already in finite-volume formulation, this guarantees conservation of momentum. The key point in the conservative formulation of the advection term on unstructured grids lies in the choice of a closed pair of advective fluxes and advected quantities. The advected quantity is defined in a cell circumcentre, and the advective fluxes that transport this quantity are defined on the cell faces that surround this cell.

Computing the shallow water equations (Swash) using an upwind scheme (discretization of advection terms) in the momentum equations and setting a discharge per unit width at the right boundary of $0.5 \text{ m}^2/\text{s}$ and a fixed water level of 0 m at the left boundary, it can be noted that there is small energy head loss across the bend. Water levels and velocity magnitudes have been requested to the model and Figs. 4.2 and 4.3 show the results.

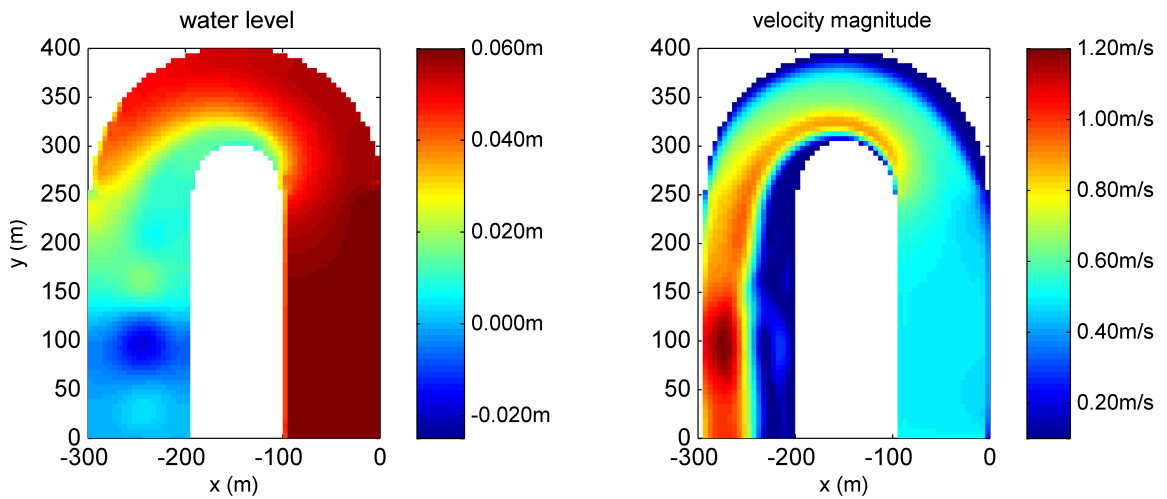


Figure 4.2: Water level and velocity magnitude in a river bend with a rectilinear (Cartesian) grid.

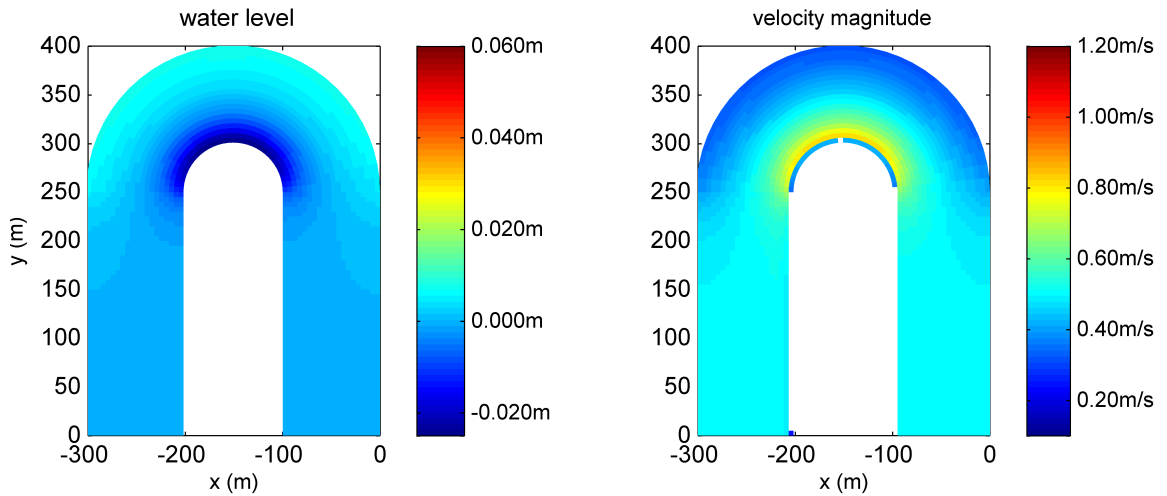


Figure 4.3: Water level and velocity magnitude in a river bend with a curvilinear grid.

The rectilinear grid displays a larger rise of the water level upstream the bend. This is due to the fact that the water flow has to follow a larger path (in the model grid) than what it is actually followed in reality. In other words:

Since grid cells are squared and their sides not perpendicular to the flow streamlines, during the computations the water flows depict a staircase pattern in the bend due because the equations are solved perpendicularly to the sides of the grid cell. Therefore, the path followed by a particle will be always larger than in reality.

Since the water level is fixed downstream and a constant discharge flows from the upstream part, a larger distance (path of the water particles) will require a larger water level upstream so that water can be driven through the bend. This additional increment of the water elevation is in the order of a few tenths of a millimeter (in this case).

On the other hand, the curvilinear grid perfectly suits the flow circulation and shallow water equations are always calculated parallel to the flow direction, thus not creating

artificial boundary effects like in the former case. For such a reason, the water level upstream the bend is the same than downstream.

The aforementioned artificial boundary effects are the product of an inaccurate matching of the actual boundary and the sides of the boundary cells (Kramer and Stelling 2008).

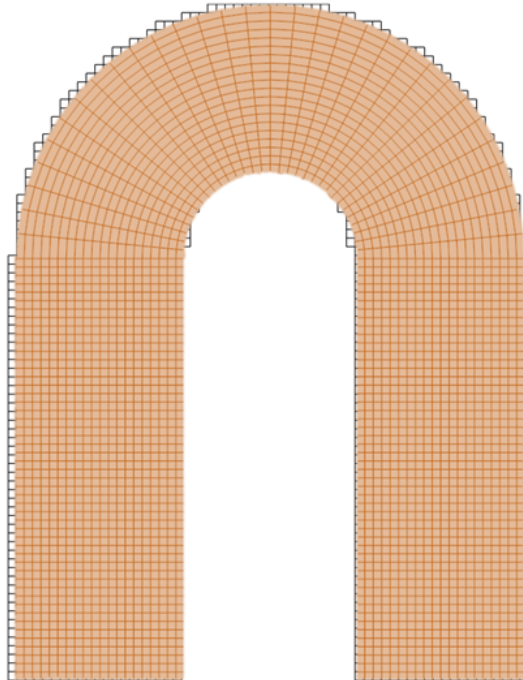


Figure 4.4: Curvilinear grid superposed over the rectilinear grid.

4.2 Time Step Assessment

Do the two grids allow for the same (small) time step?

The time integration is discretized using the Backward Euler method (or implicit Euler method). This implicit scheme is unconditionally stable which means that the schemes stable over a wide range of time steps (high cost per time step). Furthermore, these constitute excellent iterative solvers for steady-state problems. Therefore, for (small) time steps both grids will allow computations.

Chapter 5

The Vertical Structure of Barotropic Currents: Wind Driven Circulation in a Lake

Goal

Test the performance of the turbulence models (two different ones in Swash) for the case of a closed basin with wind forcing. In such wind driven basins near the surface layer the water flows in the direction of the wind (neglecting Coriolis effect), while continuity requires a return flow in the deeper water layers. With constant wind forcing a stationary circulation will be established eventually.

For the one-dimensional situation, the following script has been implemented in order to carry out the computations of the model:

```
PROJECT 'Exercise6', '1'  
'Wind driven circulation in a lake'  
SET CORI NAUT  
MODE DYN ONED  
CGRID 0. 0. 0. 1000. 0. 10 0  
VERT 20 1 2 2 5 10 10 20 15 10 5 5 5 2 2 1 1 1 1 1 1 PERC  
INPGRID BOTTOM 0. 0. 0. 1 0 1000. 0.  
READINP BOTTOM 1. 'FlatBottom.bot' 1 0 FREE  
INPGRID WLEV 0. 0. 0. 1 0 1000. 0.  
READINP WLEV 1. 'Surface.wlv' 1 0 FREE  
INIT ZERO  
WIND 5 270 CON REL  
FRIC LOG ROUGH 0.2  
VISC V KEPS  
TIMEI METH IMPLICIT  
POINT 'GAUGE' 500. 0.  
TABLE 'GAUGE' HEAD 't64tur01.tab' ZK VELK VISC TKE  
GROUP 'SYSTEM' SUBG 1 11 1 1  
TABLE 'SYSTEM' HEAD 'lake.tab' DIST WATL BOTLEV  
COMPUTE 20140424.000000 1 SEC 20140425.000000  
STOP
```

The nautical convention has been implemented (influencing the definition of the wind forcing). The system length has been set equal to 1,000 m, using a computational grid comprised by ten cells of 100 m length each.

In order to accurate the results of the vertically distributed parameters (such as the velocity and the vertical eddy viscosity) a non-equidistant sigma layer distribution has been introduced. A total number of 20 layers with different thicknesses (see script above) compose the vertical structure.

Furthermore, with regard to the viscosity, the vertical mixing is modelled by using the standard $k - \epsilon$ model. On the other hand, bottom friction obeys the logarithmic wall-law with a relatively high Nikuradse roughness length (20 cm, corresponding to very coarse sediments).

Moreover, a wind field has been introduced with a constant velocity of 5 m/s blowing from the west. A one-day simulation has been computed and different questions are assessed below.

5.1 Assessment of the Vertical Gradient of the Flow Velocity

What happens at the level where $\partial u / \partial z = 0$?

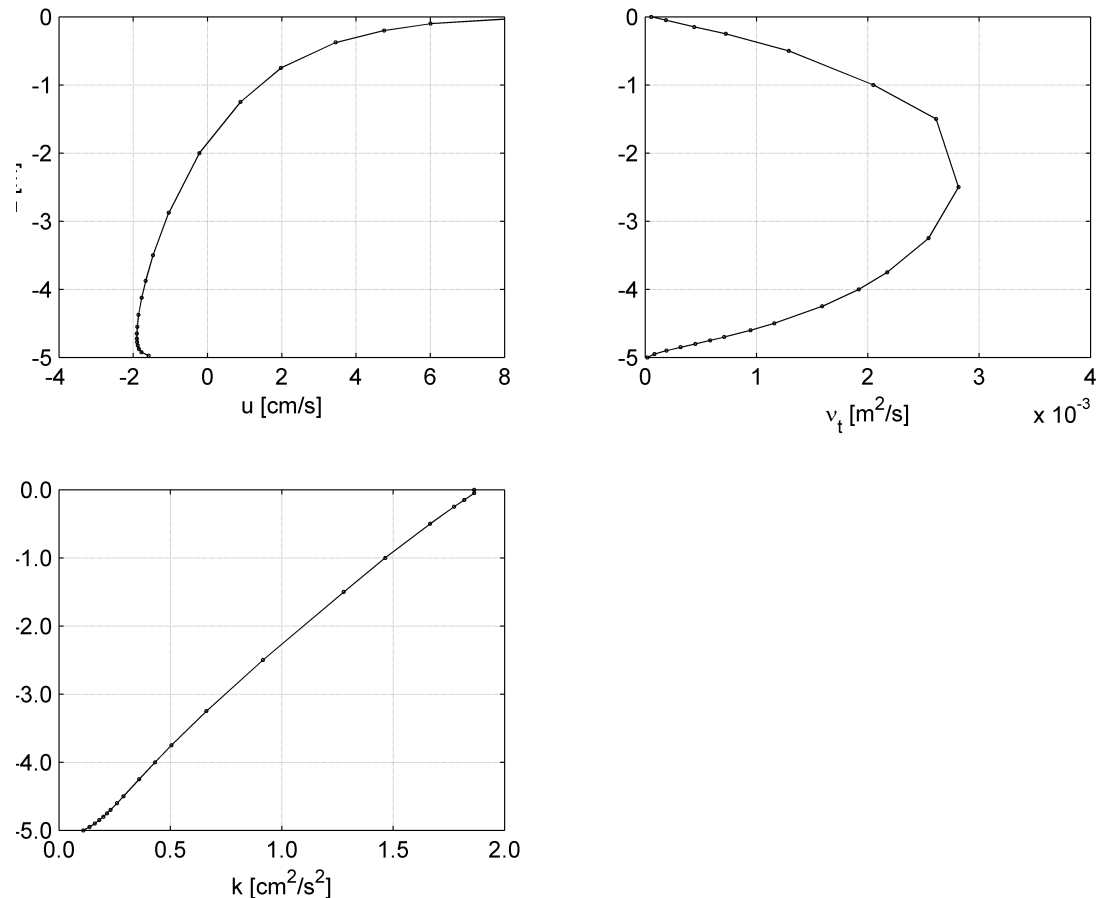


Figure 5.1: (a) Vertical distribution of the flow velocity, (b) vertical distribution of the vertical eddy viscosity per layer interface (in m^2/s) and (c) vertical distribution of the turbulent kinetic energy per layer interface (in cm^2/s^2).

It can be seen from 5.1 that $\partial u / \partial z = 0$ roughly takes place when the eddy viscosity is maximum. A conclusion can be therefore drawn: the larger the viscosity, the lower the velocity. Viscosity is due to the friction between neighboring particles (or layers) in a fluid that are moving at different velocities. A large viscosity denotes that large resistance to gradual deformation is enforced by the fluid, thus leading to a decrease in velocity. From the Figure 1(a) it can be observed that the velocity directions are different starting from $z = -2$ m (where the flow velocity is null $u = 0$ m/s), thus showing that a wind driven circulation is developing.

Furthermore, it can be seen from the 5.2 that the wind is actually creating a surface set-up towards the east boundary. The resulting circulation is generated since a balance with this surface gradient must exist. Eastwards directed flow (occurring near the surface) coincides with the direction of the wind (surface layers are dragged by the wind pulse) and below the 2 m of depth, the current is westwards directed.

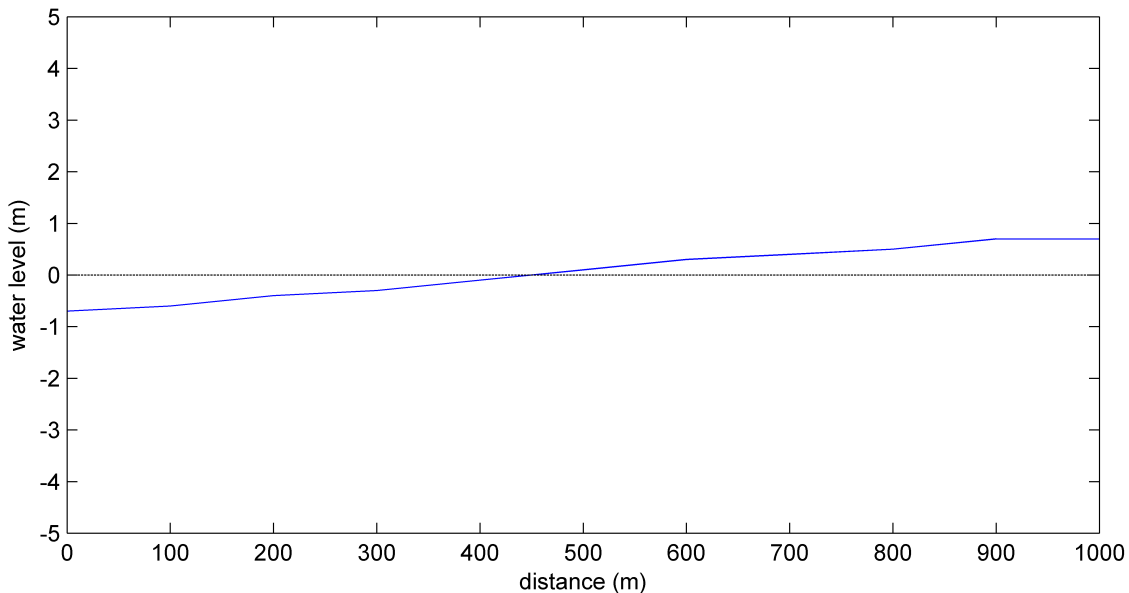


Figure 5.2: Water level at the lake.

5.2 Influence of the Background Viscosity on the Spin-Up Time

K-epsilon ($k-\epsilon$) turbulence model is the most common model used in Computational Fluid Dynamics (CFD) to simulate turbulent conditions. It is a two equation model which gives a general description of turbulence by means of two transport equations (PDEs). The original impetus for the K-epsilon model was to improve the mixing-length model, as well as to find an alternative to algebraically prescribing turbulent length scales in moderate to high complexity flows. The first transported variable determines the energy in the turbulence and is called turbulent kinetic energy (k). The second transported variable is the turbulent dissipation (ϵ) which determines the rate of dissipation of the turbulent kinetic energy.

What is the influence of the background viscosity on the spin-up time and on the final stationary results?

The background viscosity accounts for all forms of unresolved vertical mixing. Small background viscosity allows small-scale eddies to reduce stratification and increase the kinematic energy in the nearshore region. However, large vertical background viscosity interacts with the vertical parameterization scheme. Eddy viscosity is large in the whole field (Tseng, Meneveau, and Parlange 2006).

The background viscosity is set by default equal to zero. The value must be small compared to the vertical viscosity calculated by the standard $k-\epsilon$ model. Experiences suggest a value of 10^{-4} to 10^{-3} m²/s. The following command allows the user to modify the value of the background viscosity in the Swash model:

```
SET BACKVISC=10E-3
```

The influence of the background viscosity on the spin-up time will be assessed by analysing the evolution of the vertical gradient of the velocity (the distribution of the flow velocity per layer). A rough estimate of the spin-up time will be given when the vertical profile is virtually stationary.

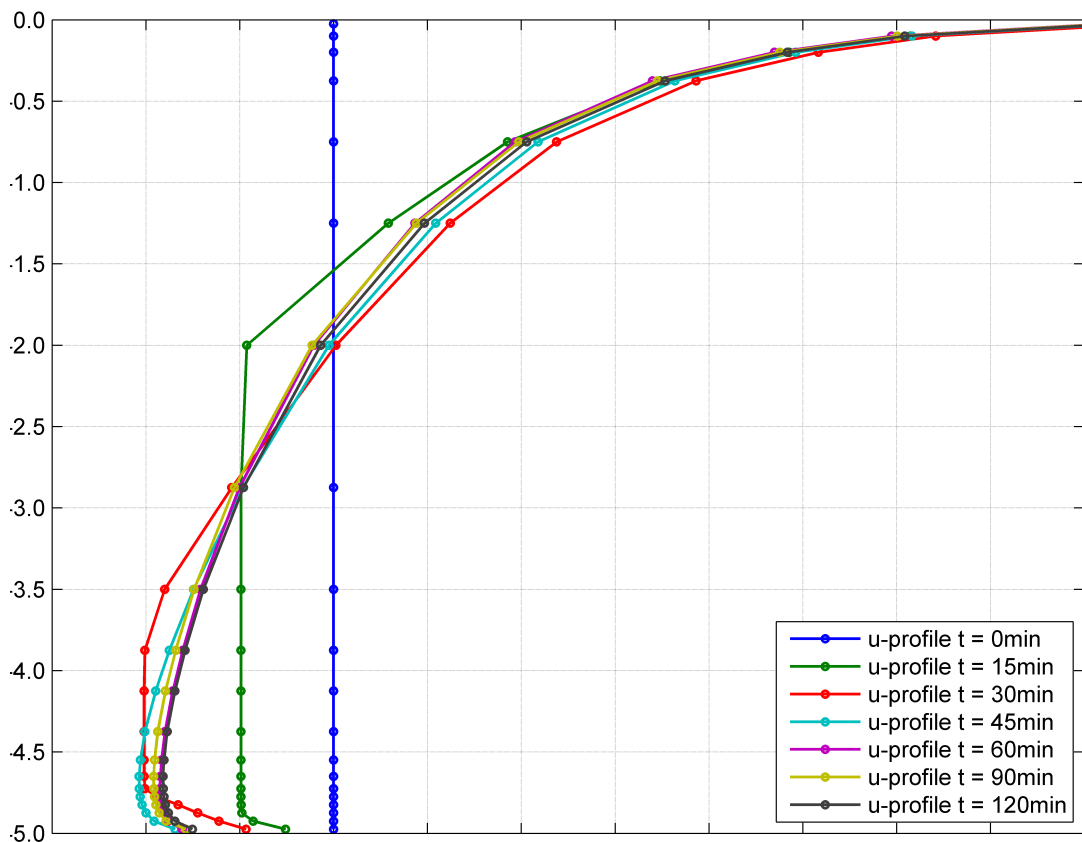


Figure 5.3: Time-evolution of the velocity profile (over depth) for the absence of background viscosity situation.

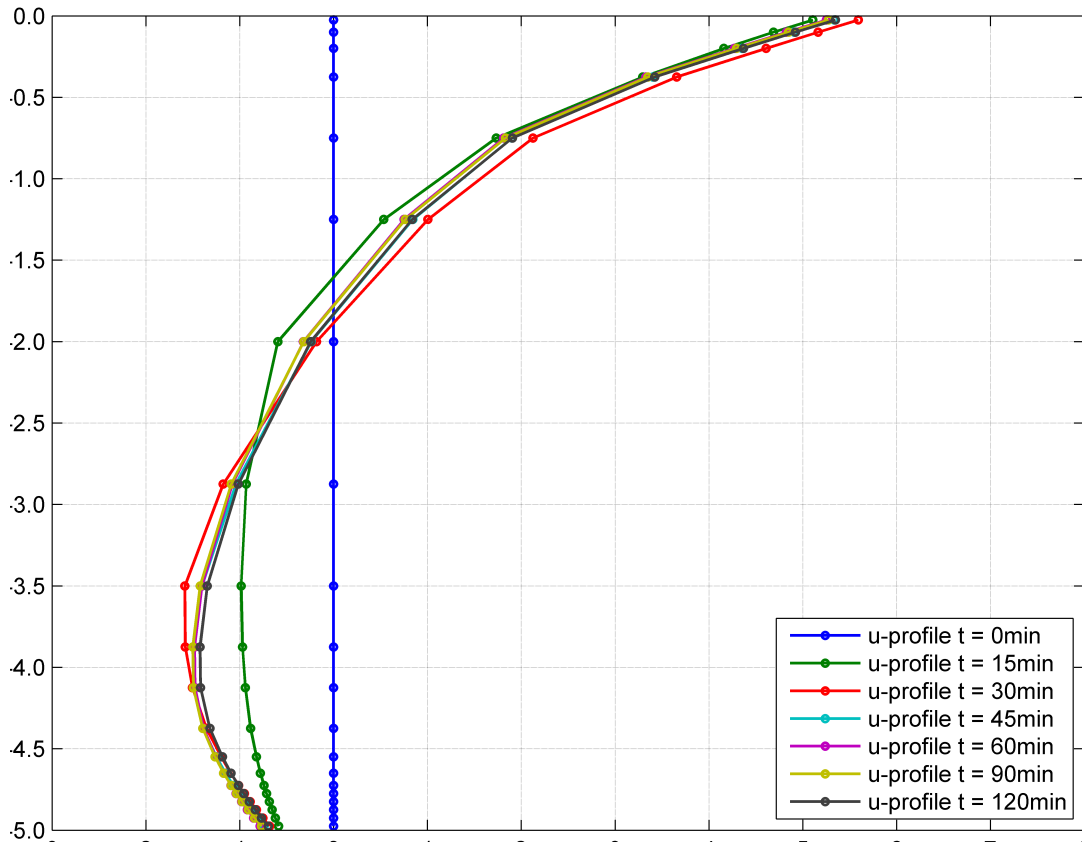


Figure 5.4: Time-evolution of the velocity profile (over depth) for a background viscosity of $10^{-3} \text{ m}^2/\text{s}$.

From the Figs. 5.3 and 5.4 it can be clearly seen that the spin-up time is reduced for the latter case, in which a background viscosity value is set. This result is in accordance with what it was expected. The vertical mixing is enhanced and overall larger viscosity will damp faster the effects associated with the spin-up.

The final stationary situation can also be deducted from these figures. Additionally, Figs. 5.5, 5.6 and 5.7 display a more comprehensible comparison of both cases (with and without background viscosity).

When background viscosity is taken into account, the velocity magnitudes decrease both at the surface and bottom. The eddy viscosity also decreases and the turbulent kinetic energy shows a significant fall at the top layer whereas the shape fairly remains constant next to the bottom. All three variables converge faster than in the case where no background viscosity is considered (thus reducing the spin-up time) and present different distributions (as shown in the figures).

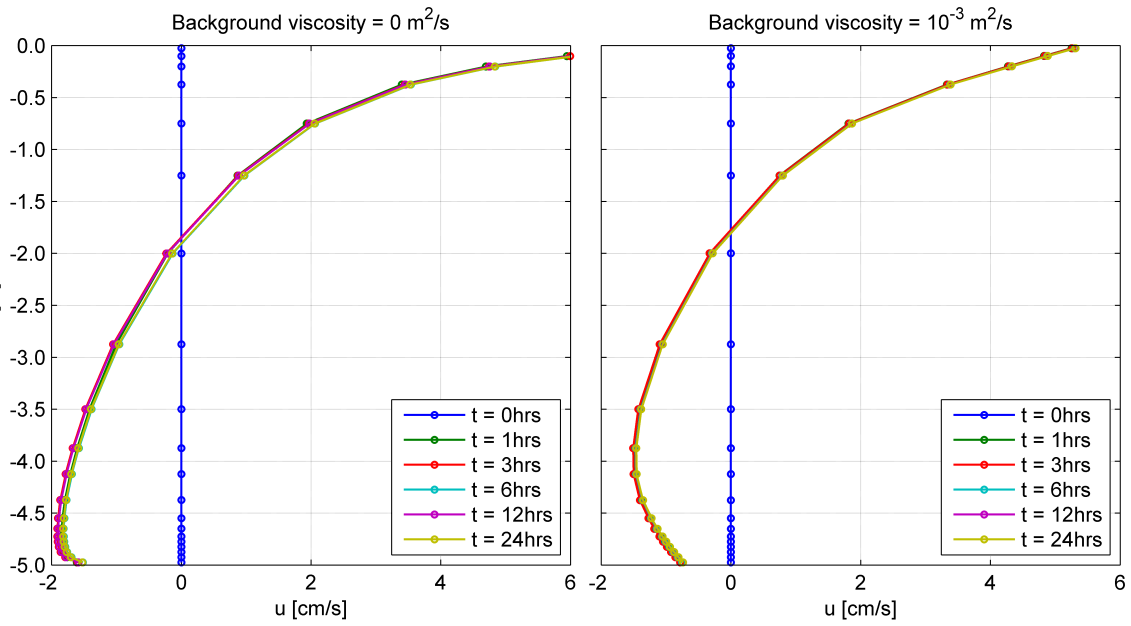


Figure 5.5: Time-evolution of vertical distribution of the flow velocity with and without background viscosity.

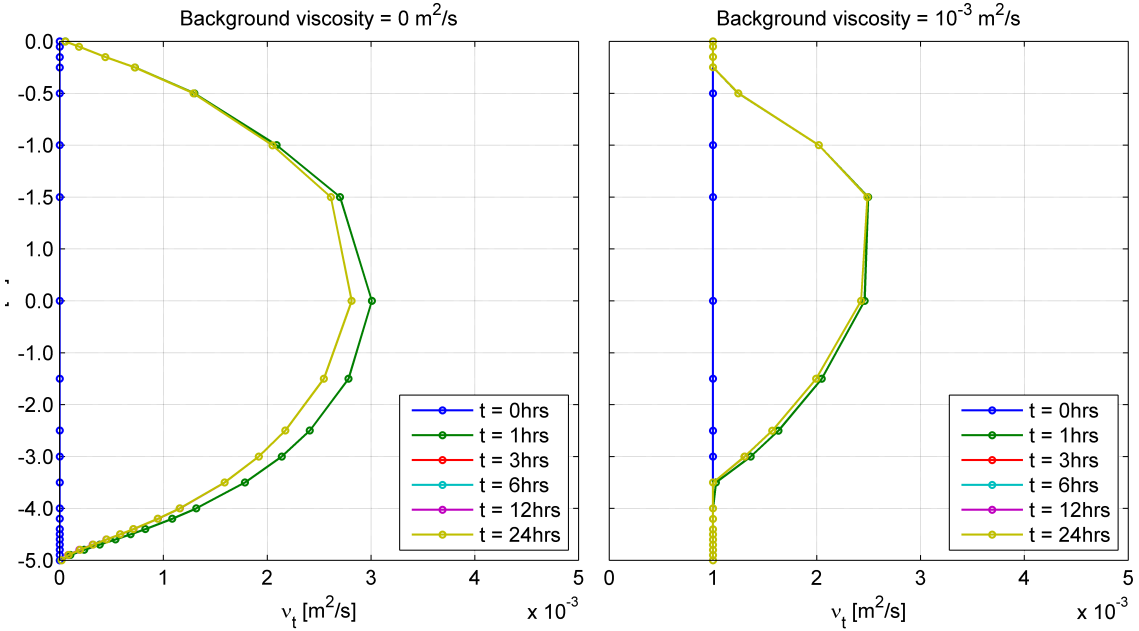


Figure 5.6: Time-evolution of vertical distribution of the vertical eddy viscosity per layer interface with and without background viscosity.

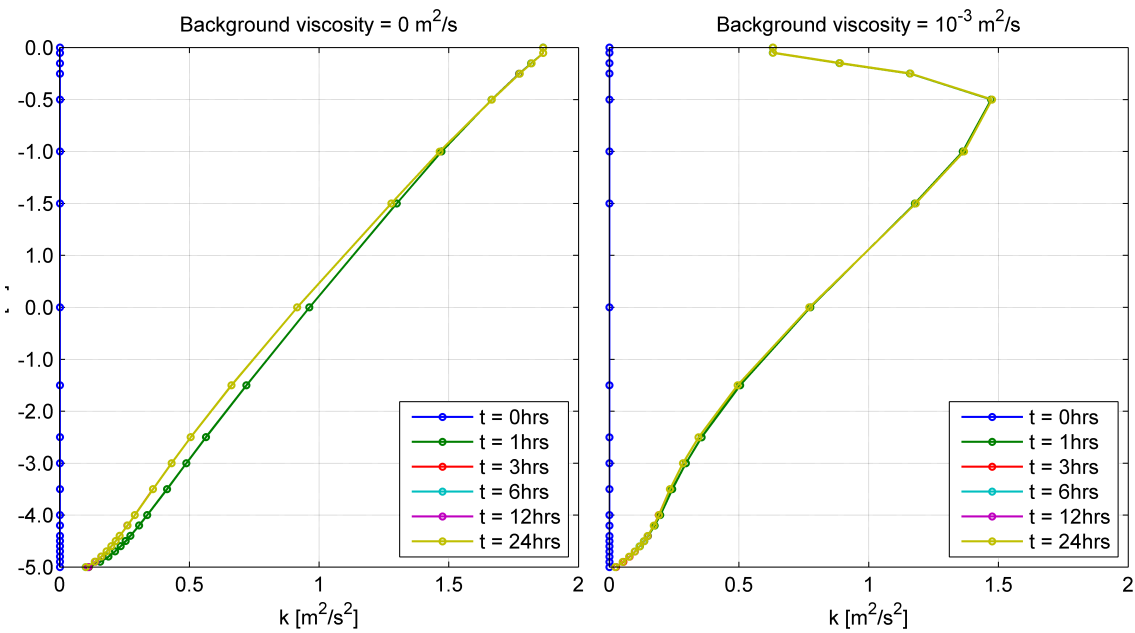


Figure 5.7: Time-evolution of vertical distribution of the turbulent kinetic energy per layer interface with and without background viscosity.

5.3 The Turbulent Kinetic Energy Profile

What does the shear stress profile (τ) or turbulent kinetic energy (k) look like and how does that relate to theory? Assess the τ profile or k -profile both during spin-up and during the stationary situation (You may compute both wind and bottom stress by means of the k -profile).

The turbulent kinetic energy profile will be assessed in the present study. The 5.8 shows the evolution of the k -profile during the early stages of the simulation. It can be observed that the turbulent kinetic energy is initially constant over the depth. However, as soon as the wind starts blowing, stresses (due to the dragging of the wind over the surface) are developed on the water surface and thus imply an increase of the turbulence (or, in other words, turbulent kinetic energy). One can also visualize the fact that the stresses (turbulent kinetic energy) is much faster developed in the surface rather than at the bottom. Equilibrium (stationary situation) is achieved at the bottom although the convergence occurs much faster at the surface.

The wind and bottom stresses may be computed from the k -profile and it can be concluded that the magnitude of the stresses at the surface will be larger than at the bottom (due to the fact that the wind is continuously blowing and hence producing more turbulent kinetic energy).

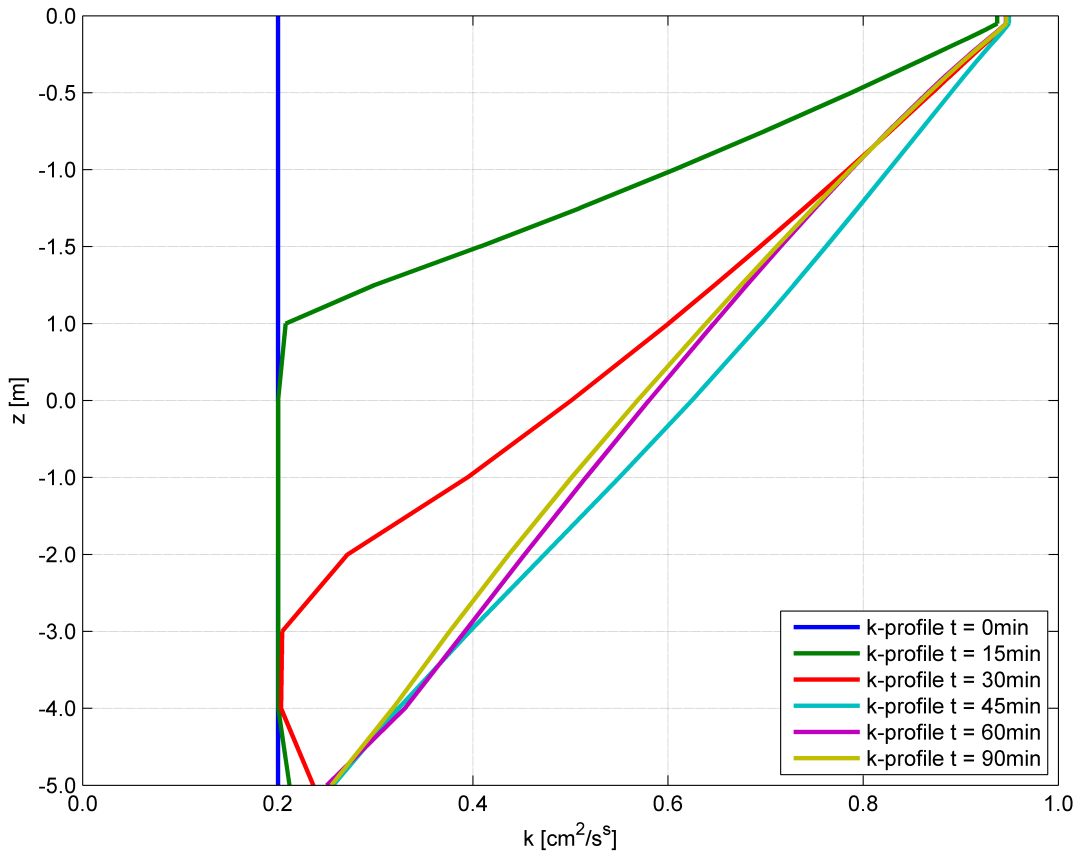


Figure 5.8: Evolution of the turbulent kinetic energy profile.

5.4 Gradually Increasing (Ramping) Wind

How can you affect the spin-up time by specifying a gradually increasing (ramping) wind, rather than a stepwise increasing wind?

When initial conditions are such that initial velocities and water levels are equal to zero and a wind field immediately blows over the surface (say, at 10 m/s), there are large differences between the initial conditions and the forcing. Therefore, all kind of wiggles are expected to grow and a much larger spin-up time will take place.

However, when a gradually increasing wind is applied, a matching between the external forcing and the initial conditions can be found. The elevation of the water surface evolves accordingly with the evolution of the wind field and, hence, the spin-up time will be effectively reduced.

5.5 Two-Dimensional System

The following script has been used so as to build the system characteristics. The bottom grid is depicted in the Fig. 5.9 and a regular wind field is blowing from the west.

```
PROJECT 'Exercise6' '2'
'Wind driven circulation in a lake'
SET CORI NAUT
MODE DYN TWOD
CGRID 0. 0. 0. 1000. 1000. 25 25
VERT 10 5 5 10 15 15 15 15 10 5 5 PERC
INPGRID BOTTOM 0. 0. 0. 25 25 40. 40.
READINP BOTTOM 1. 'Bathymetry.bot' 1 0 FREE
INPGRID WLEV 0. 0. 0. 1 1 1000. 1000.
READINP WLEV 1. 'Surface.wlv' 1 0 FREE
INIT ZERO
WIND 5 270 CON REL
FRIC LOG ROUGH 0.2
VISC V KEPS
TIMEI METH IMPLICIT 1.
FRA 'COMPGRID' 0. 0. 0. 1000. 1000. 25 25
TABLE 'COMPGRID' NOHEAD 't64tur02.mat' LAY 3 XP ZK VELK VZ
FRA 'SYSTEM' 0. 0. 0. 1000. 1000. 25 25
TABLE 'SYSTEM' HEAD 'lake.tab' WATL WIND
COMPUTE 20140424.000000 1 SEC 20140425.000000
STOP
```

Pay attention to the behavior near the borders of the closed basin:

What happens if you make the last grid cell next to the borders much larger in the grid editor?

Unfortunately, this effect cannot be implemented in Swash since grid cells are by definition equally spaced. Anyhow, it has been manually created a bottom grid file and computations have been carried out in order to understand the behavior of the surface elevation when a regularly distributed wind field is acting over the whole surface of the lake.

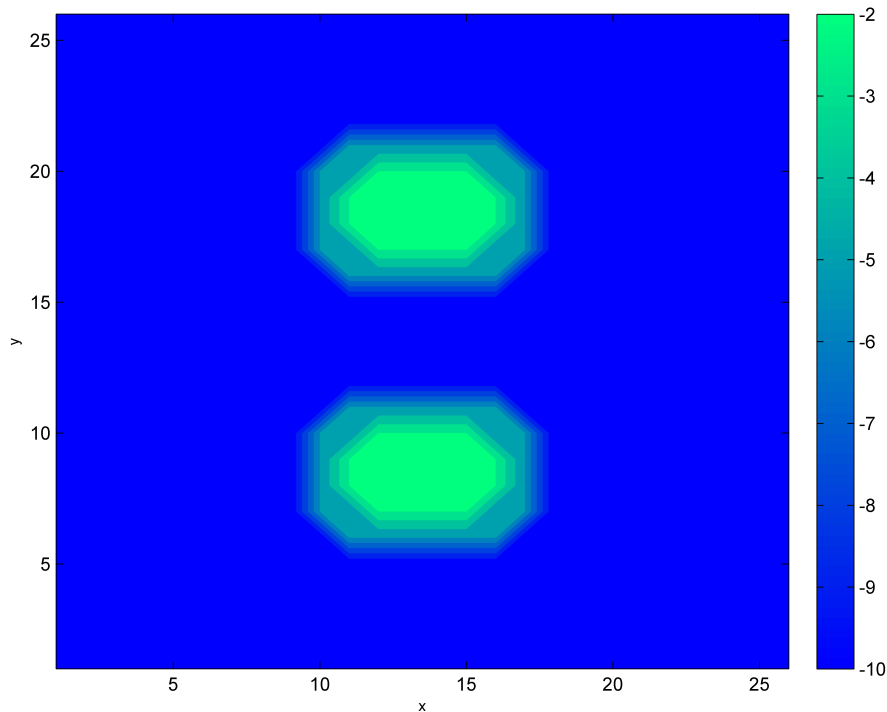


Figure 5.9: Bathymetry of the lake (vertical borders).

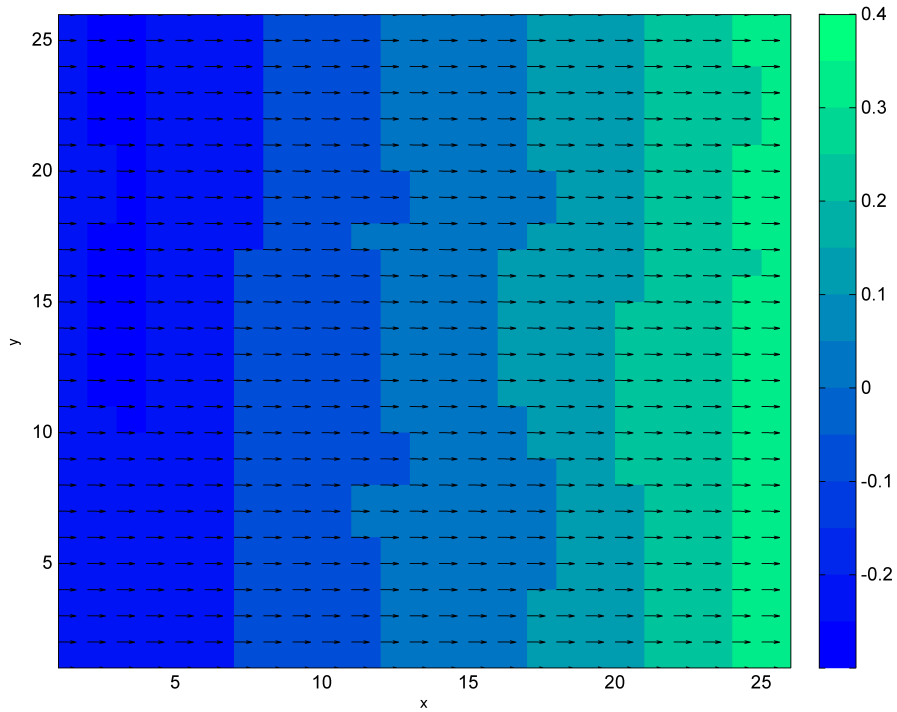


Figure 5.10: Water levels and wind directions (vectors) at the lake (vertical borders).

It can be seen that the water level set-up at the east side of the lake is slightly interrupted when it coincides (with reference to the y-axis) with the same latitude as the submerged islands (sheltering effect). In order to more clearly visualize such effect, the

islands are to be raised until they are no longer submerged (overtopping may occur though).

What happens if you adapt the depth file, such that near the edges of the lake become gradually more shallow?

The bathymetry of the lake has been transformed as suggested in the statement and it can be observed in the Fig. 5.11. The computed results can be similarly seen in the Fig. 5.12.

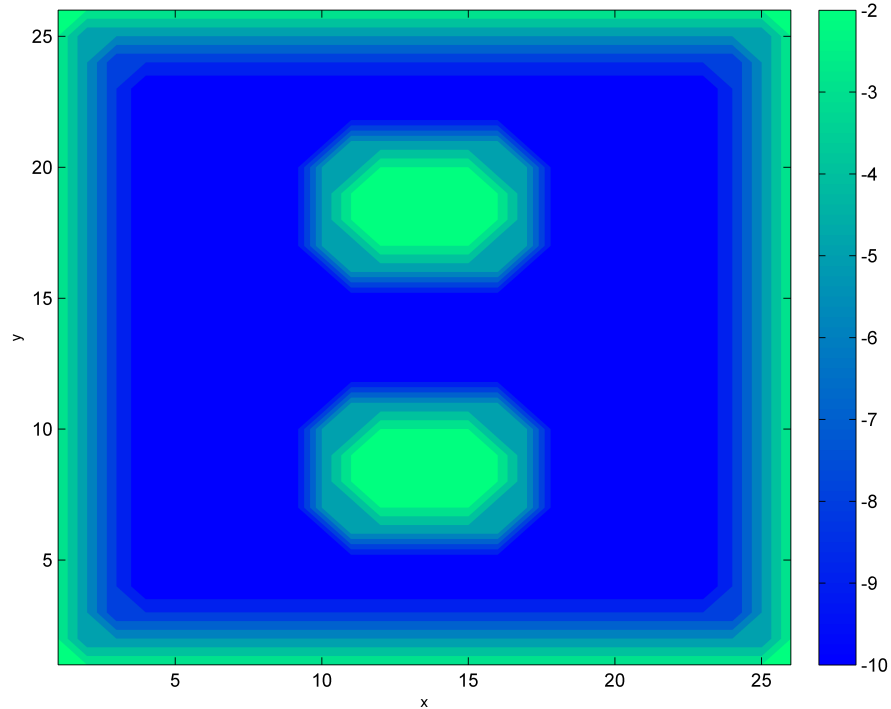


Figure 5.11: Bathymetry of the lake (gradually sloping borders).

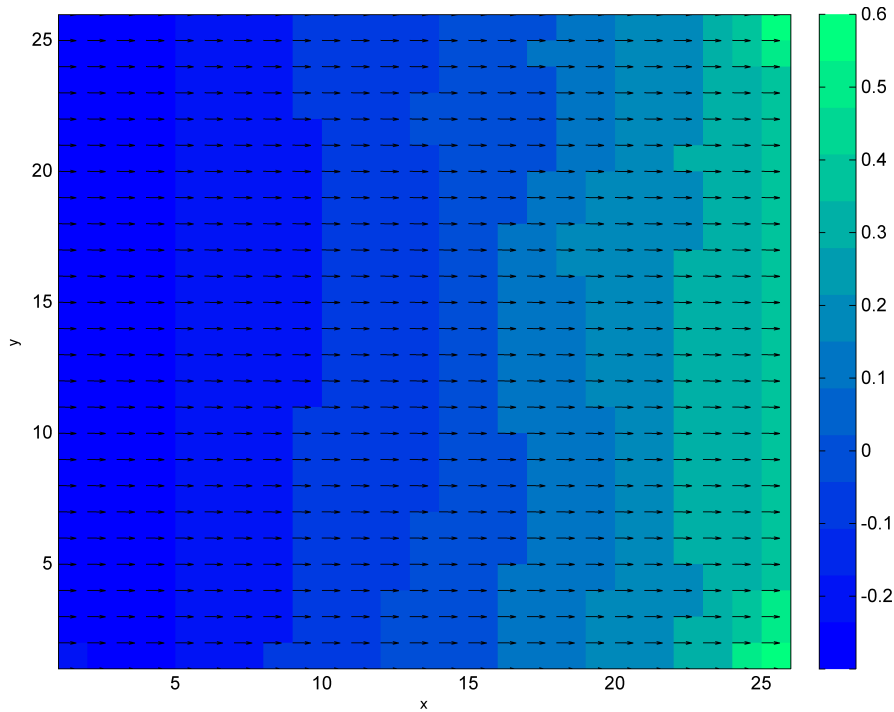


Figure 5.12: Water levels and wind directions (vectors) at the lake (gradually sloping borders).

Figs. 5.11 and 5.12 have been examined in order to understand the influence of the gently sloping shores of the lake. It can be observed that in the latter case, the surface elevation is much larger (33%) than in the first case where the edges of the lake were completely vertical. This outcome seems to be reasonable since the fact that the region near the eastern shore is shallower this time will imply that shallow water mechanisms will have larger effects (convergence of energy due to shoaling). Water will pile up in a superior manner in the latter case yielding a larger set-up at the east boundary (see Fig. 5.12).

The assessment of the flow circulation over depth is of importance. Therefore, the model has been requested to output the horizontal and vertical flow velocities per layer interface and have eventually been plotted.

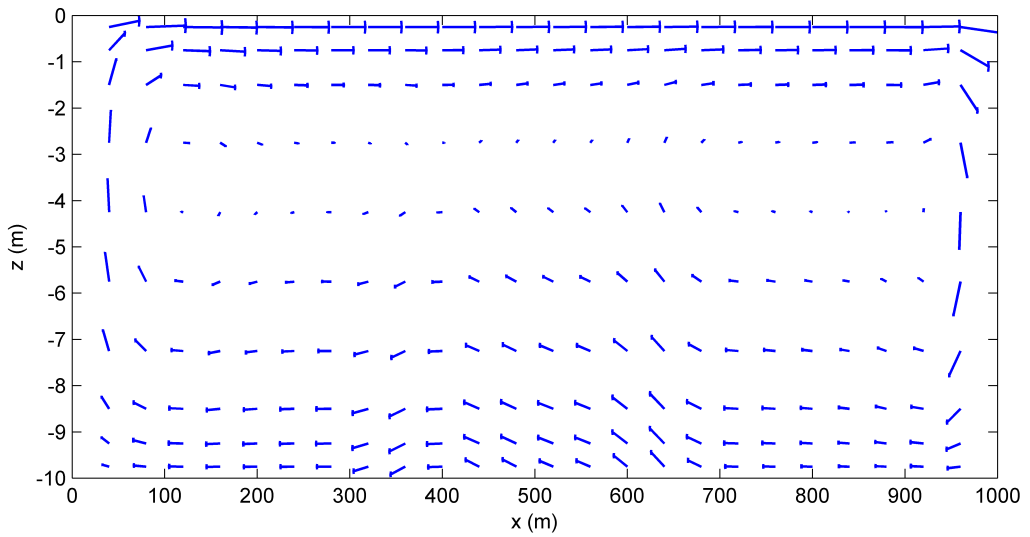


Figure 5.13: Flow circulation at a latitude of 160 m ($y=5$) (vertical borders).

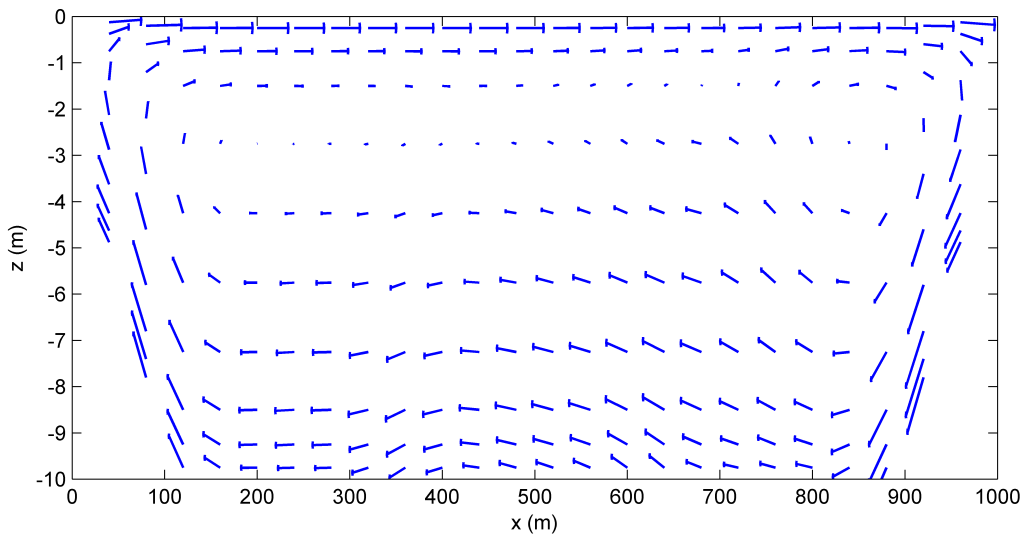


Figure 5.14: Flow circulation at a latitude of 160 m ($y=5$) (sloping borders).

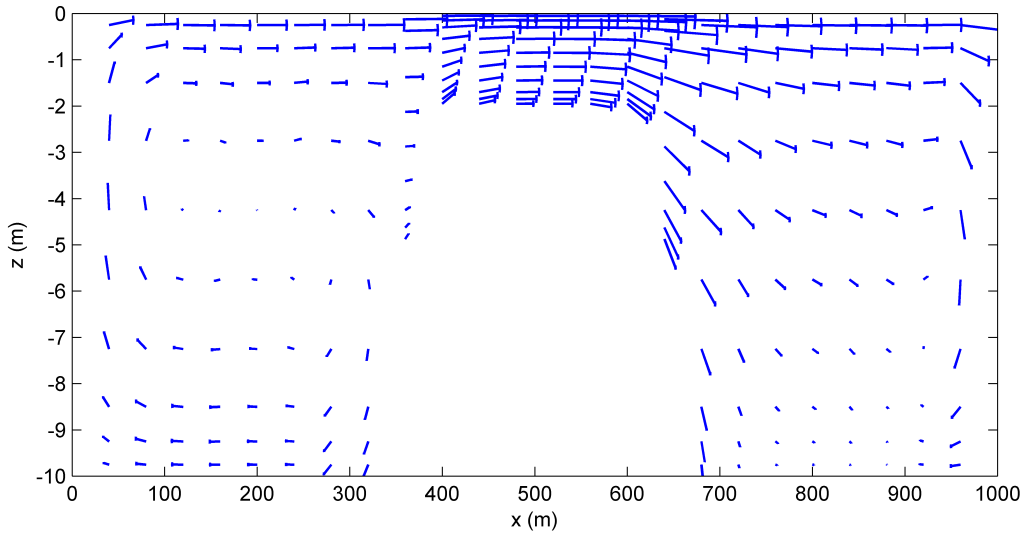


Figure 5.15: Flow circulation at a latitude of 320 m ($y=9$) (vertical borders).

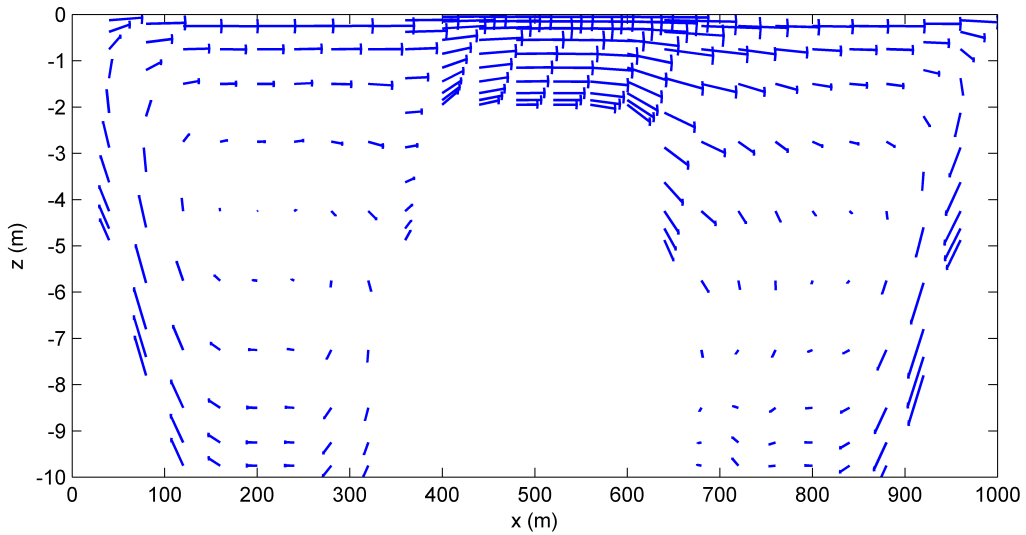


Figure 5.16: Flow circulation at a latitude of 320 m ($y=9$) (sloping borders).

Figs. 5.13, 5.14, 5.15 and 5.16 show the flow circulation over the total distance of the lake. The last two figures have been plotted in order to analyze the cross-section that exactly passes through the middle of the bottom bump and aim to display the circulation pattern above these obstacles. As expected, velocities are maximized at these locations due to the fact that the effective areas are much smaller. Clockwise flow circulation can be found at each side of the shallow area. It is likely that the flow is driven back to the left semi-basin along the bed (otherwise the water would pile up at the right semi-basin and eventually the left one would become empty). However, it cannot be visualized from the Figs. 5.15 and 5.16 maybe due to the fact that the vertical layer resolution is not high enough to capture the flow circulation above the bump.

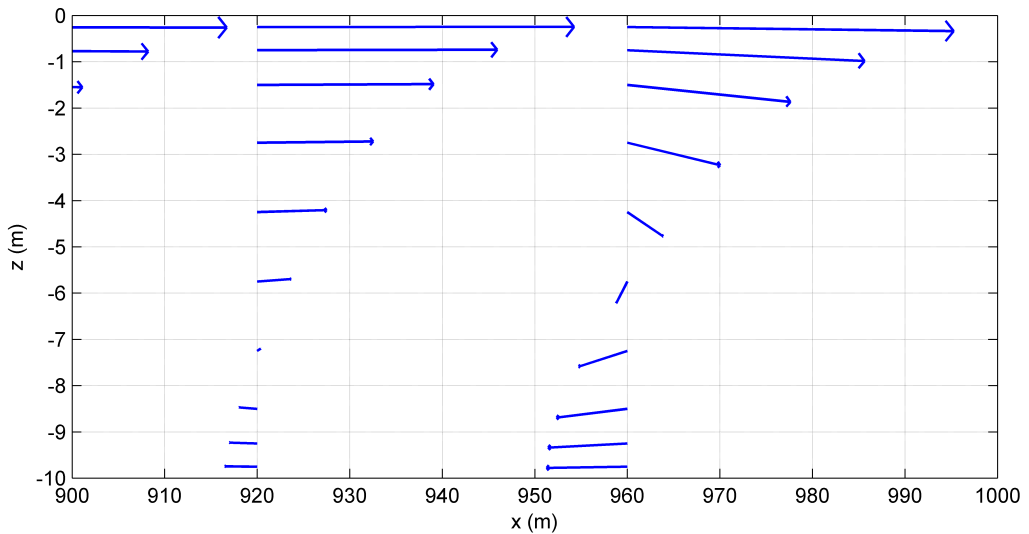


Figure 5.17: Flow circulation near the easternmost border (vertical borders).

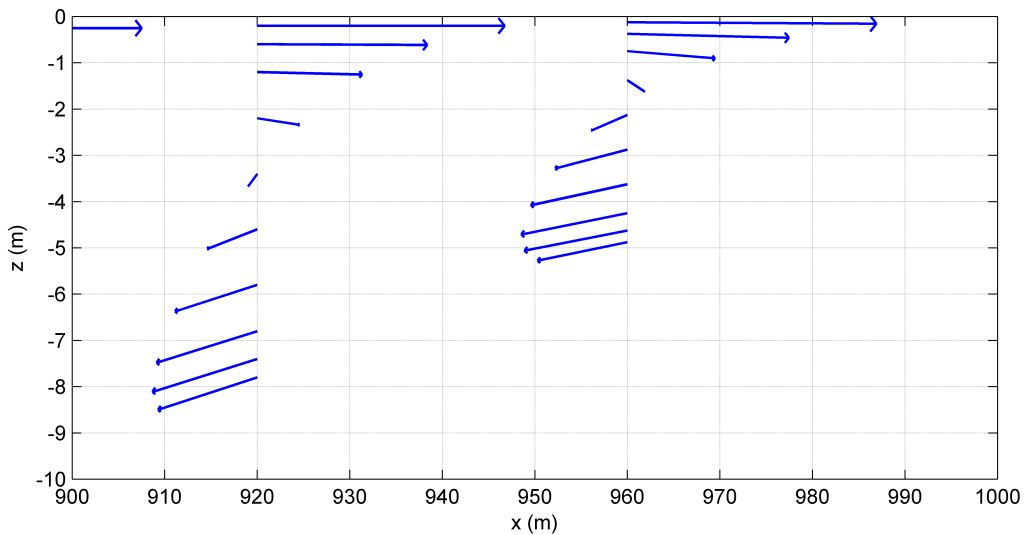


Figure 5.18: Flow circulation near the easternmost border (sloping borders).

However, the focus is on the borders of the closed basin. Figs 5.17 and 5.18 depict the flow circulation at these regions and it can be observed that larger velocities occur for the vertical borders case.

Furthermore, since water cannot evacuate the system, when it approaches the last grid cell it immediately flows downwards. The narrower the last grid cell, the larger expected velocities in the vertical direction. On the contrary, the wider the last grid cell, the lower vertical velocities may occur.

5.6 Differences With Depth-Averaged Simulations

What is the essential difference between a depth averaged simulation and a 3D simulation of a lake under wind forcing? Which one would suffice when the

objective is to predict surges , and which one when the objective is to calculate the spreading of substances (sediments, algae, oil spills, nutrients, pollution)?

Depth-averaged simulations work well to determine the set-up at a basin (the total wind force is identical to the total pressure force, *i.e.* the water elevation). On the other hand, in case a substance is dissolved in the lake, since a balance between the pressure gradient in one direction and in the opposite direction (at a grid cell) exists, the substance would move in a depth-averaged simulation. Therefore, a depth-averaged simulation would suffice the objective of predicting a surge but not the spreading of substances.

A vertical layer distribution yields the gradient of an arbitrary (hydraulic) property over the depth. It is known that, *e.g.* at a lake where a wind forcing is blowing over the water surface, flow circulation at the top layers will behave accordingly to the wind circulation whereas in a reverse fashion near the bottom. Therefore, it may occur (as it happens in the present system) that this circular circulation could drive (near the bottom) an arbitrary substance towards the west when an east-directed wind is blowing. Hence, a proper estimation of the spreading of substances ought to be done implementing a multilayered scheme.

Chapter 6

Standing Short Wave in a Closed Basin

6.1 Creating a Standing Wave in a Closed Basin

Consider a closed basin. Set up your model such to get a standing wave.

The following script has been written in order to reproduce a standing wave in a closed basin of 20 m long and 10 m deep. Since the boundaries have to be closed, no wave forcing can be imposed to create such a wave inside the basin. Nevertheless, using a specific initial surface elevation, a standing wave can be artificially created.

For that purpose, a sinusoidal water surface will be introduced:

$$\zeta(x) = a \cos\left(\frac{2\pi}{L}x + \phi\right), \quad 0 \leq x \leq 20 \quad (6.1)$$

where ζ is the surface elevation, a ($= 0.1$ m) is the amplitude of the standing wave, L is the length of the wave ($= 20$ m) and ϕ is the phase shifting ($= 0^\circ$). The abovementioned script is shown below:

```
PROJ 'Exercise7' '1'
MODE DYN ONED
CGRID 0. 0. 0. 20. 0. 20 0
INPGRID BOTTOM 0. 0. 0. 1 0 20. 1.
READINP BOTTOM 1. 'FlatBottom.bot' 1 0 FREE
INPGRID WLEV 0. 0. 0. 20 0 1. 1.
READINP WLEV 1. 'SinSurface.wlv' 1 0 FREE
FRIC CONST 0.
VISC 0.
NONHYD BOX PREC ILU
DISCRET UPW NONE
DISCRET UPW UMOM V NONE
DISCRET CORRDEP NONE
GROUP 'POINT' 10. 0.
TABLE 'GAUGE' NOHEAD 'Gauge.tbl' TSEC WATL OUTPUT 000000.000 0.01 SEC
TEST 1,0
COMPUTE 000000.000 0.01 SEC 000030.000
STOP
```

The following commands provide the specified characteristics below:

FRIC CONST 0.

VISC 0.

Neither friction nor viscosity is enabled.

NONHYD BOX PREC ILU

Include non-hydrostatic pressure to shallow water equations. Keller-box scheme (time integration follows 1st order implicit Euler method). ILU preconditioner implemented.

DISCRET UPW NONE

DISCRET UPW UMOM V NONE

No upwind is applied (discretization of advection terms), hence the standard central difference scheme is applied.

DISCRET CORRDEP NONE

No upwind is applied (for interpolation of water depths), hence the standard central difference scheme is applied.

Next are presented the time series of the computed surface elevation obtained at the gauge location:

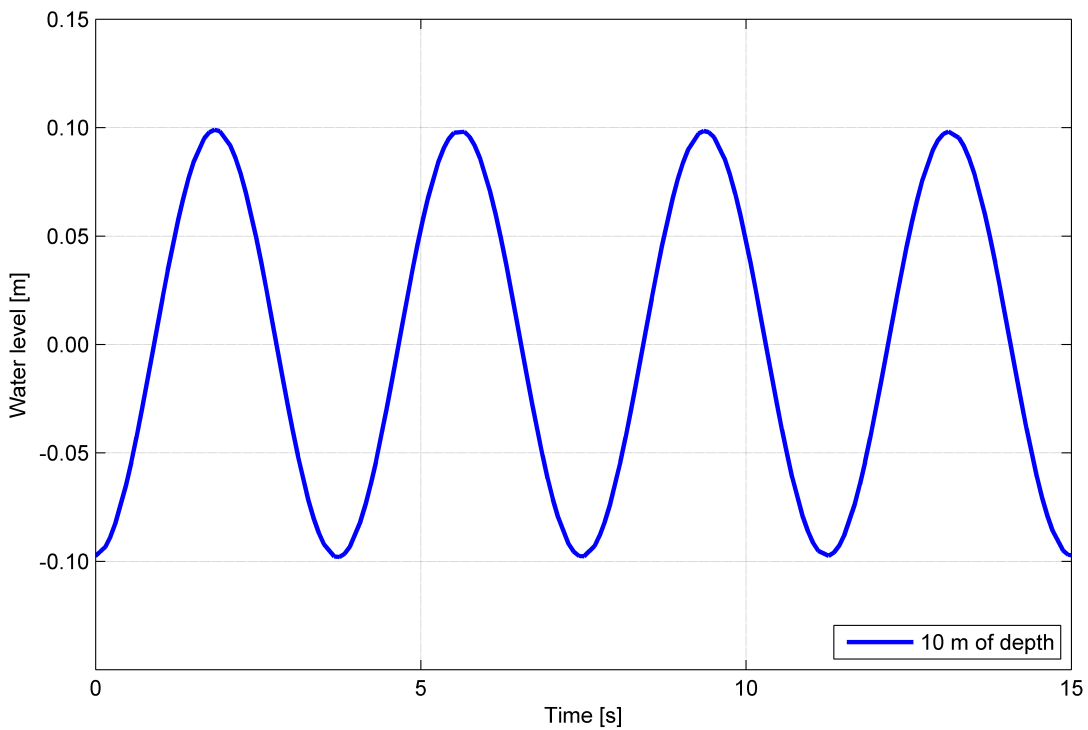


Figure 6.1: Computed time series of surface elevation at gauge point for the standing wave in closed basin of 10 m depth.

6.2 Creation of a Short Wave

Choose the right dimensions in order to get a short wave.

Given a fixed length of the closed basin, shorter waves can be reproduced by decreasing the depth. However, care must be taken since very shallow basins may induce offsetting effects on the waves. The Fig. 6.2 displays several time series of standing waves for basins with a depth larger than the original one (10 m).

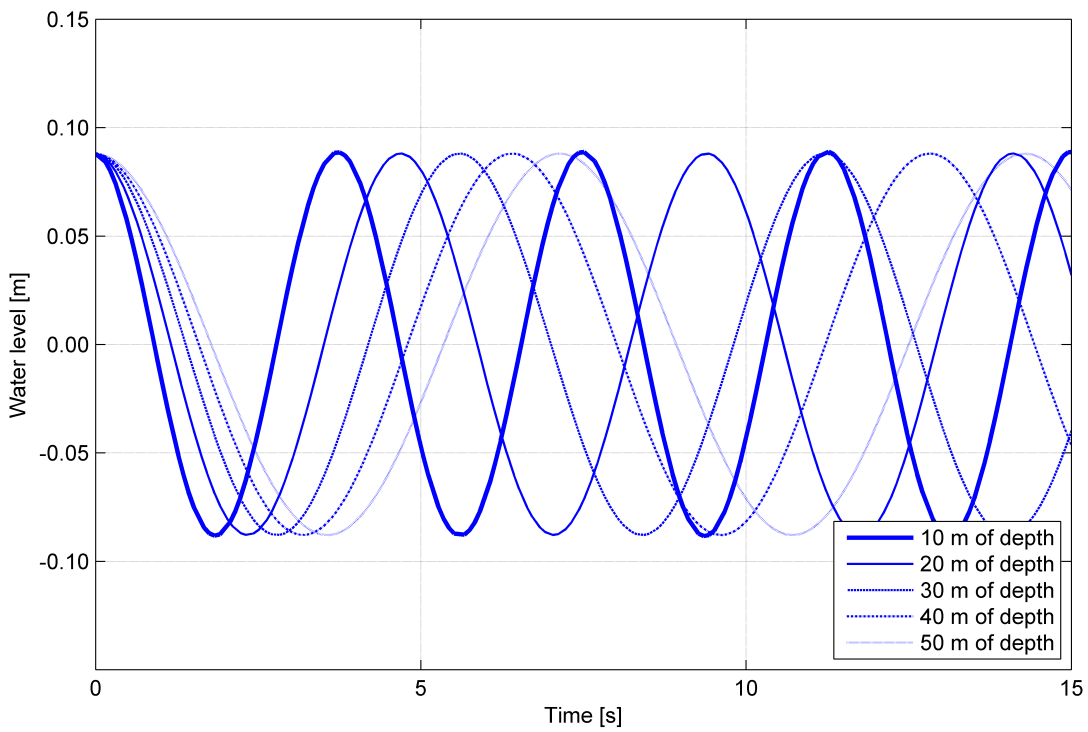


Figure 6.2: Computed time series of surface elevation at gauge point for the standing wave in closed basin (deeper).

As it has been said, it can be concluded that larger depths lead to longer waves (larger periods). On the other hand, when the bottom is rises shorter waves can be obtained (the reduction of the wave period is not as high as the depicted in Fig. 6.2) although nonlinearities are found when the basin depth is further reduced. Even though it is not clearly seen, Fig. 6.3 attempts to show the nonlinear pattern that exhibits the water surface when a rather shallow depth is present.

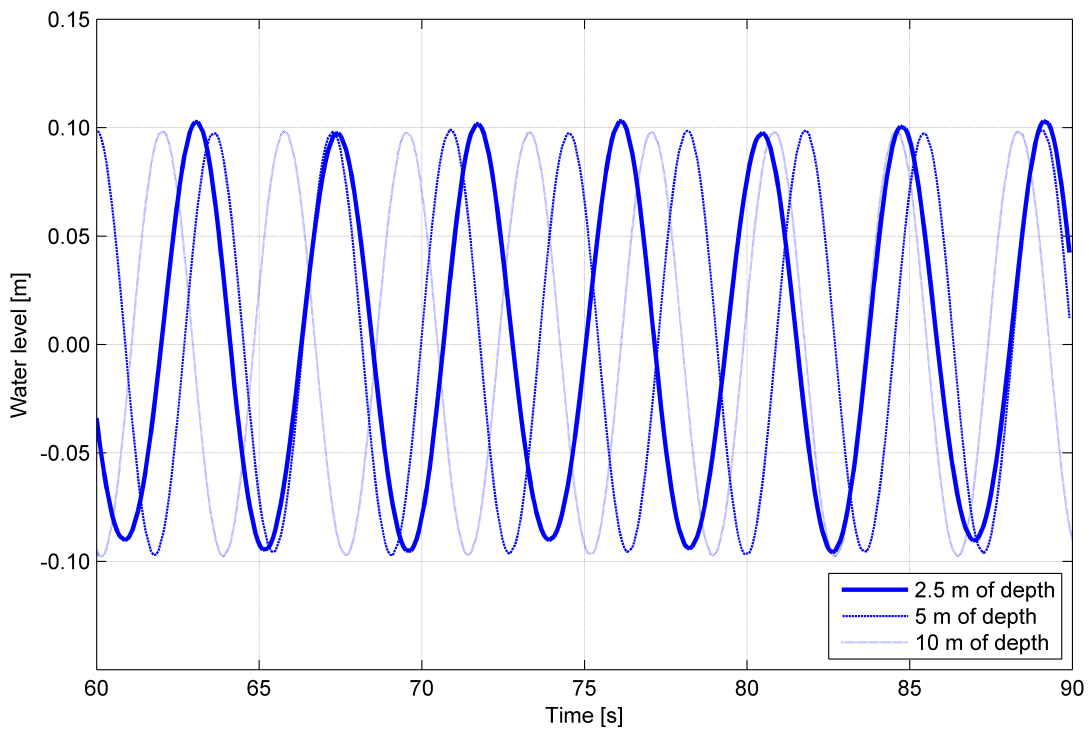


Figure 6.3: Computed time series of surface elevation at gauge point for the standing wave in closed basin (shallow).

Alternatively, the wave period can be modified by widening or narrowing the basin. For the present study, a fixed bottom level equal to the original one (-10 m) is to be kept. Different basin lengths have been implemented always providing a wave length of the standing wave equal to it.

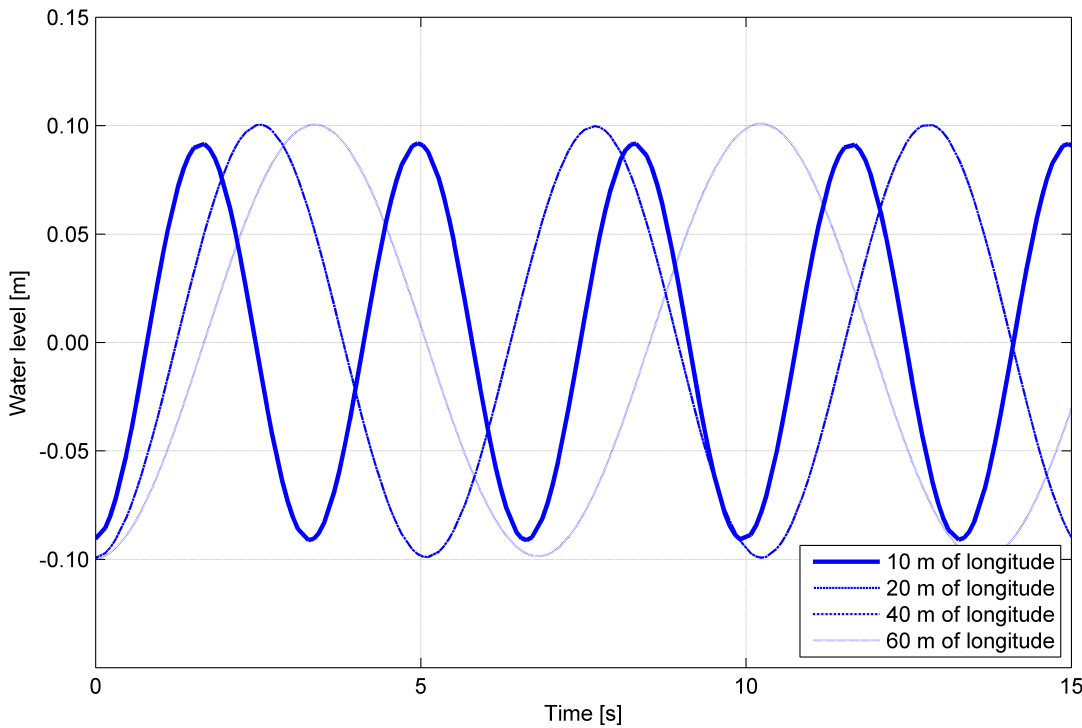


Figure 6.4: Computed time series of surface elevation at gauge point for the standing wave in closed basin (different longitudes).

From the Fig. 6.4 it can be concluded that longer waves (in the time domain) take place when the longitude of the basin is increased. However, differences in the wave heights have also been spotted. This may have to do with the fact that the wave is recursively enlarged when a larger longitude is applied. Nevertheless, the main goal is to foresee the trend and it has already been mentioned above.

6.3 Number of Grid Points per Wave Length

Think about the number of grid points per wave length.

Assume that the computational grid is comprised by n grid points ($n-1$ grid cells). If the initial water surface is defined by a 2^{nd} -order harmonic, i.e. the wavelength of the standing wave equals the length of the basin, the total number of n grid points will be used to define the wave. Therefore, the following relationship can be stated:

$$\lambda = L \rightarrow n$$

However, if a 3^{rd} -order harmonic is initially imposed as water surface, the number of grid points per wavelength is:

$$\lambda = \frac{2}{3} L \rightarrow \frac{2}{3} n$$

This procedure can be reproduced for higher harmonics leading to the following expression, that relates the number of grid points per wavelength for an arbitrary harmonic i :

$$\lambda_i = \frac{2}{i} L \quad \rightarrow \quad \frac{2}{i} n$$

Thereafter, the higher the harmonic the shorter the wavelength and, hence, fewer grid points per wavelength. This will lead to a decrease of the resolution of the water surface (and eventually the model will crash since the length of the grid cells will not be small enough to capture the oscillations of the short standing waves). Higher harmonics would thus require more grid points and, therefore, a larger computational cost.

6.4 Linear Wave Modelling

We want to model a linear wave. Why do we want this? How can we obtain this?

Linear waves are described by linear equations, i.e. those where in each term of the equation the dependent variable and its derivatives are at most first degree (raised to the first power).

This means that the superposition principle applies, and linear combinations of simple solutions can be used to form more complex solutions.

On the other hand, nonlinear waves are described by nonlinear equations, and therefore the superposition principle does not generally apply. This means that nonlinear wave equations are more difficult to analyse mathematically and that no general analytical method for their solution exists.

Neglecting nonlinearities (computation of the nonlinear source terms) can be seen a good approximation and will avoid complexities that involve computational high cost.

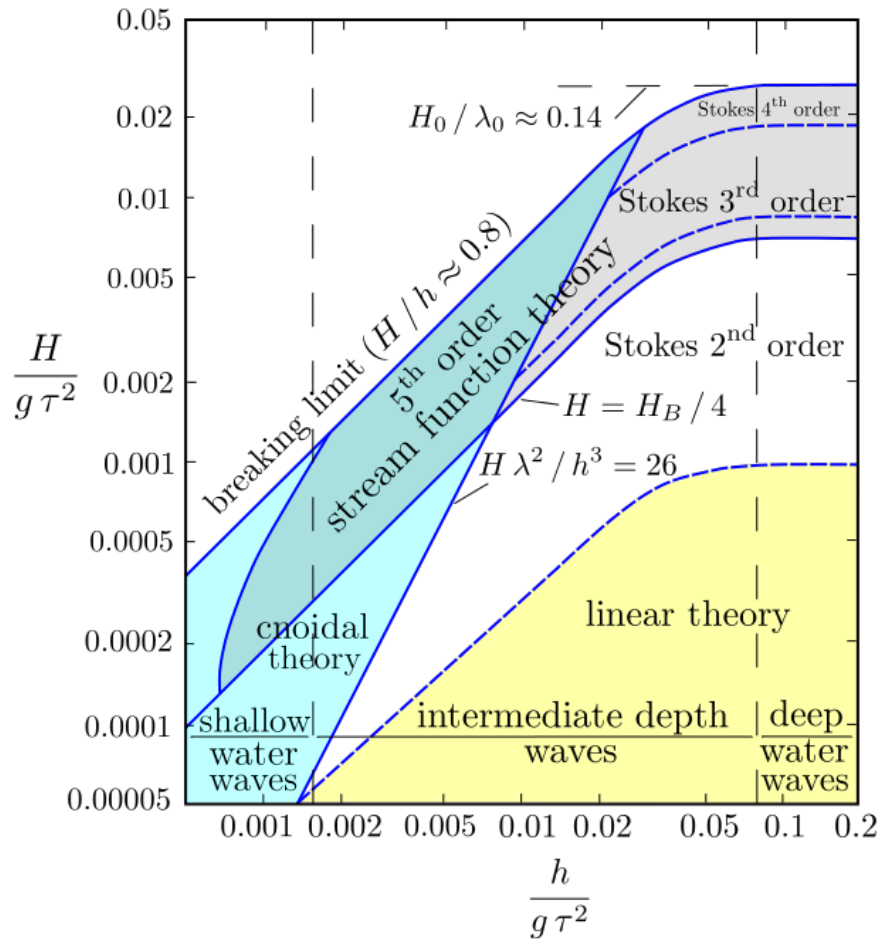


Figure 6.5: Validity of wave theories.

Linear wave theory needs to be thus satisfied:

- not too steep waves at deep water: $ak \ll 1$ for kh large, or
- small amplitude waves at shallow water: $a < h$ for kh small.

It can be seen that linear waves will be obtained providing that a rather small amplitude is considered. The basin depth is set to 10 m for all different cases (Fig. 6.6). The original case is completely linear (0.1 m). An original amplitude of the standing wave of 2 m yields a fairly linear wave although a gradual decrease over time can be observed. An amplitude of 5 m yields a nonlinear situation, where the wave length decreases over time. Lastly, an amplitude equal to the depth of the basin (10 m) leads to a completely nonlinear wave pattern (moving upwards along a vertical line in the Fig. 6.5).

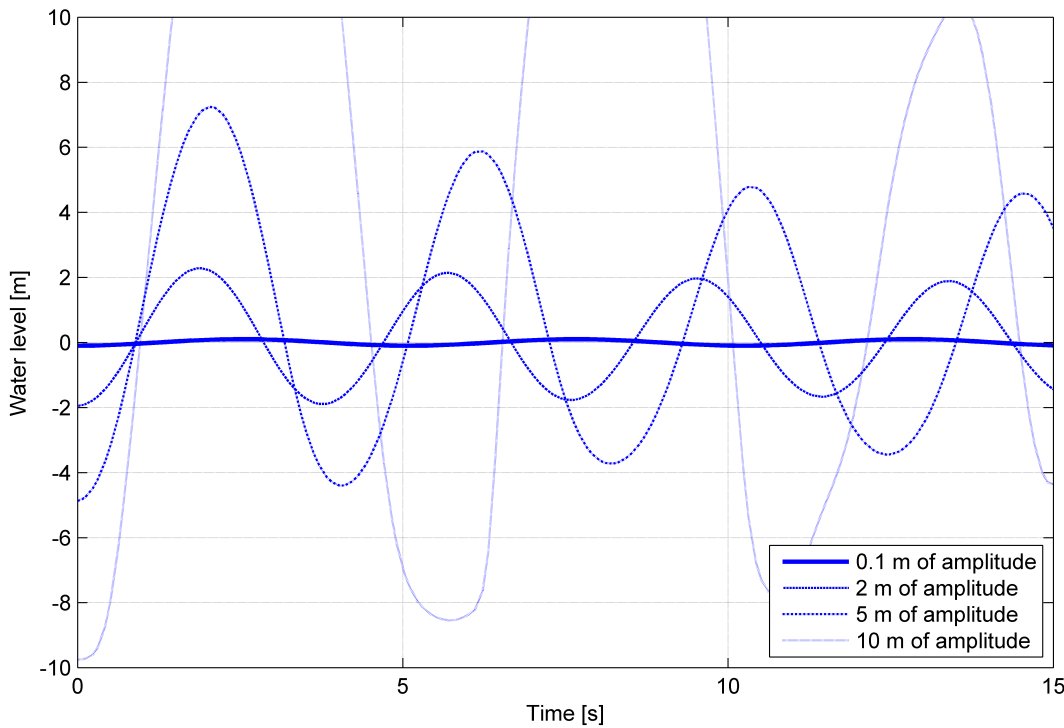


Figure 6.6: Computed time series of surface elevation at gauge point for the standing wave in closed basin (different amplitudes).

6.5 Assessment of the Phase Speed (fixed bottom level)

Assess the phase speed of the wave and compare it with the dispersion relation.

The phase speed (or celerity) c can be estimated from the wave period as:

$$c = \frac{L}{T} \quad (6.2)$$

where L is the wave length and T is the wave period. The wave length has been forced to be equal to the longitude of the basin (20 m) and the wave period is estimated using the upwards(downwards) zero-crossing method.

On the other hand, the celerity can be alternatively derived from the dispersion relation using the wave number k ($=2\pi/L$) and the water depth (10 m).

$$\omega = \sqrt{gk \tanh kh} \quad \rightarrow \quad c = \frac{\omega}{k} = \sqrt{\frac{g}{k} \tanh kh} \quad (6.3)$$

For the given conditions, the wave period can be calculated from the time series of the Fig. 6.1.

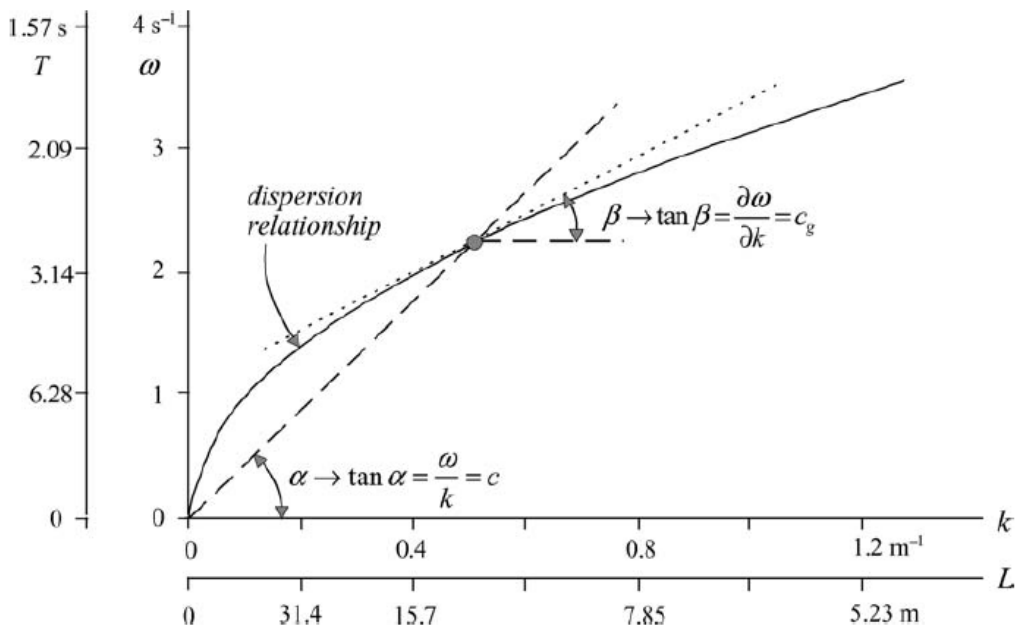


Figure 6.7: The dispersion relationship, the phase velocity c and the group velocity c_g (depth 100 m).

Fig. 6.7 shows the relationship between the dispersion relation and the phase speed. It can be seen that the dispersion relation (continuous line) crosses the group celerity (dotted line) and wave celerity (dashed line) at a specific point. This represents the limit between dispersive and non-dispersive waves.

Waves become dispersive when are longer (larger wave lengths and wave periods), which normally occurs at larger water depths, and their phase speed is smaller than the dispersion relationship. Waves become non-dispersive when are shorter (short wave lengths and wave periods), which normally occurs at shallower water depths, and their phase speed (which is the same as the group velocity) is larger than the dispersion relationship (see Fig 6.7).

Table 6.1: Dispersion relationship and phase speed results for a depth of 10 m.

h [m]	Dispersion relation [m/s]	Phase speed [m/s]	kh [-]	T [s]
10	5.577	5.333	3.142	3.75

The results (Table 6.1) denote that considered waves are dispersive, meaning that the phase speed (wave celerity) is smaller than the phase speed found with the dispersion relation (see the slopes in the Fig. 6.7). This is also related to the linear wave theory. Present waves are linear, which means that they are dispersive, otherwise the wave celerity would be larger than the dispersion relation and waves may start breaking (nonlinearities).

The dimensionless depth kh yields a measure for the dispersion of the waves:

- when $kh > 1$ waves become dispersive ($kh = \pi$ deep water boundary),
- when $kh < 1$ waves become non-dispersive ($kh = \pi/10$ shallow water boundary).

Since $kh = \pi$, the present standing wave would fall under the category of dispersive. This conclusion is in accordance with the previous statement and reaffirms the veracity of the assumption made in section 6.4, where this particular wave was already described as a linear wave.

6.6 Hydrostatic and non-Hydrostatic Modes

Try both modes: hydrostatic and non-hydrostatic . What do you see and why?

Global/basin-scale phenomenon are fundamentally hydrostatic; convective processes on the kilometer scale are fundamentally nonhydrostatic: large scale ocean circulations, tides and storm surges.

Somewhere between the geostrophic and convective scales (10 km to 1 km) the hydrostatic approximation breaks down: the “grey area” in the Fig. 6.8.

Nonhydrostatic models based on the incompressible Navier Stokes equations are valid across the whole range of scales but in oceanography have been hitherto used for process studies on the convective scale (see Marshall et al. 1997)

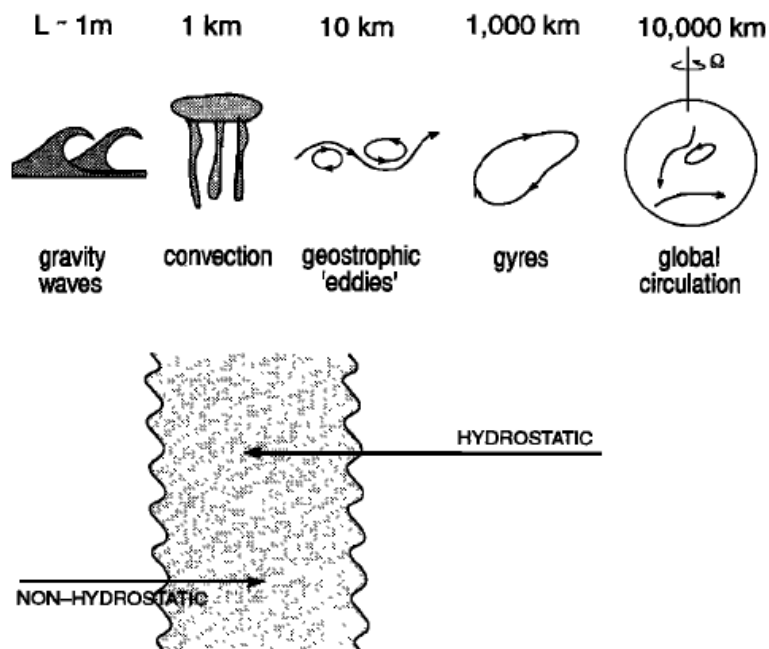


Figure 6.8: Application of hydrostatic and non-hydrostatic modes for different scales.

Given this brief introduction to the hydrostatic/non-hydrostatic nature of phenomena, following an update of the Swash code for the present section is required. The command (NONHYD BOX PREC ILU) has been omitted; by doing so the pressure is assumed to be hydrostatic. In order to include the non-hydrostatic pressure in the shallow water equations, the aforementioned command will be introduced.

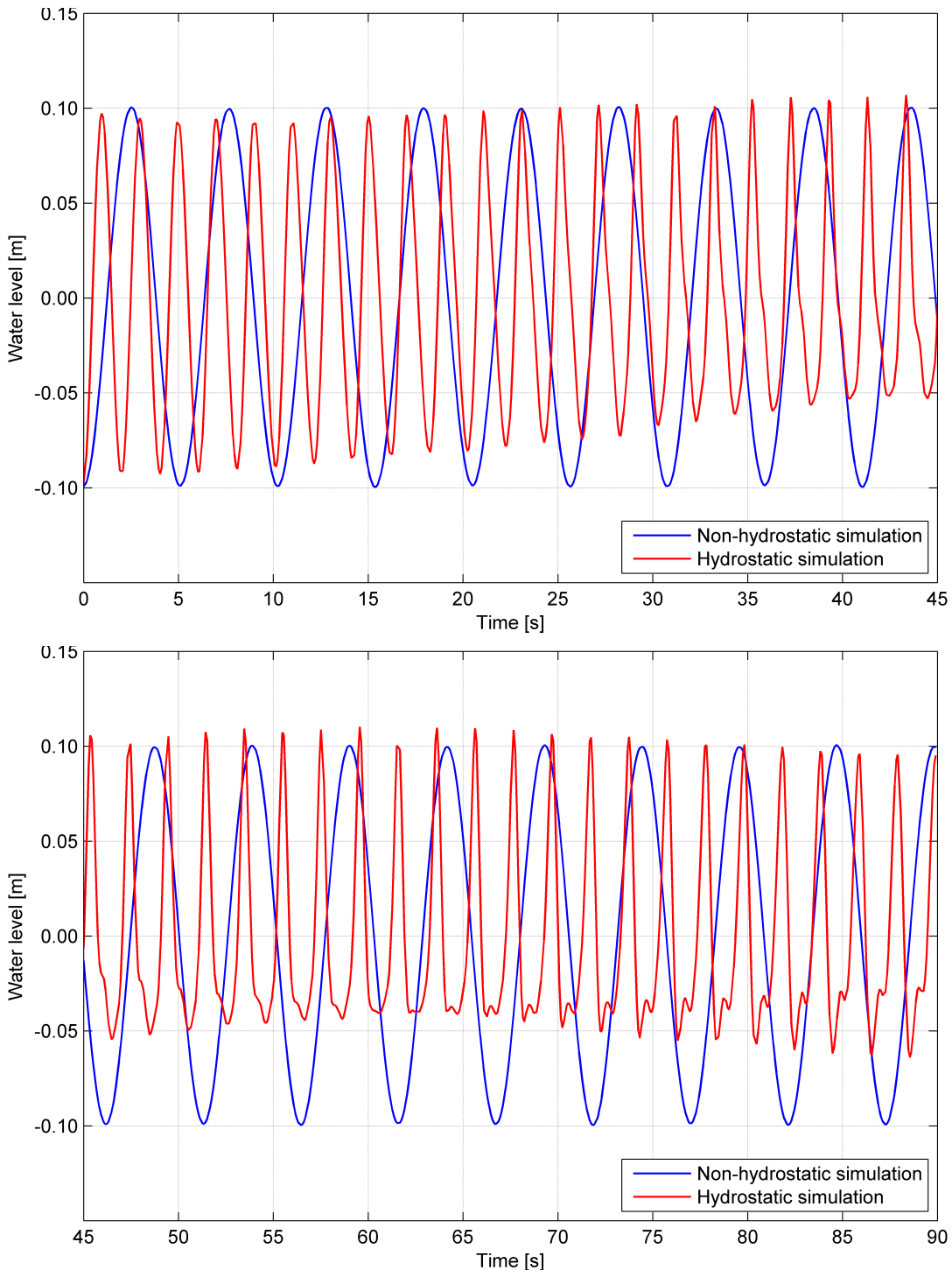


Figure 6.9: Computed time series of surface elevation at gauge point for the standing wave in closed basin (hydrostatic and non-hydrostatic simulations).

From the Fig. 6.9 the next appreciations can be written:

- Horizontal transfer of energy occurs (from the borders to the center of the basin where initially a minimum was set). The amplitude near the borders decreases and it is enhanced in the center. This effect is reversed afterwards.
- The nodes and antinodes are no longer conserved.

- The standing wave fades away (nonlinearities arise).
- The spin-up time is infinite (a large time series have been plotted and a cyclic behavior is displayed by the water surface).

During the course of this exercise, and specially in this section, the following Matlab script has been written in order to visualize the evolution of the water surface:

```

load system.tbl
m = 21;           % Number of grid points
t = 3000;          % Simulation time (msec)
dist = system(1:m,1);
watlevx = system(:,2);
depthx = system(:,3);

figure()
for i = 1:t
    k = m*(i-1);
    plot(dist,watlevx(1+k:m+k),...
        'MarkerStyle','o',...
        'MarkerSize',2);
    xlabel('Water level [m]');
    ylabel('Distance [m]');
    set(gcf,'Color',[1 1 1]);
    grid
    axis([0 20 -0.1 0.1]);
    M(i) = getframe(gcf);
    pause(1/24) % 24fps
end

```

where the input was requested from the Swash model through:

```

GROUP 'SYSTEM' 1 21 1 1
TABLE 'SYSTEM' NOHEAD 'system.tbl' DIST WATL OUTPUT 000000.000 0.1 SEC

```

To sum up, it has been seen that the hydrostatic mode is not suitable for the present system since not only its scale is not high enough but nonlinear effects lead to a vanishing of the standing wave (partly due to the former aspect).

6.7 Assessment of the Phase Speed (variable bottom level)

Try different bottom depths and assess the phase speed again. Conclusion?

The assessment of the phase speed will be based on the results found in sections 6.2 and 6.5. Depths up to 50 m are to be considered, and a comparison between the phase speed and the dispersion relationship is given in the Table 6.2.

Table 6.2: Dispersion relationship and phase speed results for depths of 10 m to 50 m.

h [m]	Dispersion relation [m/s]	Phase speed [m/s]	kh [-]	T [s]
10	5.577	5.333	3.142	3.75
20	5.588	4.255	6.283	4.70
30	5.588	3.571	9.425	5.60
40	5.588	3.125	12.566	6.40
50	5.588	2.817	15.708	7.10

The results found seem to be rather reasonable. The dispersion relation becomes constant since $\tanh(kh) \rightarrow 1$ due to the larger dimensionless depths.

For a given wave length (always assumed to be constant and limited to the longitude of the basin) and increasing wave periods (as it has been seen, the larger the depth the longer the wave periods) the wave celerity decreases (see equation 6.2). However, in reality waves become larger in longitude and the ratio is reversed and, hence, the phase speed gradually increases.

In this case, the phase speed should be seen as the celerity of the standing wave associated with the vertical motion. Thereafter, longer waves have been observed in the time series (Fig. 6.2) and this result directly corresponds to lower vertical velocities.

6.8 Different Number of Layers

Try different number of layers. What are your conclusions?

In this section, an additional change in the Swash script needs to be introduced. So far, a one-layer configuration (i.e. depth-averaged scheme) has been considered. However, a number of horizontal (not equally thick) layers will be used to assess the effect on the evolution of the standing wave. Various layers are implemented using the following command: VERT 4 5. 15. 20. 60. (e.g. four layers).

First, it is attempted to approach the influence of the multi-layered system on the phase speed. Therefore, the depth-averaged scheme and a two- and three-layered configuration results have been compared in the Table 6.3.

Table 6.3: Dispersion relationship and phase speed results for a depth of 10 m (different horizontal layers).

Layers	h [m]	Dispersion relation [m/s]	Phase speed [m/s]	kh [-]	T [s]
1-layer	10	5.577	5.333	3.142	3.75
2-layers	10	5.577	5.698	3.142	3.51
3-layers	10	5.577	5.714	3.142	3.50

The wave periods employed in the Table 6.3 have been estimated from the Fig. 6.10.

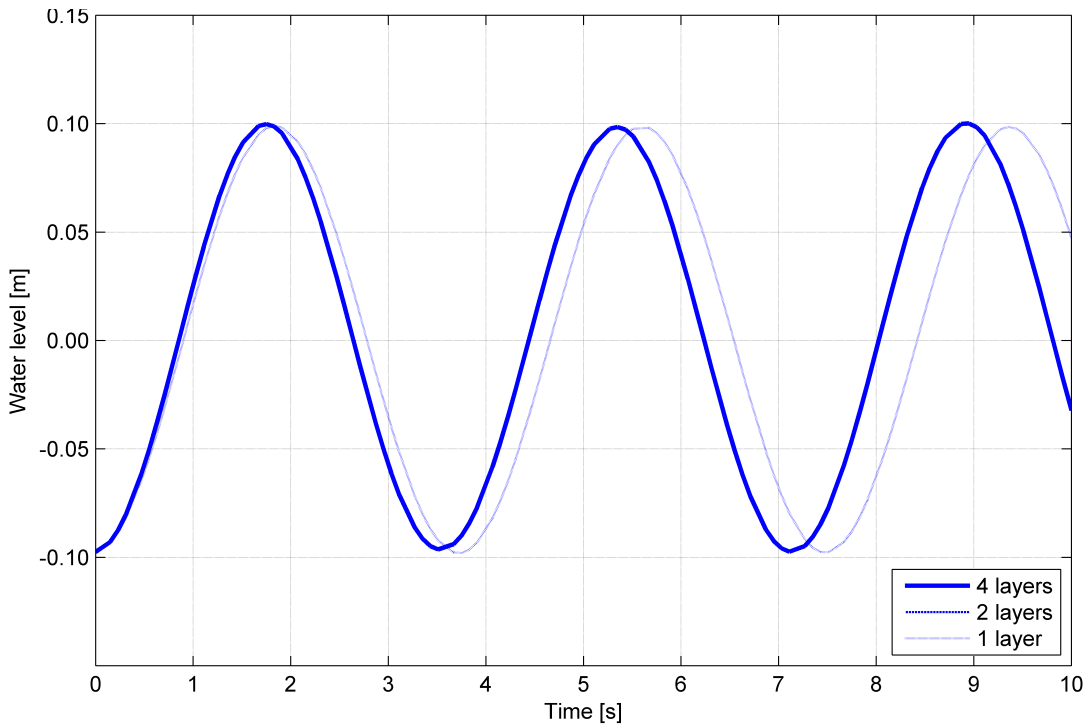


Figure 6.10: Computed time series of surface elevation at gauge point for the standing wave in closed basin (different layers).

The computed frequency of the wave is improved and equals the exact one. It is to be stressed here that we just need only two or three layers to obtain the already accurate dispersion relation, due to the use of the Keller-box scheme that allows non-hydrostatic pressure also in the surface cells (see Stelling and Zijlema 2003).

For larger depths it is important to increase the number of layers for a good estimation of the orbital velocities. A larger resolution is required in order to capture the hydrodynamic properties that take place at larger depths.

It has been found, however, that computed waves were damped during the propagation. Stelling and Zijlema 2003 stated that this is not caused by the vertical space discretization but by the splitting error of $O(\Delta t)$ introduced in the fractional step approach employed. A modified fractional step method where the splitting error is almost completely eliminated is assessed by Casulli 1999.

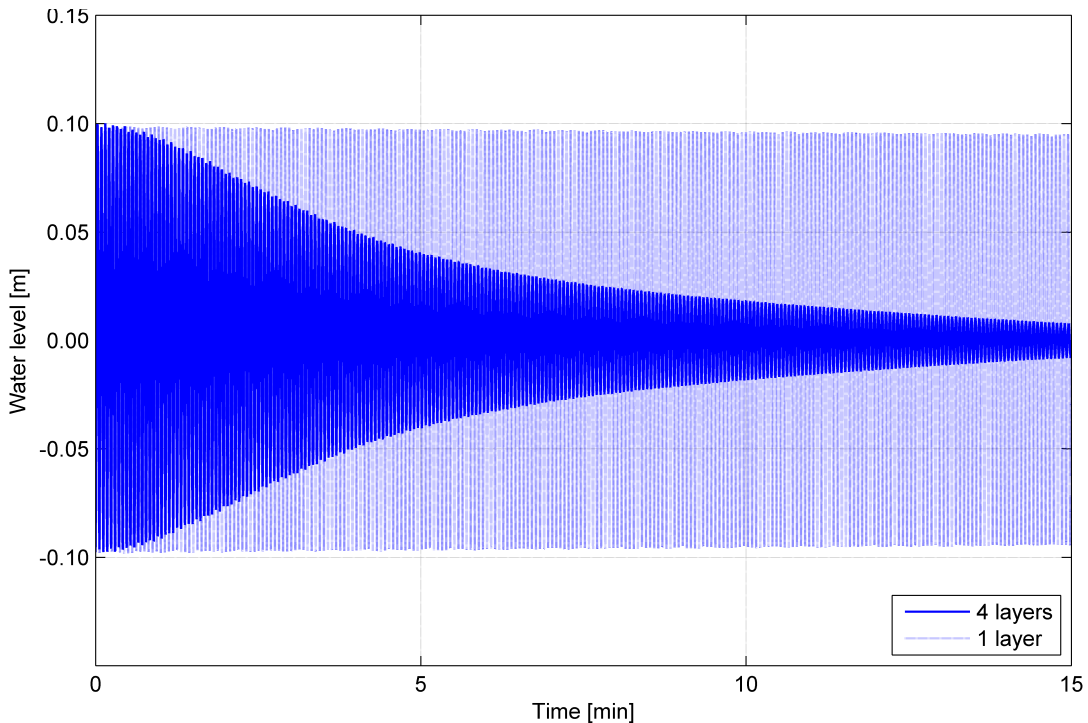


Figure 6.11: Computed time series of surface elevation at gauge point for the standing wave in closed basin (different layers).

It can be seen from the Fig. 6.11 that the case where horizontal layers are implemented (more than one) leads to a fast dissipation of the standing wave (about 25 minutes for the given conditions). However, when no layers are specified, i.e. one layer that covers the whole depth, the amplitude is virtually the same for the that time period (there is a minimum decrease). The application of vertical layers has thus a direct effect on the time-evolution of the standing wave.

6.9 θ -scheme

Try different values of θ when the θ -model is applied.

The time integration of the vertical pressure gradient is the so-called θ -scheme (a mix of explicit and implicit Euler schemes). Different values of θ can be given to the model:

- $\theta = 0.5$: second order accurate Crank-Nicolson scheme,
- $\theta = 1.0$: first order implicit Euler scheme.

Only allowed values [0.5,1.0].

So far the implicit Euler scheme has been implemented. It is also known as the backward Euler method and it is widely used in numerical methods to solve ordinary differential equations.

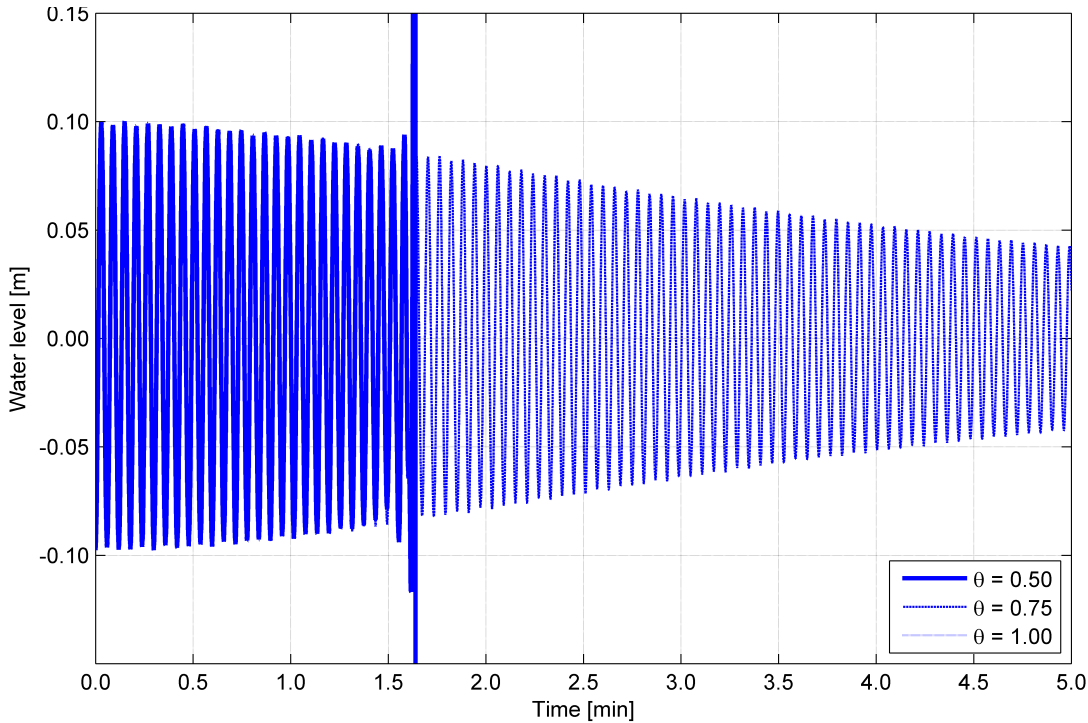


Figure 6.12: Computed time series of surface elevation at gauge point for the standing wave in closed basin (different θ s).

It can be seen from the Fig. 6.12 that no appreciable difference exists between $\theta = 1.0$ and $\theta = 0.75$. However, when $\theta = 0.5$ (Crank-Nicolson scheme) the system becomes very soon unstable. One of the main pitfalls of the latter scheme is the fact that the approximate solutions can still contain (decaying) spurious oscillations if the ratio of time step Δt and the square of the grid cell length is large enough (typically larger than $1/2$). For this reason, whenever large time steps or high spatial resolution is necessary, the less accurate (1st order method) backward Euler method is often used, which is both stable and immune to oscillations.

A multi-layered configuration of two layers has been chosen. It can be seen in detail from the Fig. 6.13 that small oscillations take place during the second 85 to 90. These are enhanced in the following time steps and finally the model computes large amplitudes (while attempting to reduce the time step) until the water level is too far below the bottom level and, hence, crashes.

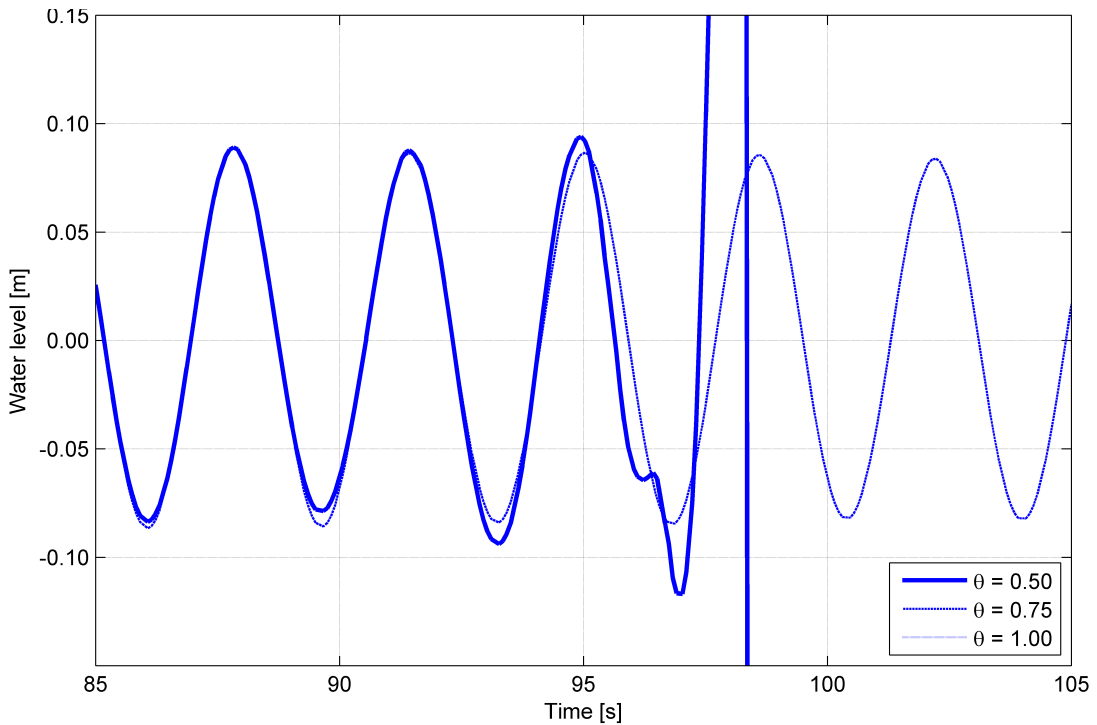


Figure 6.13: Computed time series of surface elevation at gauge point for the standing wave in closed basin (different θ s in detail).

As conclusions, the following has been observed:

- For the present phenomena, a stable method which is immune to oscillations is required. Thereafter, the larger θ values need to be larger than 0.5.
- Alternatively, short time steps (or a high resolution grid) may be applied in order to mitigate oscillations although the computational cost would be much higher.

Bibliography

- Casulli, V. (1999). "A semi-implicit finite difference method for non-hydrostatic, free-surface flows". In: *International Journal for Numerical Methods in Fluids*. DOI: 10.1002/(SICI)1097-0363(19990630)30:4<425::AID-FLD847>3.0.CO;2-D.
- Kernkamp, H.W.J. et al. (2011). "Efficient scheme for the shallow water equations on unstructured grids with application to the Continental Shelf". In: *Ocean Dynamics*. DOI: 10.1007/s10236-011-0423-6.
- Kramer, S.C. and G.S. Stelling (2008). "A conservative unstructured scheme for rapidly varied flows". In: *International Journal for Numerical Methods in Fluids*. DOI: 10.1002/fld.1722.
- Marshall, J. et al. (1997). "Hydrostatic, quasi-hydrostatic, and nonhydrostatic ocean modeling". In: *Journal of Geophysical Research*. DOI: 10.1029/96jc02776.
- Stelling, G.S. and S.P.A. Duinmeijer (2003). "A staggered conservative scheme for every Froude number in rapidly varying shallow water flows". In: *International Journal for Numerical Methods in Fluids*. DOI: 10.1002/fld.537.
- Stelling, G.S. and M. Zijlema (2003). "An accurate and efficient finite-difference algorithm for non-hydrostatic free surface flow with application to wave propagation". In: *International Journal for Numerical Methods in Fluids*. DOI: 10.1002/fld.595.
- Tseng, Y.H., C. Meneveau, and M.B. Parlange (2006). "Modeling flow around bluff bodies and predicting urban dispersion using large eddy simulation". In: *Environmental Science and Technology*. DOI: 10.1021/es051708m.
- Zijlema, M. and G.S. Stelling (2005). "Further experiences with computing non-hydrostatic free-surface flows involving water waves". In: *International Journal for Numerical Methods in Fluids*. DOI: 10.1002/fld.821.